# 6

# Advances in Thermoelectric Energy Conversion Nanocomposites

Lusheng Su and Yong X. Gan
*Department of Mechanical, Industrial and Manufacturing Engineering*
*College of Engineering, University of Toledo, Toledo, OH 43606,*
*USA*

## 1. Introduction

The painstaking exploring for alternative energy resources is at the research leading edge because energy plays an irreplacable role in the whole world. As a result, how to achieve high-efficient energy conversion rate has become more and more crucial under the condition of limited resources. Thermoelectric (TE) nanocomposite materials, which can generate electricity from heat, could be an alternative solution for global sustainable energy. Whether the power generation by TE nanocomposite materials could be employed as a reliable substitution for getting limited energy resources or not is contingent upon the fact that synthesized TE nanomaterials possess higher thermoelectric conversion efficiency than traditional bulk materials. The inherent characteristics of the promising TE materials like potential high efficiencies and environmentally clean from the use of geothermal and solar heat made the substitution a reality (Weidenkaff et al., 2008). Moreover, as of the rapid development of the modern fabrication and characterization techniques, especially the emerging of nanoscale composite materials, a brand-new period of manufacturing nanocomposites is approaching. The enormous needs for sustainable energy combined with recent advances in thermoelectrics inspire an increasing excitement as always.

Through several decades' endeavors of the researchers, TE nanocomposites have been applied widely to an advanced level. Practical applications have been found such as renewable energies (Robert et al., 2007), electrical power generation, such as thermoelectric generators providing power in remote terrestrial and extraterrestrial like deep space exploration (Snyder & Toberer, 2008), air-warming systems (Cosnier et al., 2008), cooling systems (Lineykin & Sam, 2007) like solid-state Peltier coolers with precise thermoelectric effects for optoelectronics and passengers' seat in aotomobiles, and like thermoelectric micro-coolers with high cooling power density, short response time and device scalability which are very suitable for high-power and compacted microelectronic devices (Liao & She, 2007) and self-powering sensors (biomedicine, environmental monitoring, gas sensing, radio frequency field detector, infrared rays detector such as $SrSi_2$ (Hashimoto et al., 2007) and mobile phones in the future (Dragoman & Dragoman. 2007)).

High efficient utilization of waste heat energy from the surrouding environment is attributed to TE technology application. Considerable quantity of power is generated by heat energy with typical efficiencies in the range from 30% to 40% efficiency. At such rates,

it is estimated that 15 terawatts of the power energy generated by heat energy is lost to the environment. To efficiently convert lost heat into electricity, thermoelectric nanocomposite materials can be used to accomplish this mission. Automobile exhuast and industrial manufacturing processes all generate an enormous amount of unused waste heat that could be high-efficiently converted to electricity by using silent, scalable and reliable TE devices which can scavenge waste heat from the environment. This technology can be employed in the vehicle field for the new generation vehicles with electrical power from waste engine heat from exhaust systems and radiators. One critical merit of thermoelectric nanocomposite is their scalability. For example, waste heat (Gelbstein et al., 2008) and co-generation sources could be as small as a home water heater, or as large as inductrial sources. This technology of energy conversion from waste heat into electrical energy is very important to develop alternative energy technologies in the reduction of our dependence on fossil fuels. To better understand the thermoelectric nanocomposites, knowledge in the fields such as solid-state chemistry, solid-state physics, thermal transport measurement and high-temperature electronics is required.

### 1.1 Development of thermoelectric materials

Thermoelectrics have long been considered inefficient for its most applications. TE nanocomposites have not resurged until last century when theoretical studies predicted that thermoelectric efficiency could be greatly improved through quantum confinement of the electron charge carriers. The electron energy band in a quantum confined structure is narrow and thus producing effective masses and therefore high Seebeck coefficient. In addition, heterostructured nanocomposites may decouple the Seebeck coefficient and electrical conductivity because of electron filtering which could progressively gain enhanced value of ZT. From the mid-1950 to the present, most of the bulk thermoelectric materials (like clathrates, skutterudites and Zintl phases) were found with high-efficiency. The pioneering work was performed and put into practice by Professor Abram (Nolasa et al., 1998). Professor Abram Ioffe and his collaborators did precursory work (Dresselhaus et al., 1999) on introducing semiconductors as promising thermoelectric materials. Then people gradually selected heavy elements from lower right part of the periodic table to synthesize semiconducting compounds. As a result, the lattice thermal conductivity can be reduced through manufacturing mixed or doped crystals. The more efficient thermoelectric materials at that time existed in the $Bi_{2(1-x)}Sb_{2x}Te_{3(1-y)}Se_{3y}$ family (Koga et al., 1997) right because of their lower thermal conductivity. Professor Abram's contributions to more efficient semiconducting materials paved a way for a quite active time when people are expressing great interests in thermoelectric materials. The representative ones are $Bi_2Te_3$, $Bi_2Se_3$, and $Sb_2Te_3$. The high potential of $Bi_2Te_3$ as a thermoelectric material made it still the basis in the thermoelectric field up to present.

Over the past 30 years, $Bi_{2(1-x)}Sb_{2x}Te_{3(1-y)}Se_{3y}$ and $Si_{1-y}Ge_y$ alloys have been extensively studied and optimized as TE materials for their applications like refrigeration and power generation. These conventional TE materials have experienced extensive investigation and there appears little room for future improvement in common bulk materials. As time goes by, a new class of TE compounds emerged and was investigated due to its higher performances. The comparison of ZT values between the traditional TE materials ($CsBi_4Te_6$, $Bi_2Te_3$, PbTe and $Si_{1-x}Ge_x$) and the new TE materials ($AgPb_mSbTe_{2+m}$, $Zn_4Sb_3$, $Yb_{0.19}Co_4Sb_{12}$ and $CeFe_{4-x}Co_xSb_{12}$) can be seen from Fig. 1.

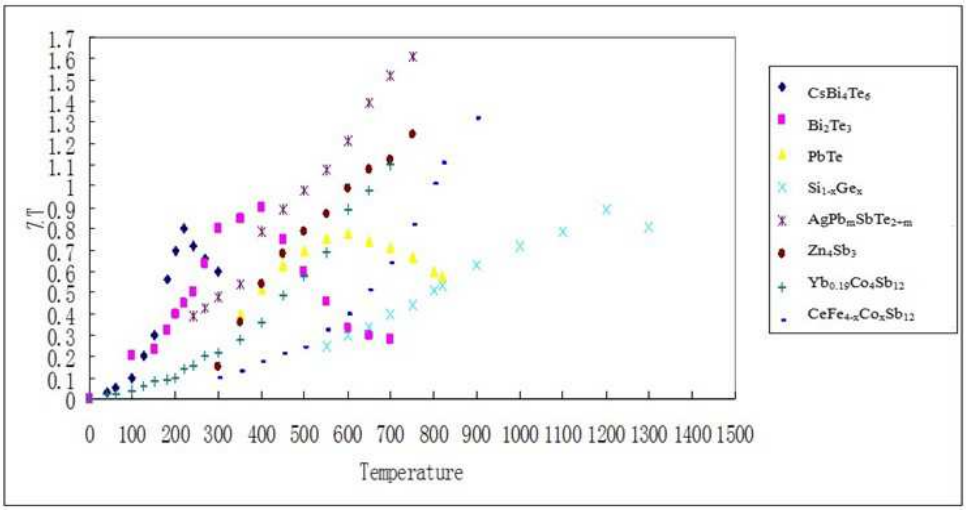


Fig. 1. Relations between temperatures (K) and ZT values. Data source from (Tritt et al., 2006)

During later 90s, researchers discovered that low dimension structures, as occurs in quantum wells (2D) or quantum wires (1D) can enhance the thermoelectric figure of merit rather than their bulk counterparts like two-dimensional PbTe quantum-well and 1D or 2D bismuth which are poor thermo-electrics in 3D. Although the low-dimensional TE materials like superlattices and nanowires could have a chance to improve ZT values due to the decoupling of the three parameters, it is still hard to employ superlattices and nanowires in large-scale energy conversion applications dut to their limitations in cost and heat transfer issures. Recently, many researchers used nanocomposite materials (polymers and inorganic materials) as the novel TE materials because composite materials have the properties from both the inorganic materials and polymers which could have higher values of figure of merit.

### 1.2 Thermoelectric effect

The thermoelectric effect is the direct conversion of thermal energy into electric energy through a themoelectric installation and vice versa. The Seebeck effect is the direct conversion of thermal energy into electrical energy. This effect was revealed by an Estonian-German physicist Thomas Johann Seebeck. The explanation of the thermoelectric mode (TE) is that the applied temperature gradient facilitates charged carriers, say electrons and holes in semiconductors, in the materials to diffuse from one end to another: hot charge carriers in the materials diffuse from the hot end to the cold end because of a lower density of hot carriers at the cold end and cold charge carriers diffuse from the cold end to the hot end. Consequently, the current is induced from the teperature diffecence between two ends of the materials. The reasons for the phenomenon of thermoelectric effect is that there are too many free charge carriers which will carry both charge and heat in metals and semiconductors. A net charge will be generated due to the build-up of charge carriers diffusing from the hot end to the cold end when a temperature gradient applied to a material. A net charge will produce an electrostatic potential. This phenomenon, known as Seebeck effect, is the basis of thermoelectric energy generation. (Snyder & Toberer, 2008)

The converse energy conversion process (ET) is well known as Peltier effect, which converts electrical energy into thermal energy.This phenomenon was discovered in 1834 by a French physicist called Jean-Charles Peltier who observed that when an electrical current is passed through the junction of two dissimilar materials, heat is either rejected or absorbed at the junction depending on the direction of the current. The Peltier effect is due largely to the difference in Fermi energies of the two materials. So the thermoelectric effect may also be called the Peltier-Seebeck effect. The thermoelectric effects have wide and practical applications across the whole world. The devices employing Seebeck effect called thermogenerators can convert various heat sources into electrical energy: turning waste heat from power plants and automobiles into electrical power, conversing radioisotope energy to support space probes and enhancing energy conversion efficiencies of solar cells by utilizing low frequency heat from the sun to a large extent. The devices using Peltier effect can create a compact refrigerator etc.

### 1.3 Measurements of thermoelectric nanocomposites

This section will first introduce the general measurements of the thermoelectric effect. Then this section emphasizes what sources can generate the thermal conduction and thus states the ways to reduce thermal conductivity. What's more, the internal conflicting factors that limit the maximum themoelectric performance is explained with several principles. Following that the relation of the carrier concentration and thermoelectric performance will be stated. Then, other equivalent measurements of thermoelectric performance will be introduced. At last, this section will talk about the thermoelectric devices' efficiency.

The main measurement of the performance of the thermoelectric nanocomposites is the dimensionless quantity ZT (see Eqn. 1). As a measurement standard, ZT is taken as the general expression of thermoelectric materials' effectiveness. Let T be the temperature (in Kelvin) and Z be the thermoelectric figure of merit. Then the dimensionless figure of merit has the following form of expression:

$$ZT=\alpha^2\sigma T/\kappa \tag{1}$$

In this equation, $\alpha$ stands for Seebeck coefficient measured in volts per kelvin (V/K), $\sigma$ denotes the electrical conductivity measured in siemens per meter (S/m) and $\kappa$ denotes the thermal conductivity measured in watts per kelvin per meter (W/K·m). $\alpha$ is the measurement of the induced voltages in response to temperature differences across the materials. It is called the thermoelectric power, or thermopower, or Seebeck coefficient. Typically the unit of the Seebeck coefficient is volts per kelvin, while in practice, it is more prevalent to use microvolts per kelvin (μV/K). The Seebeck coefficient can be represented by $\alpha$ which has the expression of delta V over delta T. Meanwhile, the Seebeck coefficient can also be defined as the following equation (Eqn. 2):

$$\alpha = \frac{8\pi^2 k_b^2}{3eh^2} m^* T \left(\frac{\pi}{3n}\right)^{\frac{2}{3}} \tag{2}$$

Where n is the carrier concentration; m* is the effective mass of the carrier; T is the temperature; e is the elementary charge; $k_b$ is Boltzmann's constant; h is Planck's constant.

Moreover, the Seebeck coefficient can also be defined as the following equation (Eqn. 3):

$$\alpha = \frac{\pi^2 k_b T}{3e}\left(\frac{\partial \ln \sigma}{\partial \varepsilon}\right)_{\varepsilon=E_F} \quad (3)$$

Where $k_b$ is Boltzmann's constant; T is the temperature; e is the elementary charge; σ is the electrical conductivity and $E_F$ is the Fermi energy.

Thermal conductivity stems from two aspects: $\kappa_e$ (electrons and holes transporting heat) and $\kappa_l$ (phonons travelling through the lattice). This means $\kappa=\kappa_e+\kappa_l$. Most of the $\kappa_e$ is directly related to the electrical conductivity based on Wiedemann-Franz Law: the higher the electrical conductivity, the higher $\kappa_l$ becomes. The Wiedemann–Franz law (see Eqn. 4), states that the electrical thermal conductivity ($\kappa_e$) is proportional to the electrical conductivity and the temperature (T).

$$\kappa_e = \sigma LT = ne\mu LT \text{ (For semiconductor)} \quad (4)$$

In above equation, L is the Lorenz factor with the value of $2.4\times10^{-8}$ $J^2K^{-2}C^{-2}$ for free electrons; σ is the electrical conductivity; T is the temperature; n is the carrier concentration; e is elementary charge; μ is carrier mobility.

Based on the above stated Weidemann-Franz law, it is necessary to minimize $\kappa_l$ instead of $\kappa_e$. In semiconductors, electron thermal conductivity is less than lattice thermal conductivity. Therefore, it is easier to decrease lattice thermal conductivity while maintaining the electrical conductivity. A phonon-glass and electron-crystal approach is proposed by G. A. Slack stating that phonons which are responsble for thermal conductivity must experience the material as they would in a glass meaning a high degree of phonon scattering, the lower the thermal conductivity; while electrons must experience the material as a crystal meaning little scattering maintaining the electrical conductivity. As a result of these two methosds, figure of merit will be optimized. This phonon-glass and electron crystal could also be explained as materials possessing electrical properties of a crystalline structure and thermal properties of an amorphous or glass-like material.

The higher value ZT of a material, the more preferable it is as a thermoelectric material for greater thermodynamic efficiency. It is very difficult to simultaneously achieve increased $\alpha^2\sigma$ and reduced κ due to interdependence of the three parameters. In other words, the three parameters are all functions of carrier concentration and are interrelated with each other. As a general rule, a rise in thermopower implies a decrease in electrical conductivity due to carrier density considerations which could be proved by the Seebeck coefficient equation, and an increase in electrical conductivity results in an increase in thermal conductivity based on Wiedemann Franz law. To assure a large Seebeck coefficient, there should be only one single type of carrier rather than mixed n-type and p-type conduction resulting in cancelling out the induced Seebeck voltages. In general, semiconductors have larger Seebeck coefficient than metals because doped semiconductors bear excessive electrons or holes, the contributions to Seebeck coefficient of which can not be cancelled out like metals. That is the main reason that semiconductors have a promising future as the thermoelectric materials. This could be demonstrated by the Fig. 2.

Figure 2 indicated the striking balance between large Seebeck coefficient and high electrical conductivity in TE nanocomposites which should be complied with maximizing the figure of merit ZT. The peak value is shown approximately at carrier concentration between $10^{19}$ and $10^{21}$ carriers per $cm^3$ with very high mobility. This is just right falls in the field between metals and semiconductors (Snyder & Toberer, 2008) which is the primary reason that

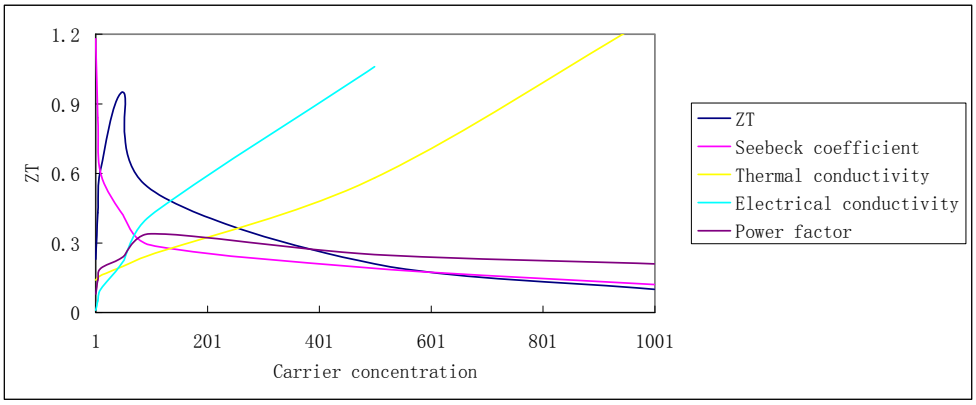


Fig. 2. Relations between Carrier concentration ($10^{18}/cm^3$) and related ZT factors. Data source from (Snyder & Toberer, 2008)

doped semiconductors were found with promising applications in TE nanocomposites. Generally speaking, maximizing the thermoelectric figure of merit refers to a compromise of thermal conductivity, Seebeck coefficient and electrical conductivity. From Fig. 2, thermoelectric power factor will maximize at higher carrier concentration than ZT.

To reduce the lattice thermal conductivity, the approaches fall into three ways. The first method is to separate the electron-crystal from the phonon-glass to guarantee not destroying the crystallinity of the electron-transport part; the second method is to form superlattices by scattering phonons at interfaces of nanostructured materials; the last method is to scatter phonons within the unit cell by generating rattling structures, vacancies or points defects.

There are some other equivalent measurements for TE nanocomposites. The first equivalent measurement of ZT (Eqn. 5) is to replace the denominator in Eqn. 1.

$$ZT=T\sigma\alpha^2/(\kappa_l, \kappa_e) \tag{5}$$

In Eqn. 5, σ,T and α are the same terms, $\kappa_l$ and $\kappa_e$ are the lattice contributions to the thermal conductivity and electronic contributions to the thermal conductivity respectively.

The second equivalent measurement of ZT is determined by Eqn. 6.

$$ZT=m^{1.5}\mu T/\kappa_l \tag{6}$$

In Eqn. 6, m is the effective mass, μ is the carrier mobility, $\kappa_l$ is the lattice thermal conductivity and T is the absolute temperature. A large m results in a high Seebeck coefficient, large μ is good for high electrical conductivity, and the thermal conductivity $\kappa_l$ relies heavily on the crystal structure.

For materials with high electrical conductivity or very low lattice thermal conductivity, the ZT can be defined by Eqn. 7:

$$ZT=\frac{\alpha^2/L}{1+\frac{\kappa_l}{\kappa_e}} \tag{7}$$

In Eqn. 7, L is Lorenz factor and $\kappa_l/\kappa_e<<1$.

Moreover, the power factor (see Eqn. 8), is used more and more frequently to measure the energy conversion efficiency.The definition of power factor is the square of Seebeck coefficient divided by electrical resistivity (ρ).

$$PF=\alpha^2/\rho \tag{8}$$

Effective thernmoelectric nanocomposites should be crystalline semiconductors that can scatter phonons without significantly interrupting the electrical conductivity because crystalline semiconductors have lower carrier mobility due to lower effective masses and increased electron scattering. And glasses will usually exhibit lower lattice thermal conductivity. However, glasses are not used as TE materials because they lack the needed electron-crystal properties. As a result, thermoelectric nanocomposites should bear the properties of phonon-glass and electron-crystal. The electron-crystal can compromise the conflicting Seebeck coefficient and electrical conductivity for crystalline semiconductors. The phonon-glass requires the lattice thermal conductivity as low as possible. This new field of vision to a large extent solves the traditional TE materials' problem. Traditional thermoelectric materials employed alloying with isoelectronic elements to conserve the crystalline structure at the price of disrupting the phonon path. Many experiments successfully demonstrated specific methods to synthesize electron-crystal and phonon-glass nanocomposite materials (Snyder & Toberer, 2008).

Thermoelectric devices consisted of many couples containing n-type and p-type thermoelectric elements assembled in parallel. For instance, a TE generator employs heat flow to power an electric load through the external circuit when applied a temperature gradient. Then a voltage is generated due to the Seebeck coefficient, or the heat flow derives the electrical current. So, it is important to know the measurement of the TE devices. A thermoelectric device's conversion efficiency η (see Eqn. 9), and modified figure of merit Zτ (see Eqn. 10), can be defined as:

$$\eta=\frac{T_h-T_c}{T_h}*\frac{\sqrt{1+Z\tau}-1}{\sqrt{1+Z\tau}+\frac{T_c}{T_h}} \tag{9}$$

$$Z\tau=\frac{(S_p-S_n)^2\tau^2}{[(\rho_n\kappa_n)^{0.5}+(\rho_p\kappa_p)^{0.5}]^2} \tag{10}$$

In Eqn. 9 and Eqn. 10, $T_h$ is the temperature at the hot junction, $T_c$ is the temperature at the surface being cooled, Zτ is the modified figure of merit, ρ is the electrical resistivity, τ is the average temperature between the hot and cold surface and subscripts n and p stand for n-type and p-type semiconducting materials.

In conclusion, semiconductor nanomaterials, which can get higher Seebeck coefficient and elevated electrical conductivity and lower thermal conductivity simultaneously or at least amelioration of some of the above three goals, give contributions to higher values of ZT, that means higher energy conversion efficiencies. To date, the best reported ZT value is between 2 and 3. Higher values of ZT for thermoelectrics are more suitable for future competition especially through nanocomposite materials.

## 2. Fabrication of thermoelectric materials

Before the discussions of thermoelectric materials' advancement, it is necessary to introduce the themoelectric materials fabrication methods to obtain a comprehensive and clear panorama. Then the thermoelectric, photoelectric, electromagnetic, electrochemical and mechanoelectric characteristics of any material can be well investigated. The 'fabrication' here has two different meanings: chemical fabrication and physical fabrication. It is obvious that chemical fabrication means that a new substance has been produced from the starting materials, while physical fabrication stands for a transformation among different physical states like gas, solid or liquid. Consequently, the following parts will explain the commonly used approaches of fabricating thermoelectric materials.

### 2.1 Fabrication from gas to solid phase

Numerous techniques refer to the concentration of gas compounds on solid-state materials. The most straightforward fabrication way is to use the phase or state transformation process from gas state to solid state to deposit a thin film or multilayers on an appropriate substrate. Among various methods based on phase transformations, the typical methods are Physical Vapor Depostion and Chemical Vapor Deposion

**Physical vapor depostion**

Physical vapor deposition depicts a purely physical process such as high temperature vacuum evaporation or plasma sputter bombardment, and this process can deposit thin films on a wafer or substrate through condensation of vaporized materials without any chemical reaction. PVD generally consists of evaporative deposition, electron beam PVD, sputter depostion, cathodic arc deposition, pulse laser deposition and molecular-beam epitaxy. And the most prevalent methods are the sputter deposition and molecular-beam epitaxy (MBE). MBE it the fabrication technique that can permit precise control over deposition composition. It can totally solve the basic problem involved in the general PVD. That is, it is hard to control the deposition composition especially when the starting reaction material is a complicated compound. Molecular-beam epitaxy happened in high vacuum or ultra high vacuum and most apprarent aspect of MBE is the low thin film growth rate(typically bewteen 300 nm and 1000 nm/hour) which in turn promted the films to grow epitaxially. As a rule in solid source MBE, ultra-pure elements such as gallium and arsenic are heated in different quasi-knudsen effusion cells until they begin to gradually sublimate, then the gaseous elements of such materials will condense on the substrate. Sputtering is another commonly used PVD method. It is a process in which atoms are expelled from a solid target by bombardment with energetic ions from an electrically excieted, low-pressure plasma. Owing to collisions, ejected ions or clusters of atoms will be deposited on the specific film substrate.

It is reported that ErAs nanoparticels were epitaxially doped into $[InGaAS]_{1-x}[InAlAs]_x$ using molecular beam epitaxy (MBE) (Zeng et al., 2009). One common example of sputtering is the preparation of bismuth telluride thin films. Many methods have been attempted to prepare the bismuth telluride(n-type and-228 μV/K, p-type 81 μV/K) thin films, including pulsed laser flash evaporation, ion-beam sputtering, metal organic chemical vapor deposition, molecular beam epitaxy, and electrodeposition techniques, while sputtering is the most easy and economic way. Both p-type and n-type bismuth telluride thin films were prepared by sequential sputter deposition of elemental Bi and Te layers and post-annealing

treatment. Periodic Bi/Te multilayer structures were sputter-deposited at room temperature and transformed into bismuth telluride via Bi/Te interfacial reaction during post thermal annealing (Liao & She, 2007).

**Chemical vapor deposition**

Compared with Physical Vapor Deposition (PVD), Chemical Vapor Deposition (CVD) gained much attention with its high growth rate and low cost of reaction equipment and it is the most helpful microfabrication technique which is used to produce high-purity and high-value thin films of semiconducting materials. In a typical CVD microfabrication process, gaseous precursors will react or decompose on the surface of a substrate or wafer to acquire the desired deposition thin film. Then the redundant gas or volatile by-products will be removed by gas flow through the reaction chamber. The deposition forms of CVD method include monocrystalline, polycrystalline, amorphous and epitaxial such as nanofibers, filaments, nanotubes, and various semiconductor compounds. The deposition rate is temperature-dependent in a typical CVD microfabrication process. When the temperature is high, mass-transfer will decide the whole deposition rate; on the other hand, if the temperature is low, the deposition rate will be determined based on chemical reaction. As a result, it is quite important to maintain a uniform temperature distribution to guarantee homogeneous deposition. Moreover, there is one special deposition technique called vapor-liquid-solid(VLS) deposition which involves multiphase catalyst-assisted heterogeneous chemical reactions. In this process, the reactants come from gas phase, while the liquid catalyst expedites the the deposition on the substrate. Similar to VLS, laser-assisted catalytic growth is another promising technique used for fabrication of nanostructure deposition. This method employs catalyst-assisted, multiphase chemical reaction which is the same with VLS. The differences between these two methods are laser-assisted catalytic growth not only hailing from gases but also from bombardment of laser beams. Catalyst such as Fe, Ni, and Au can be prepared on the substrate. Consequently, nanostructures and core/shell coaxial nanotubes can be synthesized through this technique.

Here we only introduce some common classicifications. According to operation pressure, CVD will be divided into atmospheric pressure CVD (APCVD), low-pressure CVD (LPCVD) and ultrahigh vaccum CVD (UHVCD). In view of plasma methods, the CVD includes microwave plasma-assisted CVD (MPCVD), plasma-enhanced CVD (PECVD), remote plasma-enhanced CVD (RPECVD), atomic layer CVD (ALCVD) combustion chemical vapor deposition(CCVD) rapid themal CVD (RTCVD) and vapor phase epitaxy (VPE).

The following examples are given to illustrate the applications of CVD. Zinc-doped cubic boron nitride thin films were prepared by films deposited in pure Ar (Nose & Yoshida, 2007). The crystals of $FeSb_2$ were prepared by the self-flux method or by the chemical vapor transport method (Sun et al., 2009). A key application of LPCVD is employed for fabricating polycrystalline Si by heating silane in a low pressure reactor through pyrolysis, in this process, the by-product $H_2$ will escape from the growing film of solid silicon. This reaction can be expressed as $SiH_4 = Si\downarrow + 2H_2\uparrow$.

Another prominenet use of LPCVD is to fabricate $SiO_2$ nanoscale particals. In a CVD chamber, silane and oxygen can react with each other through the reaction $SiH_4 + 2O_2 = SiO_2\downarrow + 2H_2O$. Moreover, using LPCVD can synthesize the inert silicon nitride like $Si_3N_4$ through equation $3SiCl_2H_2 + 4NH_3 = Si_3N_4\downarrow + 6H_2\uparrow + 6HCl\uparrow$. PECVD can enhance CVD through electrical plasma;

this process can also be called glow-discharge decomposition. This method is generally used to produce thin films of amorphous or polycrystalline semiconductors. Microcrystalline Si can be manufactured through the dilution of $SiH_4$ by $H_2$ at higher wafer temperature. This technique is simultaneously used to fabricate crystalline diamond thin films from a hydrocarbon-hydrogen gas mixture. Also $SiO_2$ can be obtained through the disassembling of tetraethoxysilane or through the chemical reaction of dichlorosilane and nitrous oxide following the equation of $SiCl_2H_2+2N_2O=SiO_2\downarrow+2N_2\uparrow+2HCl\uparrow$.

As for the VLS, due to the influence of catalyst, one-dimensional nanostructure such as nanofibers and nanowires generated from the interface between the liquid and solid. Au-catalyzed VLS growth of phosphorus-doped silicon nanowires, indium nitride nanowires in a dissociated ammonia environment and germanium nanowires with great crystallographic orientations at 350 °C were well fabricated with fabulous shape and orientation. Perhaps the most obvious advantage of laser-assisted catalytic technique is the fabrication of ordered longitudinal herostructure such as herojunctions and superlattices of Si/SiGe.

### 2.2 Fabrication from liquid to solid phase

Crystalline and non-crystalline materials can be fabricated starting from the liquid phase when the desired materials are in big volumn, which means materials manufacturing takes place in the liquid phase in which it is easy to manipulate and achieve. This section will introduce the methods of liquid phase deposition and Sol-gel deposition.

**Liquid phase deposition**

Using liquid phase deposition onto substrate or wafer is a common way of fabricating nanoparticles, nanorods and nanotubes. Yttrium aluminium garnet nanopowder was synthesized with an average grain size of 80 nm. Single crystalline ZnO nanorods with smallest diameter of about 5 nm were fabricated at ambient temperature in liquid phase.Also, $CdS/TiO_2$ hybrid coaxial nanocables using liquid phase deposition were synthesized by soaking porous anodic aluminum oxide template into mixed solutions. Prior literature has suggested that the fabrication of PbS, CuS and CdS nanorods can occur either by electrodeposition or injection of reactants within the channel pores of either anodic aluminum oxide or mesoporous silica templates. Parallel nanowires of CdS and ZnS (Zhang et al., 2009) with the diameter as small as 3 nm templated was another example synthesized by hexagonal liquid crystals (Li et al., 1999).

**Sol-gel deposition**

Sol-gel deposition which is well known as chemical solution depostion is widely used in the field of materials fabrication like metal oxide. This method's starting material is a sol, which is a colloidal dispersion of small paticles suspended in liquid. Then under appropriate conditions, the sol can form a continous network of connected particles called a gel, which is discrete particle. The sol-gel process can fabricate gel materials in a wide range of forms and structures. The precusor sol can be deposited on a wafer to be cast into specific desired shape in a container. This approach that allows the great control over the product's composition is a cheap and low-temperature technique.This method can typically be used in the synthesis of refractory oxide at relatively low temperature like fabrication of $SiO_2$ glass at operating temperature of 1200 degree centigrade. Nanocrystals like $TiO_2$, ZnO and $SnO_2$ oxides were fabricated recently employing sol-gel method.

### 2.3 Fabrication from solid to solid phase

This section will introduce the fabrication ways from solid state to solid state: hot pressing, spark plasma sintering, electrodeposition and doping technique will be recounted.

**Hot pressing**

Hot pressing is used for fabricating powder or powder compact with high pressure and high temperature as a result of which sintering process was begetted. Hot pressing is primarily employed to synthesize hard and brittle materials. One of prevalent examples is the reinforcement of cutting tools and technical ceramics. The hot pressing technique can be found in the form of induction heating, indirect resistance heating and direct hot pressing. In the process of inductive heating, a high frequency electromagnetic field by electronic generator and induction coil is exerted on the mould so that the the heat will be generated wihtin the mould. The merit of it is the pressure and inductive power is not dependent. The disadvantages are the the high expenditure of high-frequency generator and the dependence on satisfactory thermal conductivity and inductive coupling. The indirect resistance heating technique placed the mould in a graphite heating chamber which will cause the heat transferred into the mould. The benefit of this method is indenpendent from mould's conductivity, heat and pressure. Also a high temperature is easy to attain. But the demerit is it will take longer time to heat up the mould and heat transfer from furnace to the mould surface. The direct hot pressing is under developing. New methods called Spark Plasma Sintering (SPS) or Field Assisted Sintering Technique (FAST) have been established. These methods will be introduced in the following paragraghs.

The examples of fot pressing here are the partially filled ytterbium skutterudite materials and n-type $CoSb_3$ nanocomposites. In an argon atmosphere at 26 ksi and 650 °C for 2 h, densification of the powdered specimens into dense polycrystalline pellets was accomplished by hot pressing using graphite dies to acquire partially filled ytterbium skutterudite materials (Nolasa et al., 2000). Under the usage of hot pressing the mixture of nanoscale and micronized $CoSb_3$ powders synthesized by solvothermal method using $CoCl_2$ and $SbCl_3$ as the precursors and $NaBH_4$ as the reductant in an ethanol solution and then melting, then n-type $CoSb_3$ nanocomposites were prepared by this method (Mi et al., 2007).

**Spark plasma sintering**

In the process of Spark Plasma Sintering (SPS), the mould is directly connected to electrical power to shorten cycle time and save energy, and SPS has higher heating conversion rate. This helps increase the speed of sintering of metal power and reduce the threshold sintering teperature and pressure compared to traditional sintering process. In addition to these, in contrast to conventional hot pressing where heat is provided by external heating, SPS 's heat is generated internally. Therefore, the sintering process is fast. The TE compound $In_4Se_{3-x}$ was fabricated by SPS through a solid state reaction at 550 °C under the uniaxial pressure of 70 MPa.

There are a lot of examples of SPS for TE nanocomposites. Through SPS and the subsequent thermal treatment, the polycrystalline copper aluminates $Cu_{1-x-y}Ag_xNi_yAlO_2$ and $Cu_{1-x-y}Ag_xZn_yAlO_2$ were synthesized. These nanocomposites could be used as high temperature thermoelectric materials by partial substitution of Ag, Ni and Zn for Cu site in $CuAlO_2$ (Yanagiya et al., 2010). Bi-Te based TE p-n modulus were fabricated through SPS solid bonding for measuring their TE performances (Kima et al., 2006). The polycrystalline samples such as $BaSi_2$, $SrSi_2$, and LaSi were prepared by SPS. Among these SPS generated

materials, $SrSi_2$ exhibited a higher power factor than BaSi2 and LaSi. Also, after heating the pressed pellets of pure mixture of Sb (99.9999%), Co (99.99%) and fullerene ($C_{60}$) 99.5%, and then heating the mixed nanocomposites to 943 K under an Ar atmosphere for about 150 h, fine TE ground powders were obtained through SPS at 848 K for 15 min (Shi et al., 2004). It is reported that $Ba_yCo_4Sb_{12}$ nanocomposites with dispersed fullerene or barium fulleride have been successfully fabricated by the SPS and solid state reaction (Shi et al., 2007). Also, $SiO_2/\beta$-$Zn_4Sb_3$ core-shell nanocomposite particles with the low thermal conductivity were synthesized by SPS method (Ruan & Xiao, 2007). Moreover, $CoSb_{3-x}Te_x$ skutterudite polycrystals were synthesized by SPS along with mechanical alloying (Liu et al., 2007). Furthermore, Zn-incorporated $Ba_8Ga_{16}Zn_xGe_{30-x}$ clathrates were fabricated with the methods of SPS and solid-state reaction (Deng et al., 2007). To enhance the bulk material s' densities, highly aligned $Ca_3Co_4O_9$ and similar formula ceramics can be treated by SPS to achieve this purpose (Zhou et al., 2003).

**Electrodeposition**

Electrodeposition is the process that employs electrical current to reduce cations of a specific material within the solution and deposits nanoparticles on the surface of cathodes to synthesize a thin layer of the material with desired properties. This process bestowed many merits like depositing on complicated surfaces and synthesizing functionally-gradient materials.

Fig. 3 shows how the electrodeposition worked. The set-up for electrodeposition includes the anode, the cathode and a specific solution. They are connected to a power supply such as battery. When the external power supply is switched on, the metal at the anode will be oxidized with a positive charge. These cations will meet anions in the solution, and thus they are reduced at the cathode to deposit in the specific metal. Taking an acid solution as an example, copper is oxidized at the anode becoming $Cu^{2+}$ by losing two electrons. Then

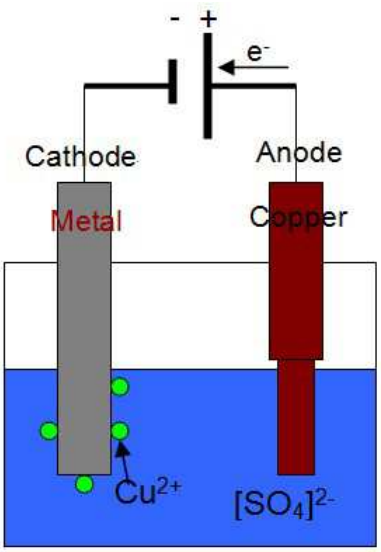


Fig. 3. Electroplating of a metal with copper in a copper sulfate bath.

the $Cu^{2+}$ will meet up the anion $SO_4^{2-}$ in the solution to form copper sulfate. At the cathode, the $Cu^{2+}$ is reduced to metallic copper by gaining two electrons. The result is the effective transfer of copper from the anode source to a specific metallic cathode.The reaction mechanism of electrodeposition has been extensively studied recently to gain expected and improving properties of various materials.

The application of electrodeposition has an extensive range.The most cheap and easy way to synthesize polyaniline is utilizing the electrodeposition method and using a stainless steel as the template. It is reported that electrodeposition of nanometer-sized alumina particles in a copper matrix was prepared and well studied. It is found that PbTe can be deposited on copper and nanoporous nickel through electroplating (Madhavaram et al., 2009). Also, a multitude of nanoparticles were inserted into metallic or ceramic coatings: submicron polymeric particles were electrodeposited into copper; SiC particles were incorporated into Ni matrix. Simultanesouly, the morphology and mechanical properties of electrodeposited $Al_2O_3$ nanoparticles that solidated copper matrix were studied. Additionally, nanostructured devices such as microgears and pulp systems were possible when using electrodeposition method. Here is the most popular thermoelectric material $Bi_2Te_3$ that has been studies for years. Extensive studies on $Bi_2Te_3$ doping have been carried out by many researchers for the optical, thermoelectric and electrical properties. And this material's growth technique was achieved by vacuum deposition technique, sol–gel, spray pyrolysis, screen printing etc. While the most economical method of fabricating bismuth telluride thin film is by cathode electrochemical deposition technique. Thin films of bismuth telluride can be grown by cathode electrochemical deposition technique on conducting glass and Mo sheet substrates. They can easily be used as a low band gap dopant in the materials for large-scale photovoltaic applications. The quality and composition of the deposited films can be easily controlled by controlling electrochemical parameters. The as-deposited bismuth telluride films are highly crystalline and compositionally and morphologically uniform throughout. This accomplishemt suggests that electrochemical deposition is a cost effective, efficient, non-hazardous process for the preparation of bismuth telluride films and large area depositions. The feasibility of preparation of bismuth telluride films was demonstrated in the aqueous electrochemical deposition process (Golia et al., 2003).

**Doping technique**

Doping is generally referred to the process of intentionally adding impurities to extremely pure semiconductors. Hence, the doping technique is used in the semiconductors to change the material' electrical properties or other characteristics. The doped-materials have a promising application for the thermoelectics. It is known that perovskite-type metal oxides are potential materials to enhance the efficiency of thermoelectric devices and cobaltite with p-type conductivity and n-type manganates are considered for the development of a ceramic thermoelectric converter. Sintered pellets and thin PLD films with the composition $La_{1-x}Ca_xMO_3$ (x= 0, 0.3, 0.4) (M=Co, Mn) were synthesized and characterized concerning their thermoelectric properties in a broad temperature range recently. It was found that similar to polycrystalline samples the electrical conductivity of $LaCoO_3$ increases significantly with 40% Ca-substitution due to the formation of $Co^{4+}$ ions while the thermopower decreases. The thermopower values of the $La_{0.8}Ca_{0.2}MnO_{3-d}$ films have a negative sign, but become large and positive at temperatures of 1000 K. Doping technique is suitable for the production of homogeneous metal or metal alloy powders. Silicon– germanium (Si–Ge) has been known as a high temperature thermoelectric element material, which has the function

of thermoelectric energy conversion by making use of a temperature difference between both ends of the element (Otakea et al., 2004).
Furthermore, a route, alternative to the conventional chemical doping, to modify a wide spectrum of physical properties of nanoscale sized films, by dynamically varying the concentration of the carriers by an applied electric field (Electric field effect doping-EFED), has been proposed recently. This theory of an electric-field-effect (EFE) induced increasing of the thermoelectric figure of merit of a thin film thermoelectric TE plate in a capacitive structure. EFED is applicable for thin films of narrow-gap semiconductors (e.g. PbTe, SnTe, PbSe, PbS, etc.) and semimetals (such as Bi) (Sandomirsky et al., 2003).

## 3. Major methods to enhance conversion efficiencies

A long pursued goal is to achieve larger ZT. Expectations appeared a decade ago, when it was theoretically proposed that superlattices and nanowires can have a much higher figure of merit than traditional bulk materials. Since then, important theoretical and experimental steps have been made, bringing us closer to the practical realization of the theoretically envisioned breakthrough. Here are three primary ways employed to improve the thermoelectric figure of merit based on (Eqn. 1): to enhance the Seebeck coefficient (thermopower) or power factor, to increase the electrical conductivity and to lower the thermal conductivity. The power factor can be enhanced by means of quantum confinement effects. The Seebeck coefficient can be increased via energy filtering and electron scattering. Typical good Seebeck coefficient's value should be larger than 200 μV/K. The low lattice thermal conductivity could be achieved from the increasing of phonon scattering by a mixed or complex structure, rattling scattering, grain-boundary scattering and huge surfaces and interfaces in nanocomposite materials. The electrical conductivity can be improved by doping or using metal-like conducting semiconductors, or in other words high-mobility carriers and very small gap will result in high electrical conductivity. Typical good electrical conductivity values should be larger than $10^3$ $\Omega^{-1}$ $cm^{-1}$. And the thermal conductivity can be lowered using doping technique of nanopartices and superlattice heterostructures.Typical good thermal conductivity value should be less than 2.0 W/m·K. Slack predicted that the low thermal conductivity can be achieved is between 0.25 W/m·K to 0.5 W/m·K. The following part will elaborate all the three methods, but not limit to any single method. For example, some thermoelectric nanocomposite mainly possesses low thermal conductivity, but at the same time, it may be provided with higher conductivity or higher themopower.

### 3.1 To increase electrical conductivity

The first method to increase ZT value is through the enhancement of electrical conductivity. Electrical conductivity is also called specific conductance, which is used to measure a specific material's capacity to conduct an electric current. The definition of electrical conductivity σ is the ratio of current density J to the electric field strength E with the expression J= σE. So the improvement of electrical conductivity is to enhance the ability to conduct electric current. This part will narrate from three aspects: doping nanocomposite materials, Co-based oxide ceramics and metal-like nanocomposite all leading to high electrical conductivity.
Improvement of electrical conductivity by doping was quite effective to increase figure of merit value. As the concentration of zinc dopant increased, the electrical conductivity of films deposited in pure Ar can be increased. For example, The electrical conductivity of zinc-

doped cubic boron nitride (cBN) thin films, prepared by sputter deposition in pure Ar, increased as the concentration of zinc dopant increased. It was found that the conductivity increment in such films was accompanied by a linear increase in the B/(B+N) ratio. It was also found that both $Al_2O_3$, $TiO_2$ or $ZrO_2$ doped ZnO and $TiO_2$ doped $Fe_2O_3$ showed a large power factor in the wide temperature range. $Fe_2O_3$'s ZT value was smaller compared with ZnO doped nanocomposites. Additionally, Ag and Zn doped $CuAlO_2$ was found to enhance the electrical conductivity (Tsuchida et al., 1996). α-$Al_2O_3$ with doped Mg nanocomposite was investigated for its electrical conductivity under the direct and alternating current with different concentrations of Mg in the temperature range 250-800 K. $Al_2O_3$ crystal is a high-temperature and good mechanical semiconductor rather than MgO doped with lithium which is brittle as a semiconductor of the p-typed. Although there are many impurities existed in the $Al_2O_3$ crystals, the electrical conductivity of $Al_2O_3$ with dopant Mg increases linearly with the concentration of Mg in both DC and AC fields (Tardı´o et al., 2001).

Oxide ceramics possess good TE properties mostly because of their thermal stability. It has already reported that (Ca, Bi, and Sr)-Co-O single crystal whiskers have the ZT values higher than 1.2 and they are suitable for practical applications. But the size of the materials limit their applications as a TE device. While the $Ca_3Co_4O_9$ (See Fig. 4) and $NaCo_2O_4$ are reported to bear great TE performances. Thus they are more favorable than traditional semiconducting materials. Moreover, the transport performance of $Ca_3Co_4O_9$ is increased significantly because of its layered structure as followes.

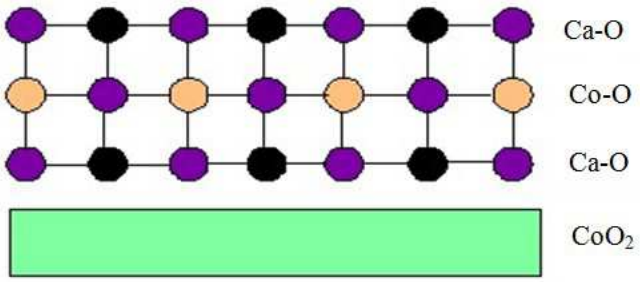


Fig. 4. Layered view of $Ca_3Co_4O_9$ after (Zhou et al., 2003).

The in-plane electrical conductivity is much larger than that of the out-of-plane electrical conductivity, showing that grain-aligned ceramics could have higher TE properties than randomly oriented ceramics with the same compositon. As a result, the fabrications of the highly grain-aligned densified TE ceramics are quite crucial for the application of polycrystalline layered structure. A ZT value of 0.8 is obtained for oxide $NaCo_2O_4$ at 1000 K. Furthermore, cation substitution can improve the ZT value. For example, an improved ZT value of $NaCo_2O_4$ can be proved from Cu-substitution for Co site; an enhanced ZT value of $Ca_3Co_4O_9$ can be proved from Bi and rare earth elements for Ca site due to increased Seebeck coefficient. $Ca_3Co_4O_9$ showed higher electrical conductivity with grain-aligned structure and had no apparent effect on the Seebeck coefficient which could reach 180 μV/K at 700 °C (Zhou et al., 2003). Polycrystalline bulks with aligned grains of the misfit-layered cobalt oxides like $[(Bi_{1-x}Pb_x)_2Ba_2O_4]_{0.5}CoO_2$ was reported to show higher electrical conductivity. The electrical conductivity of this material is four times higher than that of traditional sintered bulks. And its Seebeck coefficient is 120 μV/K at ambient temperature and its thermal conductivity is 1 W/m·K (Motohashi et al., 2008).

Some nanocomposites like green covellite copper sulfide possess metal-like electrical conductivity and chemical sensing capabilities. For example, CuS films maintain transmittance in the infrared, low reflectance in the visible and relatively high reflectance in the near-infrared region, which are ideal characteristics for solar energy adsorption. Moreover, CuS transforms into a superconductor at 1600K and has recently been used as cathode material in lithium rechargeable batteries (Zhang & Wong, 2009).

### 3.2 To enhance thermopower or Seebeck coefficient

The second way of improving the TE properties is through the increase of thermopower, or the power factor This part will first elucidate the nanocomposites with higher thermopower in carbon nanotubes, $X_3Au_3Sb_4$, $Bi_2Sr_2Co_2O_y$ whiskers, $LaCoO_3$ system, lead chalcogenide and $Ag_nPb_{18+x}SbTe_{20}$ bulk material. Then introducing some promising nanocomposites with higher power factor which is equal to the square of thermopower divided by electrical resistivity, will be stated afterwards like LaPdSb, GdPdSb, $YbAl_3$ and $In_4Se_{3-x}$.

The nanotube can be viewed as a graphene sheet rolled into a seamless cylinder with a length over diameter ratio greater than 1000. Generally, carbon nanotubes can be divided into two types. One is called single walled nanotubes (SWNTs). The other is called multiwalled nanotubes (MWNTs). Nanotubes normally can be synthesized from three methods: chemical vapor deposition, pulsed laser vaporization and electric arc discharge.

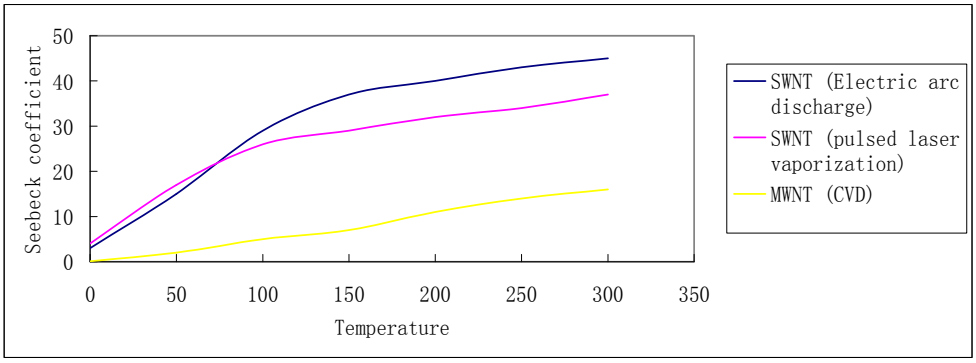


Fig. 5. Relations between temperature (T) and Seebeck coefficient (μV/K) for different carbon nanotubes. Data source from (Apparao et al., 2006)

Fig. 5 shows the general comparison of Seebeck coefficient carton nanotubes with three different fabrication methods: SWNT synthesized by the electric arc discharge and pulsed laser vaporization and MWNT produced by CVD. Clearly, the SWNT (45 μV/K) has a much higher Seebeck coefficient than MWNT (17 μV/K). The positive of the Seebeck coefficient proves both SWNTs and MWNTs are p-type materials (Apparao et al., 2006).

Taking carbon nanotube as an example, ZT in nanocomposite materials could be larger than 2.5 due to electron confinement resulting from a high density of states near the Fermi level $E_F$ thus leading to high power factor, while κ decreases due to the suppression of phonon boundary scattering. On the contrary, ZT could near 0.8 as a maximum for bulk thermoelectric materials. Such nanocomposite materials are easily assembled into different shapes and can be scaled up for commercial applications. Wireless sensors in the 1–10 m

range require very low-power consumption, which does not exceed few hundreds of microwatts. For longer distances the wireless sensor networks are designed to work in a multihop mode, while large distances are covered with multiple miniaturized sensor nodes characterized by low-power consumption and low cost. The modern architecture based on a large number of wireless nodes is possible only if each node is self-powered when working inside the network. In the advanced wireless sensor and portable device architectures carbon nanotubes (CNTs) could play a double role as sensors and harvesters, generating DC voltages necessary for the operation of small wireless sensors in the multihop mode. CNTs are very effective sensors, with many applications in environmental monitoring, biomedicine, or automotive industry. Smart biological devices could be implemented using this harvesting principle, but the generated power is of few picowatts, which is not enough for wireless applications. However, thermoelectric power devices based on CNTs could be the key elements of self-powering devices of wireless sensors as well as of any low-consumption portable device (Dragoman & Dragoman. 2007).

The relatively earlier nanocomposites with notably performance of thermoelectricity are ternary antimonides and stannides with half-Heusler structure. The recently reported TE material like $X_3Au_3Sb_4$ has a more complex crystal structure than those earlier nanocomposites. The specific formula is $Ln_3Au_3Sb_4$ for Ln= Nd, Sm, Gd and Ho with lower thermal conductivity in the range of 1.4-1.8 W/m·K at ambient temperature because of heavy masses of the component atoms and complex structure. The highesst Seebeck coefficient ever reported is 100-200 μV/K, showing that the dominant carriers are holes enhancing with increasing temperature. The resisitivities and Seebeck coefficient can be greatly affected by the ratio of Au:Sb. Moreover, there is no influence of the electrical resisitivity resulted from the improved Seebeck coefficient for nanocomposites with mixtures of lanthanides on the large atom position (Young et al., 1999).

There are other alloys with higher Seebeck coefficient. $Bi_2Sr_2Co_2O_y$ whiskers possess high performance of thermoelectricity. The Seebeck coefficient of this material can reach 300 μV/K at 973 K. The thermal conductivity is measured about 2 W/m·K because of the phonon-phonon interactions. The ZT value is more than 1.1 which stands for about one tenth energy conversion at 973 K (Funahashi & Shikano. 2002). Due to the high Seebeck coefficient of 600 μV/K at room temperature, the $LaCoO_3$ system is a promising thermoelectric nanocomposite despite of its high electrical resistivity which lower the whole conversion efficiency. But as the temperature goes up to 750K, the electrical resistivity will drop down which again enhances the conversion efficiency. Furthermore, different substitution of a specific site will cause promotion of ZT. Substitution in the $LaCoO_3$ system like $La_{0.8}Ca_{0.2}MnO_3$ and $La_{0.6}Ca_4CoO_3$, represents a semiconducting-like behavior, which can improve the conversion efficiency. Another example of the $LaCoO_3$ system is La-Sr-Co-O compound. The polycrystalline $La_{0.8}Sr_{0.2}Co_{1-x}Mn_xO_3$ was synthesized by citrate complex method. And the TE propertied can be tuned by adjusting Co site substitution by Mn atoms. The experimental results showed that both the Seebeck coefficient and electrical resistivity will increase with the increasing Mn content. The Seebeck coefficient is positive in the temperature range between 90 K and 290 K, and the electrical resistivity indicated a metallic semiconducting temperature behavior. Also a power factor of 18 $\mu W/K^2$ is achieved with x=0.08 (Moreno et al., 2008).

Prevalent examples of wide applications with higher Seebeck coefficient existed in the lead chalcogenide which has been studied for years due to their special physical characteristic

and easy fabrication within ambient pressure. The synthesized lead chalcogenide possesses the advantages of a short growth time, high yield and cost effective. Lead chalcogenide exhibits extensive quantum-size effects in nanocrystalline form because of its smaller bandgap and larger Bohr excitation radius. Up to now, a variety of forms such as nanorods, nanowires, nanotubes, nanocubes and nanoflowers have been successfully fabricated under controllable conditions. Parkin and co-worders used a method to fabricate lead chalcogenides in liquid ammonia at room-temperature. Later, it is reported that the synthesized size of PbS, PbSe and PbTe nanotubes is 200-300 nm, 50-120 nm and 30-60 nm respectively fabricated in hydrazine hydrate saturated alkalline solution under the general experimental conditions. And the Seebeck coefficient value of the three composite nanotubes are 154.4 μV/K, 199.8 μV/K and 451.1 μV/K respectively (Wan et al., 2010). Through the TEM images and electron diffraction patterns, lead chalcogenide is single crystal nanotube and PbTe nanotube has the smallest size with a round-angle. It is concluded that PbTe nanotube bears the higher thernoelectric property. Additionally, PbTe nanorod's Seebeck coefficient could be up to 679.8 μV/K at room temperature. The thermopower of PbTe coating on copper and nickel was found much higher than either pure copper or copper-nickel alloy. PbTe on nanoporous nickel shows higher Seebeck coefficient than on the pure copper. It is about 50% higher on nanoporous support. The possible explanation is that the electron confinement effect of nanoporous materials causes higher thermoelectric potential (Madhavaram et al., 2009). Because of the high potential usage of PbTe as TE material, various PbTe nanocomposite materials have been successfully synthesized by solvothermal/hydrothermal fabrication, sonoelectrochemical synthesis, chemical bath method and high temperature solution-phase synthesis (Wang et al., 2009). Addtionally, n-type TE material $Ag_nPb_mSbTe_{m+2n}$ system (ZT>2) and p-type TE material $Ag_9TlTe_5$ system are reported with easier fabrication methods like mechanical alloying and SPS as powder metallurgy processes. Specifically, $Ag_nPb_{18+x}SbTe_{20}$ bulk materials with micrometer sized grains were synthesized by the powder metallurgy process. A maximum power factor of 1.766 mW/ $mK^2$ was obtained at 673 K for the $Ag_{0.8}Pb_{22}SbTe_{20}$ corresponding to a high ZT value of 1.37. The experimental results also indicated that the TE properties are highly related to the composition especially the content of Pb atom (Wang et al., 2006).

There are also some TE materials with high power factor attributing to high Seebeck coefficient. LaPdSb showed a large power factor of 50 μW/cm $K^2$ at 327 K. And GdPdSb also indicated relatively large power factor with high Seebeck coefficient and low electrical resistivity resulted from high Hall mobility (Sekimoto et al., 2006). Moreover, both n-type $YbAl_3$ and p-type $CePd_3$ showed high Seebeck coefficient values. $YbAl_3$ exihibits a high power factor as high as 5.4 W/m·K at 300 K which is nearly 4 to 5 times larger than optimized $Bi_2Te_3$ based TE materials. However, the high thermal conductivity in $YbAl_3$ limits its total TE performance. Therefore, further investigation should be done on how to reduce the thermal conductivity to achieve high ZT value. The Se-deficiency polycrystalline compound $In_4Se_{3-x}$ has the property of increasing the poewr factor and decreasing the semiconducting band gap. The experimental results showed that small Se deficiency will lower the thermal conductivity resulting from the random disorder phonon scattering. On the other hand, the thermal conductivity will increase with the increasing Se deficiency. Moreover, the power factor will increase with increaing Se deficiency between 300 K and 750 K. The power factor of $In_4Se_{3-x}$ measured may be lower than that of double-doped skutterudites because of relativiely high electrical resistivity of $In_4Se_{3-x}$. In the same

temperature range, the ZT value of $In_4Se_{3-x}$ due to high Seebeck coefficient and low thermal conductivity is comparable to the n-type PbTe and $CoSb_3$ (Rhyee et al., 2009).

### 3.3 To lower thermal conductivity

The third way to improve the TE performance or the ZT value is through reducing the total thermal conductivity. Lowering the thermal conductivity is the most focused way to obtain the high performance of TE materials. This part will elucidate the acquired accomplishments from Zintl compounds, skutterudite family, $Zn_4Sb_3$, clathrate, telluride alloys and InSb. Among these TE materials, rattlers atoms could be inserted into the voids to further lower thermal conductivity in cage-like materials skutterudites and clathrates.

**Zintl compound**

Nanocomposite Zintl have recently arised as a new class of thermoelectric materials for it has complex crystal structures. Zintl phase is the product of a reaction between alkali metals, alkaline earthes and post transition metals, metalloids. Zintal phases were named for the German chemist Eduard Zintl who investigated them in the last 30s. Zintl phases can provide the great properties for TE materials: they will form small band gap semiconductors and possess complex structures. As of the their valence compound traits, zintl phases have the semiconducting nature (Zhang et al., 2008). Zintl phases have the structural properties used for electron-crystal and phonon-glass characteristics which result in higher ZT value. They combine different regions of covalent bonding for electron-crystal properties with ionically bonded cations that can be subtstituted for tuning electronic traits and bringing disorder which generate low lattice thermal conductivity due to phonon-glass properties. Improved thermoelectric performance will be expected due to enhanced structural modifications that allow the increase in the fundamental transport parameters such as carrier mobility, carrier concentration and effective mass. The low thermal conductivity value is gained in Zintl thermoelectric materials on accounts of low velocity of optical phonon modes and point defect scattering.

A Zintl compound consists of both covalently and ionically bonded atoms. Then, the general ionic cations will give their electrons to the covalently anionic species. And Zintl phases comprise of electropositive cations (Group 1 or Group 2) which will give their electrons to electronegative anions; which in turn will form bonds to suffice for valence. Assuming the presence of both ionic and covalent contributions to the bonding type is the reason of the structural requirements of Zintl phase. The purely ionic materials possess less mibility of the charge-carrier species than covalent bonding. The conplex nanostructures with multiple strucural units in the same structure are resulting from the combination of the bonding types. It is reported that due to the reason that zintl phases possess highly electropositive alkali and alkaline-earth elements, they are air and moisture sensitive. To overcome this drawback, the air-stable antimonide analogs of zintl phases are synthesized: $X_{14}MPn_{11}$, $Yb_{14}MnSb_{11}$, $YbZn_2Sb_2$, $YbZn_{2-x}Mn_xSb_2$, $BaZn_2Sb_2$, $EuZn_2Sb_2$, $YbCd_2Sb_2$, $YbCd_{2-x}Zn_xSb_2$, $Ca_xYb_{1-x}Zn_2Sb_2$, $X_{11}Sb_{10}$ (X=Ca, Yb, and Eu), $Ca_{11}AlSb_9$, $CaZn_2Sb_2$, $BaGa_2Sb_2$, $Mo_3Sb_7$, filled skutterudite and $Zn_4Sb_3$ etc.

$X_{14}MPn_{11}$ expression conforms to zintl formulism. In this expression X means a heavy or alkaline earth metal; M is a transition or main group metal and Pn is group 15 elements such as P, As, Sb or Bi. Doping on different sites will improve the TE properties through electrical and thermal conductivities. For example, incorporating on M site will adjust the electronic parameter and incorporating on X sites will tune the disorder scattering of phonons and

carrier concentration. $Yb_{14}MnSb_{11}$ is the appropriate candidate for polar intermetallic compared with the transition metal zintl compound $Ca_{14}AlSb_{11}$. And thus $Yb_{14}MnSb_{11}$ made ideal candidates for thermoelectric materials because it possesses the properties of electron-crystal and phonon-glass. The $Yb_{14}MnSb_{11}$ has extremely low lattice thermal conductivity and high Seebeck coefficient. The experimental results showed that Seebeck coefficient is positive and will increase with increasing temperature from 300 K to 1300 K; the resistivity increases with increasing temperature and gets a maximum value at 1200 K; a notable low thermal conductivity is between 0.7-0.9 W/m·K for temperatures from 300 K to 1275 K; substitution of $La^{3+}$ for $Yb^{2+}$ on X site and substitution of $Mn^{2+}$ with $Al^{3+}$ will result to a high ZT value at lower temperature (Kauzlarich et al., 2007). $Yb_{14}MnSb_{11}$ is comprised of distinct anionic units like $Yb_{11}Sb_{10}$ rather than structrue like $CaZn_2Sb_2$ shown later. This type of zintl material consists of polyatomic $[Sb_3]^{7-}$ anions, $[MnSb_4]^{9-}$ tetrahedra in addition to isolated $Sb^{3-}$ cations and $Yb^{2+}$ cations. This compound is isostructural to zintl phase $Ca_{14}AlSb_{11}$. A high temperature melting point is anticipated due to anionic units ionically bonded together via cations. Thus, $Yb_{14}MnSb_{11}$ has a much complex structure than $CaZn_2Sb_2$. The Fig. 6 is the general $X_{14}MPn_{11}$ layered view. In this figure X means 2+ cation with, M means metal and Pn means P, As, Sb or Bi. The green, blue and red spheres denote X, Pn and M atoms respectively and yellow spheres denote X atoms which are not in the same plane.

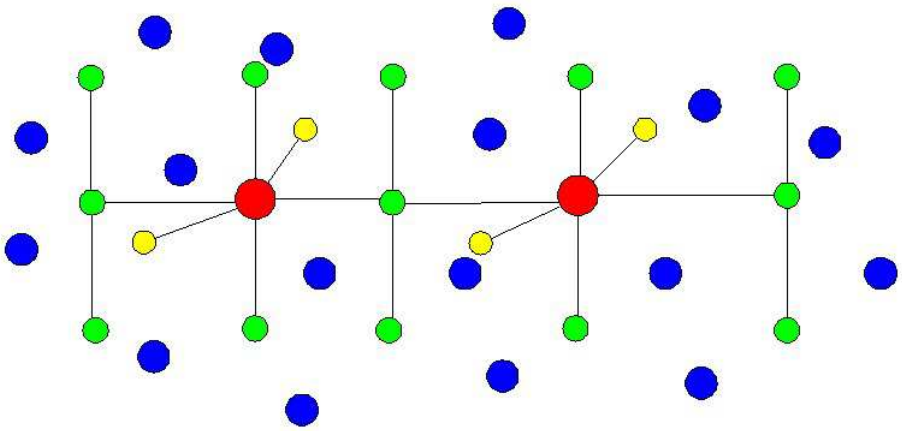

Fig. 6. Layered view of $X_{14}MPn_{11}$ structure after (Kauzlarich et al., 2007)

It is reported that $Yb_{14}MnSb_{11}$ has the ZT value of 1.0 at 900 °C along with large Seebeck coefficient and high electrical conductivity. The $Yb_{14}MnSb_{11}$ possesses a ZT value more than 1.0 up to 1275 K. In comparison, the ZT value of $Yb_{14}MnSb_{11}$ is proven that two times of the SiGe nanocomposite which is used prevalently before. The Fig. 7 showed ZT values of several p-type TE materials ($Zn_4Sb_3$, TAGS means $(GeTe)_{0.85}(AgSbTe_2)_{0.15}$, $CeFe_4Sb_{12}$, $Yb_{14}MnSb_{11}$, $CuMo_6Se_8$ and SiGe) at different temperature range. It indicated that $Yb_{14}MnSb_{11}$ possesses highest ZT value at higher temperatures. While the some other materials ($Zn_4Sb_3$, TAGS and $CeFe_4Sb_{12}$) indicated high ZT values at low temperatures.

What's more, it is reported that Zintl compound $YbZn_2Sb_2$ with isoelectronic substitution of Zn by Mn in anionic $(Zn_2Sb_2)^{2-}$ system possesses lowered thermal conductivity. The attained value of figure of merit value is between 0.61 and 0.65 at 726 K compared with the

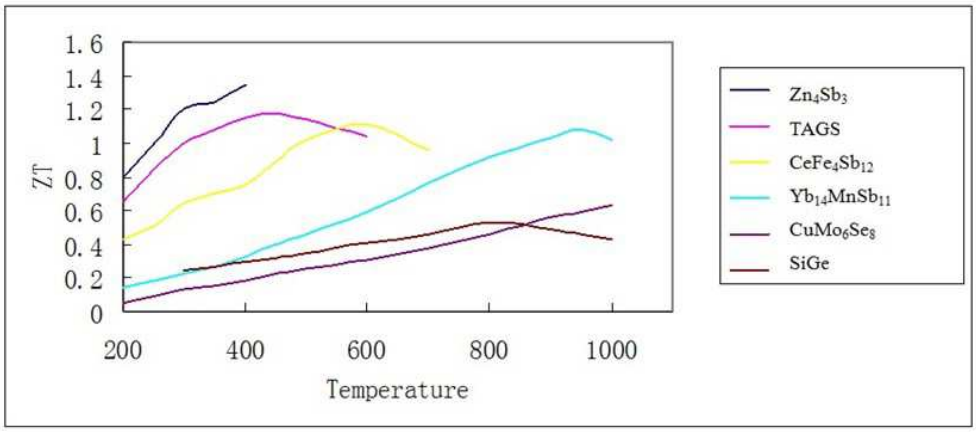


Fig. 7. Figure of merit as a function of temperature (°C) for a number of p-type materials. Data source from (Kauzlarich et al., 2007)

unsubstituted $YbZn_2Sb_2$'s ZT value of 0.48 (Zhu et al., 2008). Yb site substitution can well tune the TE properties in $YbZn_2Sb_2$. Here, through a solid-state reaction followed by certain cooling, annealing, grounding and hot-pressing densification process, the p-type $YbZn_{2-x}Mn_xSb_2$ were synthesized. The reason of the lowered thermal conductivity and significantly increased Seebeck coefficient is because the Mn substitution. As a result, ZT value of 0.65 is obtained at 726 K for x=0.05-0.15. In $YbZn_{2-x}Mn_xSb_2$ structure, the cell refinement revealed the lattice constant a increased linearly with increasing Mn content, while the lattice constant c showed a relatively small change. That means the unit cell expands in the x-y plane but little changes in the z-axis with increasing Mn contents. It can be illustrated from the Fig. 8 (Yu et al., 2008).

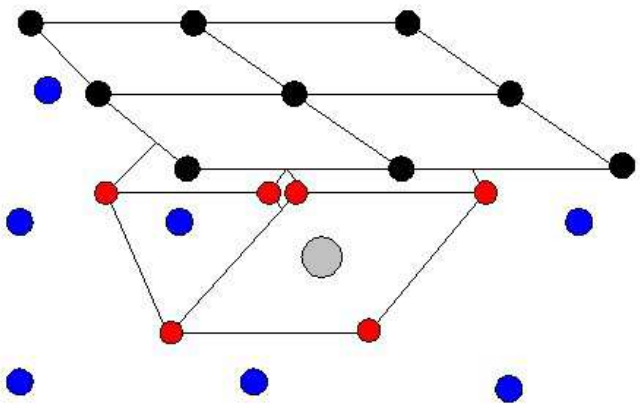

Fig. 8. $YbZn_{2-x}Mn_xSb_2$ structure view after (Yu et al., 2008). Black spheres denote Yb atoms, red spheres denote Sb atoms, blue spheres denote Zn atoms and gray sphere denotes Mn atom.

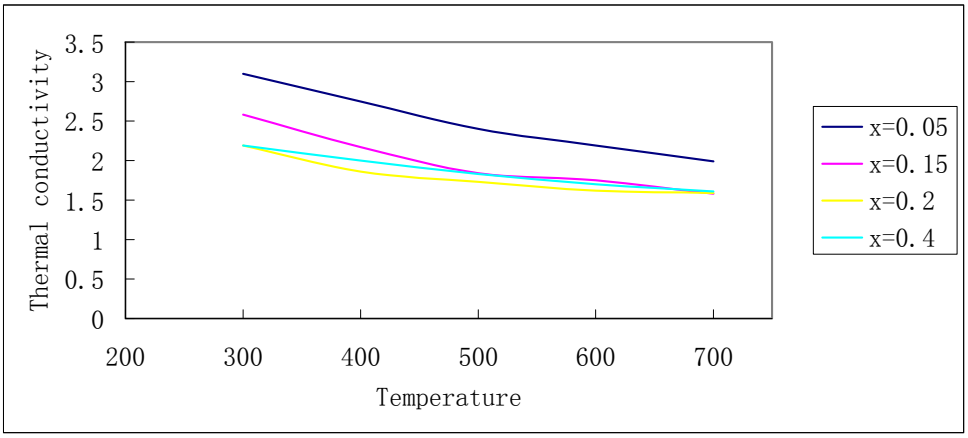


Fig. 9. Relations between temperature and thermal conductivity for $YbZn_{2-x}Mn_xSb_2$. Data source from (Yu et al., 2008)

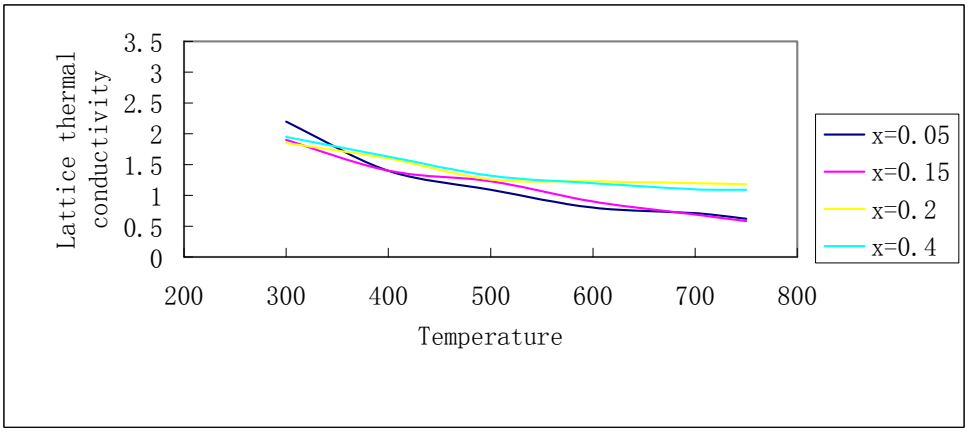


Fig. 10. Relations between temperature and lattice thermal conductivity for $YbZn_{2-x}Mn_xSb_2$. Data source from (Yu et al., 2008)

The thermal conductivity and lattice thermal conductivity at different temperatures for $YbZn_{2-x}Mn_xSb_2$ nanocomposites are shown above (See Figs. 9 and 10). It can be seen that thermal conductivity will decrease with increasing Mn substitution at ambient temperature and indicate a trend that they will converge at higher temperatures.

Meanwhile, polycrystalline sample of the title compound ($BaZn_2Sb_2$,p-type) was prepared and its thermoelectric properties from 2 to 675 K were studied. This Zintl compound shows rather low thermal conductivity, 1.6 W/m·K. The value of its thermoelectric figure of merit ZT reaches 0.31 at 675 K. A few new simple ternary Zintl phase compounds contain alkali-earth and rare-earth elements such as $Ba_4In_8Sb_{16}$, $Yb_5In_2Sb_6$, $Eu_5In_2Sb_6$, and $BaCu_2Te_2$ were synthesized and considered as potential TE materials. For the Zintl compound with low thermal conductivity, we care more about their electronic structures which could provide

some useful information such as the energy gap, effective mass, electronic components, and so on (Wang et al., 2007). Additionally, a higher figure of merit ZT at 700 K is achieved as high as more than 1 from Cd-rich nanocomposite $YbCd_2Sb_2$ and Zn substitute of Cd nanocomposite $YbCd_{2-x}Zn_xSb_2$ which have low thermal conductivity and high ZT value (Wang et al., 2009). The polycrystalline TE material $EuZn_2Sb_2$ is reported with its high Seebeck coefficient as high as 181 μV/K, low thermal conductivity as low as 0.4 W/ m K and high electrical conductivity ranging from 524-1137 S/cm. The acquired TE figure of merit is 0.92 (Zhang et al., 2008). $Ca_xYb_{1-x}Zn_2Sb_2$ expressed good thermoelectric properties as a zintl phase. The structure of $CaZn_2Sb_2$ indicates the bonding within the Zn-Sb layers between planes of $Ca^{2+}$. The covalent bonding in the $[Zn_2Sb_2]^{2-}$ layers give the electron-crystal traits like high mobility, on the other hand, the substitution like Yb can be made at the Ca position for tuning of the electron concentration and generating disorder for phonon-glass properties.

These materials comprise of electron precise Zn-Sb anionic sheets. Because both Zn and Sb have the similar electronegativity, the bonding within should have mostly covalent character. The $[Zn_2Sb_2]^{2-}$ system possesses good hole mobility because of its low polarity. The bonding of the cation is ionic and the $CaZn_2Sb_2$ is a semiconductor with a band gap of one quarter eV. Doped $YbZn_2Sb_2$ is an extremely p-type semiconductor with metal-like transport properties when less electropositive Yb cation makes it a little electron deficient. As a result, $Ca_xYb_{1-x}Zn_2Sb_2$ forms a doped polar intermetallic. The electronic band structure of the conducting $Zn_2Sb_2$ will not change notably when different components in $Ca_xYb_{1-x}Zn_2Sb_2$ except for carrier concentration. Thus, a gradually tuning of the hole concentration resulting in improvement of ZT value will emerge by alloying isoelectronic species. More importantly, the lattice thermal conduvtivity will apparently be reduced due to disorder scattering by alloying Ca atom and Yb atom on the cation position. It is also reported that Ru doped $Mo_3Sb_7$ indicated higher ZT value than pure $Mo_3Sb_7$ over 300 to 700 K. The fabricated $Mo_{3-x}Ru_xSb_7$ exhibited a complex crystalline structure related to improved thermoelectric performance, while the weak TE performance of undoped material is because its metallic nature (Candolfi et al., 2009).

A phonon-glass property can be acquired from binary zintl nanocomposite of complex structure. The Fig. 11 indicates $X_{11}Sb_{10}$ as a good example of such complex structure. This kind of structure contains 22 $X^{2+}$ cations with five $[Sb_2]^{4-}$ dumbbells and 10 $Sb^{3-}$ anions in each unit cell. It is proven that this complicated structure has notably low lattice thermal conductivity for a high melting point around 1200 K. This structure is like a semiconductor catering for electron-crystal needs. $Yb_{11}Sb_{10}$ is similar to a heavily doped semiconductor and the $Ca_{11}Sb_{10}$ is like a lightly doped semiconductor. So $X_{11}Sb_{10}$ nanocomposites indicated properties of bipolar conduction resulting in low thermopower and therefore low ZT value.

The zintl anions provide the electron-crystal electronic structure through the covalently bonded network of the complicated anions or metalloids. The following three figures indicated the covalently bonding regions separate from the ionic regions of antimony containing zintl phases. The covalent bonded regions supply electron-crystal traits like high high mobility, while the ionic region can be doped for tuning of the electrion concentration and creating disorder to give phonon-glass properties.

Complex anions ($Ca_{11}AlSb_9$), tunnel structure ($BaGa_2Sb_2$) and a layered net ($CaZn_2Sb_2$) are all semiconductors.. $CaZn_2Sb_2$ has already been explained before. $Ca_{11}AlSb_9$ comprised of 11 $Ca^{2+}$ cations which give their electrons to $[CaSb_4]^{9-}$ tetrahedron, 3 isolated anions $Sb^{3-}$ and

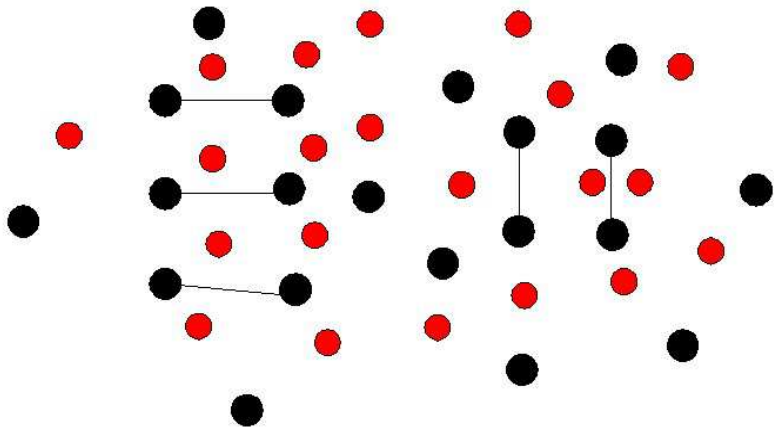

Fig. 11. Layered view of three distinct types of Sb atoms in $X_{11}Sb_{10}$ structure after (Kauzlarich et al., 2007). X is denoted by red sphere and Sb is denoted by black sphere.

$[Sb_2]^{4-}$ dumbbell. The Sb anions are six coordinated by alkaline earth cation. This nanocomposite complex structure possesses low lattice thermal conductivity. $BaGa_2Sb_2$ consists of $Ba^{2+}$ and $[Ga_2Sb_2]^{2-}$ network which is comprised of $[Ga_2Sb_{6/3}]^{2-}$ units considered as a ethane-like Ga-Ga. These kinds of $[Ga_2Sb_{6/3}]^{2-}$ units are connected in a way that leaves holes in the structures as shown above. Such as electron compound will form bonding and antibonding bands that will cause necessary semiconducting band-gap. Because the band gap emerges on accounts of the separation of bonding and antibonding states in the anions, the existence of nonbonding or partially bonding states can fill the gap region with states and make the compound metallic. On the other hand, more electronegative elements such as fulfur will reduce mobility. Thus, zintl anions coming from heavier, softer atoms will of course gain lower lattice thermal conductivity. The cations in Zintl phases provide regions that can be doped precisely to control electron concentration and interrupt phonon transport through alloying scattering. In this way, optimized characteristics of zintl phases can be achieved. (Kauzlarich et al., 2007)

$Mo_3Sb_7$ has been indicated a promising TE material because of low thermal conductivity and high Seebeck coefficient. $Mo_3Sb_7$ is a complex 3-D structure (See Fig. 12) of atoms consisted of antimony dimers, square antiprisms and empty $Sb_8$ cubes. The $Sb_8$ cubes give more room for incorporating dopants. Moreover, substitution of Te for Sb site will improve the TE property. For example, $Mo_3Sb_{7-x}Te_x$ showed a decreased thermal conductivity and inceased Seebeck coefficient leading to a ZT value of 0.8 at 1050 K. The Fig. 12 is the layered view of $Mo_3Sb_7$ structure.

**Skutterudite family**

Skutterudite is the cobalt arsenide mineral that has variable amounts of nickel and iron with the general formula like (Co, Ni, Fe)$As_3$. The thermoelectrical performances highly rely on the compositions of skutterudites. The abundant compositional types permit various physical properties for its potential applications. The general structure of skutterudite is a cubic form with space group comprising of eight corner-shared octahedra (Co,Rh or Ir)(P, As or Sb)$_6$.

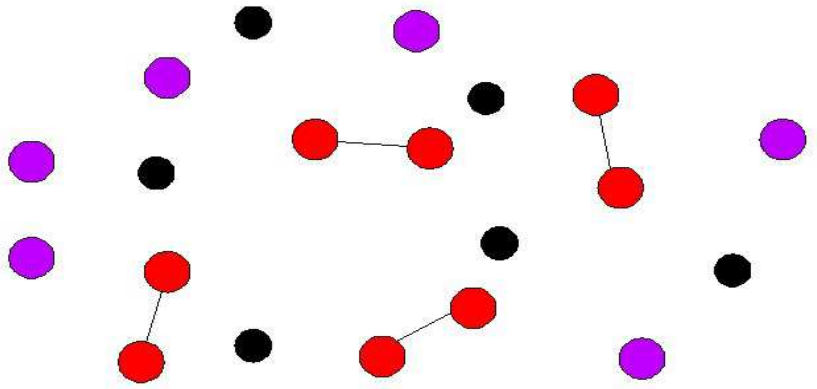

Fig. 12. A layered view of $Mo_3Sb_7$ after (Kauzlarich et al., 2007). Red spheres denote Sb-Sb bonds, purple spheres denote isolated Sb atoms and black spheres denote Mo atoms.

General skutterudites compounds showed high Seebeck coefficient and high electrical conductivity and high thermal conductivity. So how to lower the thermal conductivity had become the key point.The nanocomposite morphologies are effective in reducing thermal conductivity more than electrical conductivity, and Such nanocomposite materials are easily assembled into a variety of desired shapes and can be scaled up for commercial applications. The reason why skutterudite family of compounds could be regarded as thermoelectric nanocomposites is because the low thermal conductivity can be obtained when filling the voids with small diameter, large-mass interstitials. The filled skutterudites have reduced thermal conductivity than pure skutterudites because of rattling disorder of the void-filling ions that substantially affect the phonon scattering through the lattice. As of the more loosely bound rattlers producing local vibrational modes of lower frequency, and thus they are more effective in scattering the lower-frequency, heat-carrying phonons. The heavier and smaller the ion is in the voids, the larger the disorder that is produced and, therefore, the larger the reduction in the lattice thermal conductivity. The skutterudite antimonides are provided with large voids and therefore of ideal candidate for TE material. This concept, first introduced by Slack, is corroborated by the large atomic displacement parameters that have been observed in alkaline-earth and lanthanide-filled skutterudites.

At present, the reported studies showed that the filled skutterudites have the following fillers: rare earth elements, alkaline-earth elements (Ca, Sr, and Ba), foreign atoms (e.g. La, Ce, Nd, Sm, Eu etc) and others (Y, Tl, Sn and Ge). The continuing effort in improving the thermoelectric properties of skutterudite compounds has resulted in attempts to fill the voids in the crystal structure with ever-differing atoms.Synthesis approaches are at present underway in order to form ever more varied compounds in this diverse materials system.This section will elucidate $CoSb_3$ and the filled skutterudite materials especially the $CoSb_3$ based skutterudite materials .

$CoSb_3$ is one of the skutterudite family materials due to their similar formula. $CoSb_3$ is narrow-band gap semiconductor with a parabolic bottom of the conduction band. Due to its specific band structure, n-type $CoSb_3$ should have a high Seebeck coefficient while p-type

$CoSb_3$ should have high carrier mobility. However, the thermal conductivity of $CoSb_3$ is almost ten times higher than other state-of-the-art TE materials. Hence, the prepared $CoSb_3$ by hot pressing and SPS showed reduced thermal conductivity compared with that of the specimen fabricated by the traditional way like melting annealing/hot-pressing method which have some interial drawbacks.The slvothermal route without high temperature synthesized nanosized materials ranging from 150 nm to 250 nm and this method is economical and high efficient. An experimental ZT value of 0.61 is obtained for undoped $CoSb_3$ fabricated by SPS (Mi et al., 2007). N-type $CoSb_3$ fabricated by solvothermal method and melting is reported. Nanostructured and microstructured $CoSb_3$ powders indicated reduced thermal conductvity more than electrical conductivity. A ZT value of 0.71 is achieved for nanocomposite material with about 40% nanopowder inclusions (Mi et al., 2007).

The disorder within the unit cell can help to reduce thermal conductivity in structures containing void spaces. The skutterudite family material $CoSb_3$, containing corner-sharing $CoSb_6$ octahedra (See Fig. 13), which can be considered as a distorted variant of the $ReO_3$ structure. From the Fig. 13, it is seen that void spaces which can be filled with rattling atoms energes due to tilted octahedra.

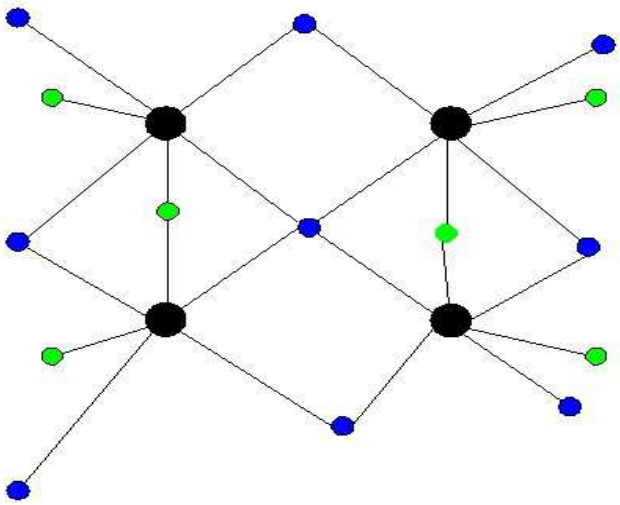

Fig. 13. The $CoSb_3$ structure as a typical skutterudite family material after (Snyder & Toberer, 2008). Black sphere denotes Co atom, blue sphere denotes Sb atom which stays in the same plane as Co atom and green sphere denotes Sb atom which is perpendicular to the plane.

In nanocomposites such as $CoSb_3$ and $IrSb_3$, which contain a high degree of covalent bonding, great electron-crystal properties can be expected because of high carrier mobilities. But the defect of this kind of strong bonding results in high lattice thermal conductivity. As a result, doping $CoSb_3$ by alloying either transition metal or the antimony site could lower the lattice thermal conductivity for this kind of skutterudite. The Fig. 14 can better show high value of thermal conductivity $CoSb_3$ can be reduced when alloying the $Co(Ru_{0.5}Pd_{0.5}Sb_3)$ or $Sb(FeSb_2Te)$ sites or filling the void spaces with $CeFe_3CoSb_{12}$ ranging from 100 °C to 500 °C.

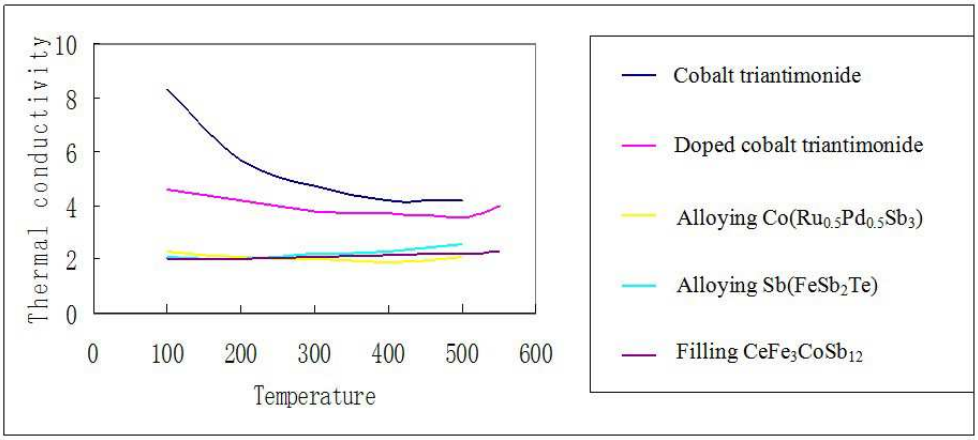


Fig. 14. Reduced thermal conductivity (W·K$^{-1}$·m$^{-1}$) with different doping and filling materials at different temperatures (°C). Data source from (Snyder & Toberer, 2008).

The following contents will elaborate the filled $CoSb_3$-based skutterudite materials including $YCoFe_3P_{12}$, $LaRh_4Sb_{12}$, $CoSb_{2.875}Te_{0.125}$, $CoSb_{2.8}Te_{0.2}$, $CoSb_{2.85}Te_{0.15}$, $M_yFe_{4-x}Co_xSb_{12}$, $Ba_{0.3}Co_{3.95}Ni_{0.05}Sb_{12}$, $Ba_xYb_yCo_4Sb_{12}$, $Sr_yCo_4Sb_{12}$, $Tl_xCo_{4-y}Fe_ySb_{12}$, $Tl_xCo_4Sb_{12-y}Sn_y$, $Yb_{0.19}Co_4Sb_{12}$, $Yb_yCo_4Sb_{12}$/ $Yb_2O_3$, $Yb_{0.2}Co_4Sb_{12+y}$, $Yb_{0.3}Co_4Sb_{12.3}$ and Fullerene-filled $CoSb_3$.

The general filled skutterudites materials reported include $YCoFe_3P_{12}$ and $LaRh_4Sb_{12}$. For example, the Y-filled compounds have larger rattling amplitudes than the La-filled, but are less stable; only the completely filled $YCoFe_3P_{12}$ is estimated to be stable at 0 K. Many other Y-filled compounds are close to being stable, however, and could possibly be stabilized by temperature and entropy effects. It is expected that P-based skutterudites like (La, Y)$CoFe_3P_{12}$ and (La, Y)$_{0.67}Co_2Fe_2P_{12}$ are potential TE materials in the future (Mangersnes et al., 2008). Additionally, filled $RhSb_3$ is also a promising TE material like $LaRh_4Sb_{12}$. It can be anticipated that doping La in the $RhSb_3$ will yield lower lattice thermal conductivity by means of La's vibration yielding considerable amplitudes (Fornari & Singh. 1999).

Many reports have also writen the filled $CoSb_3$-based skutterudite materials with improve TE properties. Doping partially by Co-site or Sb-site incorporation, filling voids and multisite substitution is an effective way to enhance TE performance. Te-doped $CoSb_3$ has a dramatically improvement on TE properties: a ZT value of 0.72 is achieved at 700 °C from fabricated $CoSb_{2.875}Te_{0.125}$ by melting annealing method as well as SPS; a ZT value of 0.83 is acquired at 427 °C from fabricated $CoSb_{2.8}Te_{0.2}$ by encapsulated induction melting method; Te-doped polycrystalline $CoSb_3$ like $CoSb_{2.85}Te_{0.15}$ with fine grains and an average grain size of 160 nm was synthesized by Mechanical alloying and SPS showing improved thermoelectric properties. The $CoSb_{2.85}Te_{0.15}$ TE material possessed the lower thermal conductivity and higher power factor leading to an enhanced ZT value of 0.93 at 547 °C (Liu et al., 2007). The mischmetal skutterudites material like $M_yFe_{4-x}Co_xSb_{12}$ was studied ranging from 300 K to 800 K. Mischmetal is an alloy of rare earth elements in various naturally-occuring propertions. A typical composition will consist of 50% cerium, 25 lanthanum and small amounts of neodymium and Praseodymium. Enhanced TE properties were found from decreasing size from micro scale to nano-scale (Zhang et al., 2010).

It is reported that Barium-filled skutterudites are among the most promising n-type materials with lower lattice thermal conductivity compared to pure $CoSb_3$, and it possess great electrical transport properties. A ZT value of 1.2 is achieved for the compound $Ba_{0.3}Co_{3.95}Ni_{0.05}Sb_{12}$ which is one of the highest experimentally determined values reported for n-type skutterudite (Zhao et al., 2006). And a ZT value of 1.3 is obtained through $Ba_yCo_4Sb_{12}$-based composites with dispersed fullerene or barium fulleride fabricated by SPS and solid state reaction. And the experimental results indicated that both the electrical and thermal conductivity will simultaneously decrease with the increasing impurity contents attributing to enhanced grain-boundary scattering of charge carriers and phonons. Moreover, a ZT value of 1.3 at 800 K is obtained from the double filled skutterudites $Ba_xYb_yCo_4Sb_{12}$. An improved lattice thermal conductivity is observed due to the reason of the combination of Ba and Yb fillers inside the voids of the skutterudite structure leading to a wide range of resonant phonon scattering (Shi et al., 2008).

Addtionally, strontium-filled skutterudites $Sr_yCo_4Sb_{12}$ have been fabricated by a melting method. The lattice parameters can increase linearly with the increase of the Sr content. The experimental resulted indicated that the thermal conductivity of $Sr_yCo_4Sb_{12}$has been decreased significantly compared with undoped $CoSb_3$. The ZT value of 0.9 of these TE materials is obtained at 850 K. Moreover, filled skutterudites such as $Tl_xCo_{4-y}Fe_ySb_{12}$ and $Tl_xCo_4Sb_{12-y}Sn_y$ have been studied for their electrical and thermal transport properties. Thallium atom is an unusual element because it is chemically silimar to other heavy metals like lead atom in some manner. It may have less effect on electrical transport than the rare earths because electronegativity of Tl is near to that of Sb. The substitution of Tl in the TE material means substantial rattling of the Tl about its equilibrium position. The resonant scattering of acoustic phonons by the Tl rattlers is considered the main reason of the quick decrease in the lattice thermal conductivity when incorporating small amout of Tl into the voids of the skutterudite structure. The Tl compounds have higher electron mobilities and lowered thermal conductivity. The maximum of ZT value of 0.8 is acquired at ambient temperature for Tl-doped $Co_4Sb_{12}$ like $Tl_{0.22}Co_4Sb_{12}$ compound (Sales et al., 2000).

A relatively high value of figure of merit in a polycrystalline skutterudite partially filled with ytterbium ions was reported. The small-diameter yet heavy-mass Yb atoms partially filling the voids of the host $CoSb_3$ system exhibit low values of thermal conductivity while they still possess the quite favorable electronic properties which are not substantially perturbed by the addition of Yb. This combination is ideal for thermoelectric applications exemplifying the ''phonon-glass electron-crystal'' concept of a thermoelectric material, resulting in ZT=0.3 at room temperature and ZT=1 at 600 K for $Yb_{0.19}Co_4Sb_{12}$ (Nolasa et al., 2000). Additionally, Yb-filled skutterudite materials incorporated with $Yb_2O_3$ is prepared by in situ reactio method. In this $Yb_yCo_4Sb_{12}$/ $Yb_2O_3$ structure, some $Yb_2O_3$ particles reside at the grain boundaries and others are dispersed within $Yb_{0.2}Co_4Sb_{12}$ grains as nanoscale inclusions. A remarkable reduction in thermal conductivity is acquired on accounts of the combination of the rattling of Yb ions inside the voids of $CoSb_3$ and the phonon scattering of the oxide defects. A maxiumu ZT value of 1.2 is obtained for $Yb_{0.21}Co_4Sb_{12}$/ $Yb_2O_3$ compound and a maximum ZT value of 1.3 is gained for $Yb_{0.25}Co_4Sb_{12}$ compound at 850 K (Zhao et al., 2006). Nanostructured $Yb_{0.2}Co_4Sb_{12+y}$ was fabricated by melt spinning techniqu with SPS. An average grain size of 150 nm was acquired, and with the increase of value y, the grain size will increase accordingly. Just because of the nanostructure of $Yb_{0.2}Co_4Sb_{12+y}$, a lowered thermal conductivity is obtained. Also, because of the moderately excessive Sb atoms, electrical transport properties are enhanced. A ZT value of 1.26 is achieved at 800 K

for $Yb_{0.2}Co_4Sb_{12+y}$ (Li et al., 2008). A method called synthetic route that can remarkably reduce the fabrication time of $Yb_{0.3}Co_4Sb_{12.3}$ is proposed leading to improved TE properties. As a result, a ZT value of 1.3 is obtained at 800 K for this single-phase, fully densified filled skutterudites. The notably reduced manufacturing time along with the improved TE performance can be employed in the practical application of skutterudite-based TE materials (Li et al., 2008).

Fullerene-filled $CoSb_3$ was studied of its structural, chemical, and transport properties Fullerene is a 60-atom carbon molecule that forms microsize clusters between the grain boundaries of $CoSb_3$. An experimental approach has proved that partial void filling is the optimizing method to improve thermoelectric properties. The advantage of partial fillingis that a random alloy mixture of filling atoms and vacancies can be established which accelerates effective point-effect scattering. Furthermore, soft phonon modes and rattling moedes which can efficiently reduce the value of lattice thermal conductivity can be created from large space for the filling atom in skutterudites and clathrates. Filling the voids with ions generates an additional source of lattice disorder like $Fe^{2+}$ frequently employed to substitute $Co^{3+}$ in pure $CoSb_3$. The result showed that dominant scattering mechanism in the electrical transport changes from impurity scattering to grain-boundary scattering near a $C_{60}$ content of mass percentage from 5% to 6%, and that thermal conductivity decreases with increasing $C_{60}$ content. The result also implies a transition from ionized impurity scattering to grain-barrier scattering occurs when the $C_{60}$ concentration increases above mass percentage of 5%. A significant increase in the thermoelectric figure of merit is achieved for doped $C_{60}$ compared to the pure $CoSb_3$ (Shi et al., 2004). At last, La doped $IrSb_3$ indicated enhanced TE efficiency by the decreasing lattice thermal conductivity because of filled La atoms rattling in the structural vacancies of the skutterudite crystal structure (Kim et al., 2004).

**$Zn_4Sb_3$**

The extremely high value of figure of merit acquired from $Zn_4Sb_3$ is coming from the remarkably glass-like thermal conductivity. The low thermal conductivity of $Zn_4Sb_3$ is coming from high levels of interstitials and corresponding local structural distortions and from domains of interstitial ordeirng, leading to disorder at multiple length scales.

In $Zn_4Sb_3$ structure, about one fifth of the Zn atoms are on three crystallographically distinct interstitial sites in ambient temperature. These interstitials are along with local lattice distortions with Zn diffusion rates as high as that of superionic conductors (Snyder & Toberer, 2008). $Zn_4Sb_3$ structure (See Fig. 15) contains following types of antimony atoms: Sb-Sb bonded dumbbels, $[Sb_2]^{4-}$ and isolated $Sb^{3-}$ without bonding to other antimonyatoms. The general zintl components can not precisely reflect the true strucuture which can be depicted by a complicated and delocalized multicenter bonding. $Zn_4Sb_3$ phase keep this delocalized multicenter bonding. However, Zn atoms will be disordered at longer length scales. Consequently, in ambient temperature with symmetry, one fifth of the Zn atoms will be in interstitail positions. Just due to the complex Zn interstitial structure, $Zn_4Sb_3$ possesses a higher ZT value to a large extent on accounts of lower lattice thermal conductivity which is less than 1 $Wm \cdot K$.

It is reported that $Zn_4Sb_3$ can be fabricated using solid state reaction (Cadavid & Rodríguez, 2008), conventional quench method and zone-melting technique etc (Pedersen & Iversen, 2008). Only the $Zn_4Sb_3$ fabricated by the last method is more thermal stable for more promising applications. The synthesized $Zn_4Sb_3$ by other two methods will partly

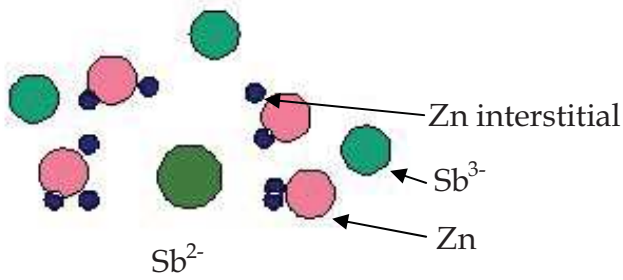


Fig. 15. A layered view of the structure of $Zn_4Sb_3$ containing electron density map indicating the existence of interstitial Zn atoms after (Kauzlarich et al., 2007)

decompose to ZnSb, ZnO and Zn below expected stability range which resulted in a notable degradation of the ZT value. Therefore, the $Zn_4Sb_3$ prepared by the zone-melting technique is a high-performance TE material. Also, compacted $Zn_4Sb_3$ synthesized by SPS is investigated with grain size less than 45 μm. The experimental and measurement result showed that there is an obvious correlation between the density and thermoelectric properties. The results indicated that changes in $Zn_4Sb_3$ compaction conditions will have a larger influence of ZT than doping (Pedersen et al., 2006). It is not sure to say that doping can improve the electron crystal traits of $Zn_4Sb_3$ But doping with small amount of metal dopants changes the subtle balance between the Zn deficiency and Zn disorder. As a resutl, it is estimated that doping with metals can enhance its carrier concentrations (Litvinchuk et al., 2008).

It is known that $Zn_4Sb_3$ possesses at least four crystalline phases, among which, only β phase $Zn_4Sb_3$ is an efficient TE material from 263 K to 765 K. β phase $Zn_4Sb_3$ possesses hexagonal rhombohedric crystal structure and its highest ZT value achieved is 1.4 at 400 °C . Single phased polycrystalline specimen was fabricated by melting and well homogenizing Zn and Sb in closed quartz ampoules. The acquired ingots were ground into powders and then hot pressed to generate crack-free specimen (Nolas et al., 2006). A method of disordering is emerging as a efficient way to lower the thermal conductivity as well as loosely bonded atoms and point defects. β phase $Zn_4Sb_3$ is a structurally disordered intermetallic compound at moderate temperature range 450 K- 650 K. So β phase $Zn_4Sb_3$ is a promisng nanocomposite material which possesses potential low thermal conductivity. The great TE properties of p-type β–$Zn_4Sb_3$ fills the gas in the ZT values between the low temperature state-of-the-art materials $Bi_2Te_3$-based alloys and the intermediate teperature materials PbTe-based alloys and Te-Ge-Sb-Ag alloys. β–$Zn_4Sb_3$'s stability is remaining stable up to 670 K under static vacuum and argon. Much effort is devoted to producing n-type materials and other isostructural compounds such as $Cd_4Sb_3$. Meanwhile, a series of $SiO_2$/β–$Zn_4Sb_3$ core-shell nanocomposites with different thickness were fabricated by coating β–$Zn_4Sb_3$ pariticles with $SiO_2$ nanoparticles prepared by hydrolyzing the tetraethoxysilane in alcohol-alkali-water solution. The experimental results and analysis indicated that $SiO_2$ nanoparticles are coated with uniformly β–$Zn_4Sb_3$. During the coating process, both the thermal conductivity and electrical conductivity gradually decrease, and at the same time, the thermopower increases compared to β–$Zn_4Sb_3$ bulk material. The results also demonstrate that the themopower will increase dramatically in high temperature range. It showed that thermal conductivity of $SiO_2$/β–$Zn_4Sb_3$ nanocomposite material with thickness of 12 nm isn only

0.56 W/m-1K-1 at 460 K. Consequently, the ZT value of $SiO_2/\beta–Zn_4Sb_3$ nanocomposite is 0.87 at 700 K (Ruan & Xiao, 2007).

**Clathrate**

Clathrates are a series of materials which possess teetrahedrally bonded atoms form of a framework of cages that can encircle relatively large metal atoms. Clathrate compounds consisting of polyhedral cages and guest atoms encapsulated in the cages are expected to exhibit relatively high electrical conductivity and Seebeck coefficient, in addition to very low thermal conductivity from their crystal structures comprising of polyhedral cages doped with a guest atom.There is a potential way to further reduce thermal conductivity for clathrates which consist of rattling atoms and large cages, that is via disorder within the unit cell containing void spaces (Snyder & Toberer, 2008). The polyhedral cages consist of group-IV and/or -III elements while the guest atoms are typically alkali metals or alkali-earth metals. The "rattling" of guest atoms in oversized cages is considered to scatter heat-carrying phonons efficiently, resulting in low thermal conductivity, while electrical conductivity remains relatively high because electronic conduction mainly takes place through the cage framework. Therefore, clathrate compounds have been investigated in recent years as promising thermoelectric materials, Clathrate compounds form in a variety of structure types, depending on the combination of different constituting cages. The rest part of this section will emphasize on the type-I clathrate and type III clathrate.

One of prominent properties of clathrates is its low glass-like thermal conductivity in type-I clathrates. A large number of clathrate types belong to the type-I with formula $X_8Y_{16}Z_{30}$ (Bentien et al., 2004). Polycrystalline $Sr_8Ga_{16}Ge_{30}$, in which Sr atom is encapsulated by the $[Ga_{16}Ge_{30}]$ framework, of single crystal of the type-I clathrate compounds are reported in the temperature range from 5 K to 300 K with stability. The compounds exhibit n-type semiconducting behavior with relatively high Seebeck coefficients and electrical conductivity, and bear carrier concentrations in the range of $10^{17}$–$10^{18}$ $cm^{-3}$ at room temperature. An enhanced ZT value of more than 1 is achieved at more than 700 K. thus exceeding that of most known materials. At the same time, the $Sr_8Ga_{16}Ge_{30}$ compound's thermal conductivity is drastically reduced, to nearly that of the theoretical minimum, while good electronic conductivity in not affected (Nolasa et al., 1998). The $Ba_8Ga_{16}Ge_{30}$ has nearly equal coefficient of thermal expansion with $Sr_8Ga_{16}Ge_{30}$ is also of the type-I clathrate and they both showed higher performance at higher temperatures. In comparison, $Sr_8Ga_{16}Ge_{30}$ has lower thermal conductivity than $Ba_8Ga_{16}Ge_{30}$ due to more notably rattling of Sr atoms in the cages (Okamoto et al., 2008). A ZT value of 1 is reported for poly crystalline $Sr_8Ga_{16}Ge_{30}$ and a ZT value of 1.7 is reported for polycrystalline $Ba_8Ga_{16}Ge_{30}$ with optimized compositions previously. And improved thermoelectric properties are expected from polycrystalline crystal $Ba_8Ga_{16}Ge_{30}$. The experimental results indicated that polycrystalline specimen of $Ba_8Ga_{16}Ge_{30}$ with optimization showed higher TE properties than reported single crystal $Ba_8Ga_{16}Ge_{30}$ (Martin et al., 2008). To date, the relatively high ZT value of 1.35 is obtained through Czochralski method at 900 K for $Ba_8Ga_{16}Ge_{30}$. Additionally, n-type $Ba_8Ga_{16}Zn_xGe_{30-x}$ was fabricated by solid-state reaction and SPS. The electrical conductivity and carrier mobility will increase with the decreasing Zn content, while the carrier concentration will increase with the increasing Zn content. Specifically, Seebeck coefficient of $Ba_8Ga_{16}Zn_{3.2}Ge_{26.8}$ will reach 250 μV/K at 300 K or 307 μV/K at around 700 K. The thermal conductivity will decrease with increasing Zn content. And it is expected that electrical conductivity and carrier concentration will increase significantly by slightly adjusting Ga content (Deng et al., 2007).

It is also reported that $Ba_8Ge_{43}$ is considered as type-I clathrate compound. The crystal structure of $Ba_8Ge_{43}$ is quite different from other type-I clathrate compound. But type-I clathrate compound is a supperlattice structure according to ususl type-I clathrate structure. The experimental indicated that this kind of material is not a good TE material because of its high electrical resistivity attrbuting from the Ge vacancies (Okamoto et al., 2006). In comparison, tellurium doped type-I clathrate compound $Ge_{30}P_{16}Te_8$ possesses lower thermal conductivity as low as of $Sr_8Ga_{16}Ge_{30}$ and $Ge_{38}Sb_8I_8$. Because the general clathrates materials are n-type, so the fabrication of this p-type clathrate compound is very crucial. $Ge_{30}P_{16}Te_8$ has a thermal conductivity of 0.9 W/m·K at ambient temperature (Kishimoto et al., 2006).
Clathrate compounds with the formula like $X_{24}(Y/Z)_{100}$ or $X_{24}Y_{32}Z_{68}$ is defined as type III clathrate compounds in which, Y and Z are tetrahedrally and trigonally bonded cage atoms, respectively. $Ba_{24}Ge_{100}$ has been reported to exhibit low lattice thermal conductivity of about 1 W/m·K but also to show a high value of electronic thermal conductivity and a small value of Seebeck coefficient. The high value of electronic thermal conductivity and the small value of Seebeck coefficient are considered to originate from the high electron concentration of $Ba_{24}Ge_{100}$. There exist 16 extra electrons per $Ba_{24}Ge_{100}$ unit formula corresponding to a higher electron concentration than usual one. As a result, the reduction of the extra electrons can enhance Te performance. The addition of Al and Ga doped into clathrate compound can decrease the thermal conductivity and increase the Seebeck coefficient. Furthermore, thermal conductivity in clathrate compounds like Ba–In–Ge ($Ba_{24}In_XGe_{100-X}$) system generally decreases with the increase in the In content because of the decrease in the number of excess electrons. And the system Ba-Al-Ge and Ba-Ga-Ge systems have the similar traits (Kim et al., 2007). It is reported that n-type $Ba_8Ga_xGe_{100-x}$ of type- III clathrate compound synshesize by arc melting, achieved a ZT value of 1.25 at 903 K. (Deng et al., 2007).

**Tellurides alloys**

This section introduces binary telluride alloys, ternary telluride alloys and many entities telluride alloys. This section will firstly state the binary telluride alloys PbTe, $In_2Te_3$ and $Ga_2Te_3$, then narrate the doped binary telluride alloys, after that recount the ternary telluride alloys and quaternary alloys, and at last will compare some TE nanocomposites with lower thermal conductivity and state the state-of-the-art telluride superlattice with highest ZT value achieved in tellurides alloys.
Synthesized lead telluride based alloys are considered as n-type and p-type thermoelectric materials with lower thermal conductivity. The achieved great thermoelectric characteristics are greatly relying on the preparation technology and the carrier concentration. PbTe has a high melting point, good chemical stability. Good chemical strength, low vapor pressure and high figure of merit. Lead telluride can be operated at 900 K and is an intermediate thermoelectric power generator which is widely employed in the army, space crafts and batteries. The outstanding property of this TE material is its low lattice thermal conduvtivity. The TE material PbTe can be acquired from the decomposition of metastable $Pb_2Sb_6Te_{11}$ into PbTe and $Sb_2Te_3$. A layered microstructure is obtained of PbTe and $Sb_2Te_3$. The inter-layered space can be adjusted by the temperature and time of the decomposition process. The ajacent PbTe and $Sb_2Te_3$ layers are crystallographically oriented, resulting in high-quality epitaxy like interfaces. Average layer spacings are 180 nm compared to a PbTe layer thickness of 40 nm. These nanoscae multilayers stands for the thin-film superlattice thermoelectric materials which have indicated notably high thermoelectric efficiency (Ikeda et al., 2007). Addtionally, the single crystalline PbTe nanowires indicated decreased thermal

conductivity with the decreasing nanowire diameter. The lower thermal condutivity is 1.29 W/m K for a 182 nm nanowire at 300 K which is half value of bulk PbTe. This kind of single crystalline PbTe nanowires can be synthesized by chemical vapor transport method with prepared length ranging from 182-436 nm in diameter. The Figs. 16 and 17 show the relations between temperature and thermal conductivity of different nanowire diameters. Based on these figures, it can be seen that the thermal conductivity will decrease as the diameter shrinks (Roh et al., 2010).

$Ga_2Te_3$ is another example telluride alloy with low thermal conductivity due to effective scattering phonons in the 2-D vacancy plane. $In_2Te_3$ was compared with $Ga_2Te_3$ for their TE performances. They have the same crystal structure and their thermal conductivities were compared in the Fig. 18. It can be seen that $In_2Te_3$'s thermal conductivity decreases with

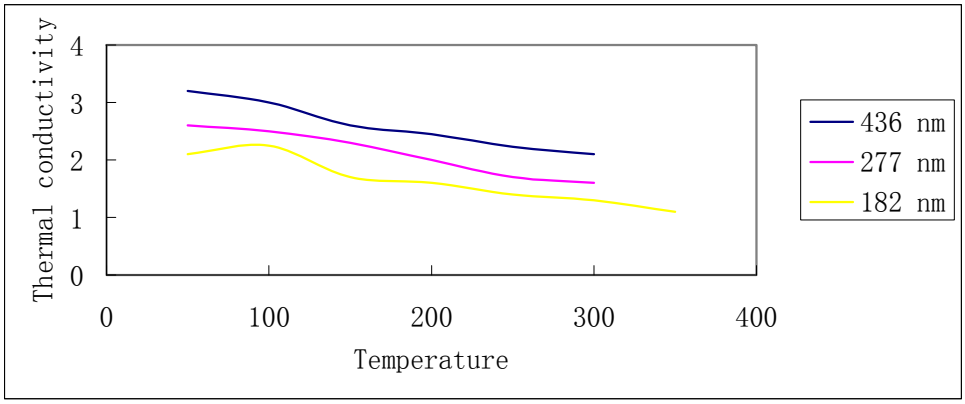


Fig. 16. The measured thermal conductivity of individual single-crystal PbTe nanowires with different diameters at different temperatures. Data source from (Roh et al., 2010)

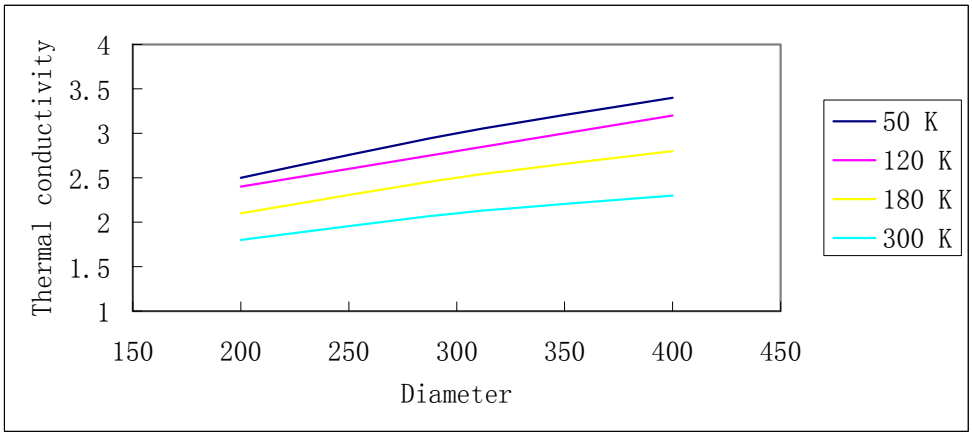


Fig. 17. The measured thermal conductivity of individual single-crystal PbTe nanowires at different temperatures with different diameters. Data source from (Roh et al., 2010)

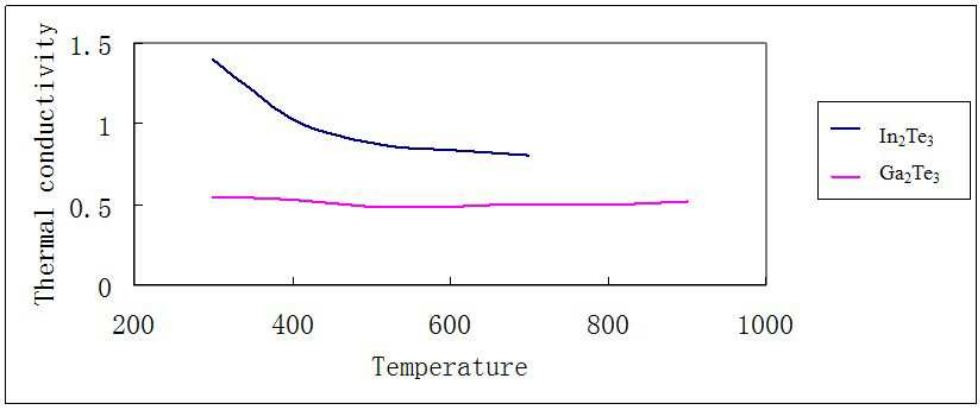


Fig. 18. Measured relations between temperature (K) and thermal conductivity (W/m·K) for $Ga_2Te_3$ and $In_2Te_3$. Data source from (Kurosaki et al., 2008)

increasing temperature, while $Ga_2Te_3$ showed a nearly flat temperature dependence. It is obvious to see that $Ga_2Te_3$ exhibits a lower thermal conductivity than $In_2Te_3$, and it has a rather low thermal conducitivity of as low as 0.5 W/m·K (Kurosaki et al., 2008).

Alloying binary tellurides ($Bi_2Te_3$, $Sb_2Te_3$, PbTe, GeTe and $Ga_2Te_3$) with other isoelectronic cations and anions can reduce the thermal conductivity rather than lower the electrical conductivity. The traditional TE materials without doping generally have a maximum value of ZT up to 1 at ambient temperature relying on the band gap of the materials. For example, the nanocomposites like $Bi_2Te_3$, PbTe and SiGe alloys (Yamashita, 2004) have ZT value of 0.9 at 400 K, 0.8 at 650 K and 0.9 at 1200 K, respectively. Because of the inherent flaws involved in these materials like their cost and scale-up, many other new preparation methods of nanocomposite have emerged like sinodal decomposition, matrix encapsulation and eutectic system. A eutectic system is a mixture of chemical compounds or elements that has a single chemical composition that freezes at a lower temperature than any other composition. This composition is knows as the eutectic composition and the temperature is knows as the eutectic temperature. The reported entectics falls in the range of semiconductor and metal compounds. Here, we will introduce the new-explored eutectic material PbTe-GeSi. The incorporation of Ge into the PbTe lowers the brittleness notably. The composition PbTe-Ge (4:1) was studied indicating that the lattice thermal conductivity was not significantly improved than PbTe itself. While when the composition of Ge is lower than 20 %, the incorporated PbTe showed an reduced thermal conductivity. Furthermore, when incorporating Ge and Si simultaneously, a remarkably reduction was observed. An enhanced ZT value up to 1.3 was achieved via PbTe-$Ge_{0.8}Si_{0.2}$ (19:1) (Sootsman et al., 2009). A maximum figure of merit as high as $3.2\times 10^{-3}$/K is achieved from p-type alloys with the composition $Bi_{24}Sb_{68}Te_{158}Se_6$. The lattice thermal conductivity is found to decrease when the telluride content is increasing (Bergvall & & Beckman, 2003). An improvement in thermoelectric property is attained of $CsBi_4Te_6$ which is a complex variant of $Bi_2Te_3$. It has a lamellar structure with slabs of $(Bi_4Te_6)^{1-}$ alternating with layers of $Cs^+$ ions. Low doping degrees will greatly influence the charge transport properties. Due to few Bi-Bi bonds and complexity of the Cs layers in $CsBi_4Te_6$, $CsBi_4Te_6$ has a lower lattice thermal conductivity than $Bi_2Te_3$. Meanwhile, an enhanced Seebeck Coefficient with slightly damage to the

mobility will be resulted in because of the anisotropic effective mass in layered $CsBi_4Te_6$. A ZT value of 0.8 is obtained at 225 K which is 40% greater than that of Bi-Sb-Te-Se alloys. Transition metal pentatellurides of the orthorhombic polytype structure $ZrTe_5$ and $HfTe_5$ exihibits large resistivity anomalies. These compoumds have the similar structure with $Bi_2Te_3$, with van der Waals gaps between the individual layers. Doped pentatellurides showed high power factors at low temperatures, surpassing the optimized $Bi_2Te_3$ value, but the high thermal conductivity is relatively high (4W/m·K-8W/m·K). Eventually, pentatellurides still need to be tuned to make them high performance TE materials. Doped crystals of the pentatellurides such as $Hf_xZr_{1-x}Te_5$ showed reduced thermal conductivity on accounts of phonon scattering (Zawilski et al., 2000).

Alloyed bismuth telluride also possesses such properties. Solid state alloying improves the thermoelectric figure of merit by decreasing lattice thermal conductivity without affecting electrical properties. Alloying engenders part disorder in the film network that may increase the scattering of phonons with minor effect on the charge carriers which have long wavelength as compared to phonons. Bismuth telluride could be easily synthesized by cathodic electrochemical deposition. The deposition process can be controlled by bridling electrochemical parameters. The as-deposited bismuth telluride films are crystalline and morphologcally smooth in the whole area.

Bismuth telluride could be employed as a thermoelectric power generator with other doped materials. It has reported that thermoelectric power generator modules contain of 0.8 mm $Bi_2Te_3$ and 50 μm thick ErAs (60% of volume): $[InGaAs]_{1-x}[InAlAs]_x$. A output power of 6.3 W was measured when the heat source temperature was at 610 K. When ErAs nanoparticles are doped into $[InGaAs]_{1-x}[InAlAs]_x$, a bending potential barrier is created at the interface between the particle and semiconductor. The Seebeck coefficient can be increased by meas of the electron filtering effects of these potential barriers. The performance of a thermoelectric generator module can be effectively enhanced by employing segmented element structures with materials whose thermoelectric properties are optimized in successive temperature ranges. A notable improvement in TE properties has been seen in the $Bi_2Te_3/Sb_2Te_3$ superlattices deposited on GaAs. Supperlattices provide the chances to enhance the ZT value by increasing Seebeck coefficient and decreasing the thermal conductivity compared to bulk materials (Touzelbaev et al., 2001). The experimental results indicated that via incorporating ErAs nanoparticles in the compound InGaAlAs, the thermal conductivity was lowered than that of $[InGaAs]_{0.8}[InAlAs]_{0.2}$. The thermal conductivity of this nanocomposite is lowered by one quarter when increasing the ErAs concentration from 0.3% to 3% (Zeng et al., 2009). An improved ZT value up to 1.04 was obtained after incorporating the n-type $Bi_2[Te_{0.94}Se_{0.06}]_3$ with I and Te by Bridgman method and anealed for 2 hours at 473 K. This speciman possesses a remarkably high power factor of $6.57\times10^{-3}$ $W/mK^2$ at 298 K which is the highest in bismuth tellurides. In comparison, $Bi_2[Te_{0.94}Se_{0.06}]_3$ doped with I, Te and CuBr fabricated by the same method indicated a lower ZT value of 0.91 at 298 K. The reason may be attributed to the addition of CuBr (Yamashita & Tomiyoshi, 2004). The Te doped p-type $(Bi_{0.25}Sb_{0.75})_2Te_3$ was synthesized by the Bridgman method at a rate of 6 cm/h. After the annealing and vacuum processes, the maximu ZT value is 1.41 at 308 K (Yamashita et al., 2003).

Neither Si nor Ge is a good TE material because Si's lattice thermal conductivity value is 150 W/m·K and Ge's lattice thermal conductivity value is 63 W/m·K which is quite large for TE materials. However, through alloying, the lattice thermal conductivity could be exceedingly reduced, like $Si_{0.7}Ge_{0.3}$'s thermal conductivity is 10 W/m·K. Using nanostructure method, a

ZT value of 1.3 is achieved for n-type silicon germanium (SiGe) bulk alloy at 900 K. The enhancement of TE performance is due to notably reduction in thermal conductivity resulted from large phonon scattering (Wang et al., 2008). Moreover, it is reported that the power factor ZT value of n-bype $Si_{1-x}Ge_x$ nanowires are larger than those p-type counterparts with the same Ge content and incorporating concentration. A maximum ZT value of 1 is achieved for n-type $Si_{0.5}Ge_{0.5}$ nanowires (Shi et al., 2010).

The charge density wave material like $CeTe_2$ indicated relatively low thermal conductivity1.25 W/m·K at 300 K and high Seebeck coefficient as high as 477 μV/K at 300 K. And also polycrystalline $Ce_{1-x}Cu_xSe_2$ series nanocomposites have been investigated. The experimental results showed a large Seebeck coefficient value of 344 μV/K and low thermal conductivity value of 0.71 W/m·K. With the increment of Cu doping concentrations, the Seebeck coefficient will decrease, referring to increase in the charge carrier concentration from Cu doping. $Ce_{1-x}Cu_xSe_2$ indicated a lower power factor than $Bi_2Te_3$ and its alloys due to the higher electrical resistivity. From the band structure calculation, the high Seebeck coefficient for the $Ce_{0.9}Cu_{0.1}Se_2$ compound is due to the localized Ce *f*-band near the Fermi level. The Figs. 19 and 20 showed the crystal structure of the stoichiometric $CeSe_2$ and $Ce_{1-x}Cu_xSe_2$ with Cu as a dopant. From the energy formation calculation, the dopant Cu at the Ce-Se block is rather advantageous than the interstitial or the Se position doping. The doped Cu atom modified the atomic coordination as shown by the red arrow (Rhyee et al., 2010).

It is reported that a high thermoelectric performance can also be obtained from the ternary alloys. Thallium compounds indicated low thermal conductivity thus exhibiting high TE performance. Particularly, bulk polycrystalline material $Ag_9TlTe_5$ showed a ZT value of 1.23 at around 700 K. What's more, polycrystalline sintered specimen of $Tl_2GeTe_3$, $Tl_4SnTe_3$ and $Tl_4PbTe_3$ showed thermoelectric figure of merits as follows: 0.29 at 473 K, 0.74 at 673 K and 0.71 at 673 K largely because of their low thermal conductivities. Although $Tl_2GeTe_3$, $Tl_4SnTe_3$ and $Tl_4PbTe_3$ did not indicate an optimized electrical conductivity, their low

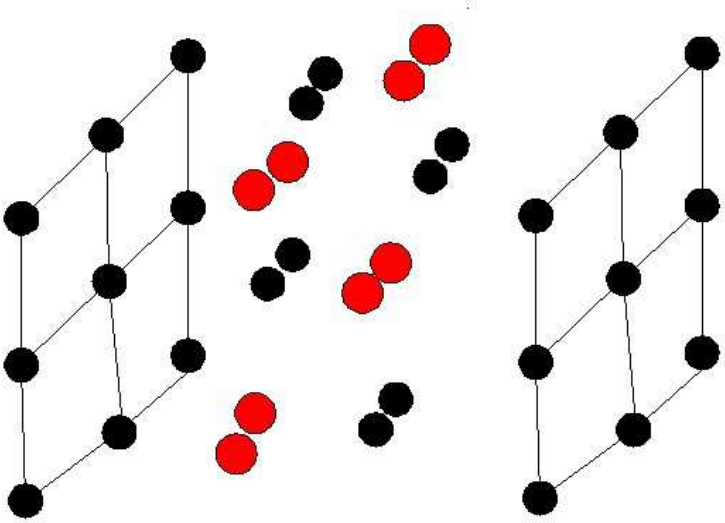

Fig. 19. Crystal structure of $CeSe_2$ after(Rhyee et al., 2010). Black spheres denote Se atoms and red spheres denote Ce atoms.

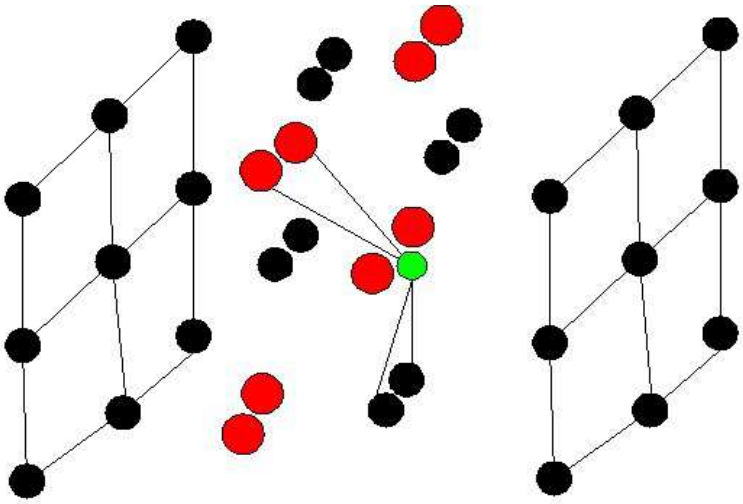

Fig. 20. Crystal structure of $Ce_{1-x}Cu_xSe_2$ after(Rhyee et al., 2010). Black spheres denote Se atoms, red spheres denote Ce atoms and green sphere denotes Cu atom.

thermal conductivity resulted from weak bonding of atoms and complicated crystal structure stands for their potential utilizations (Kosuga et al., 2006). Furthermore, $TlGaTe_2$ and $TlInTe_2$ showed semiconductorlike properties with low thermal conductivities and relatively high ZT values. And TlTe indicated an exceptionally high thermal conductivity due to its large electronic contributions and high lattice thermal conductivity (Matsumoto et al., 2008). This maybe explained from their structure (See Figs.21 and 22) : $TlGaTe_2$ and $TlInTe_2$ have the same structure, while TlTe has a more complex structure than $TlGaTe_2$ and $TlInTe_2$. Both $TlGaTe_2$ and $TlInTe_2$ have 16 atoms per unit cell, and TlTe has 32 atoms per unit cell.

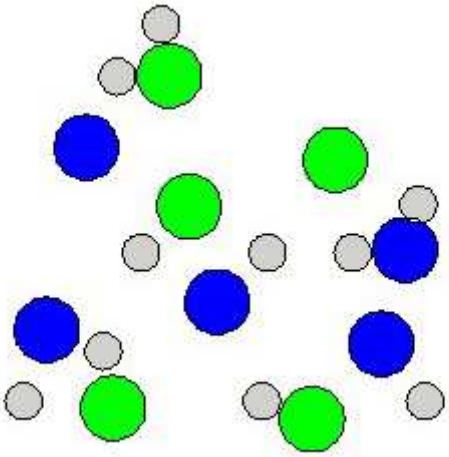

Fig. 21. Plane view of $TlGaTe_2$ and $TlInTe_2$ after (Matsumoto et al., 2008). The green, blue and gray balls represent Ga or In, Tl and Te atom respectively.

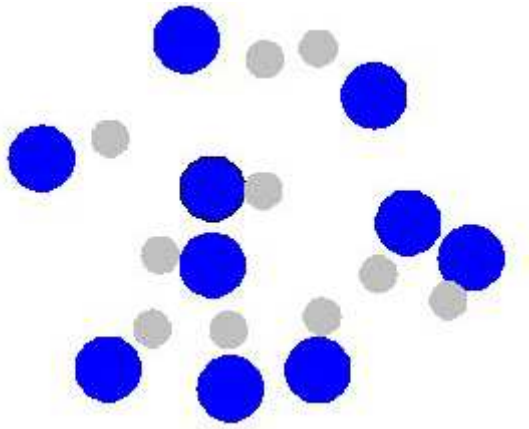

Fig. 22. Plane view of TlTe after (Matsumoto et al., 2008). The green, blue and gray balls represent Ga or In, Tl and Te atom respectively.

Although the conventional low dimension thermoelectric nanocomposites such as superlattive $Bi_2Te_3/Sb_2Te_3$ and quantum dot superlatticve $PbSe_{0.98}Te_{0.02}/PbTe$ indicated improved ZT to a large extent due to the lattice thermal conductivity, it is still hard to scale up these supperlattices for large energy conversion applications because of their limitations (Ma et al., 2008). So how to apply the TE materials into practical applications have become important. A high ZT value is achieved from silver antimony lead telluride fabricated from zone melting and crystal growth technique. A ZT value of 1.56 is obtained at 300 K from the p-type $Bi_{0.52}Sb_{1.48}Te_3$ bulk material with microstructures. This bulk material is fabricated by melt spinning technique and SPS. This microstructure contains nanocrystalline domains implanted in amorphous matrix and 5-15 nm nanocrystals with coherent grain boundary. The achieved higher ZT value is attributed to the lower thermal conductivity, and this value is more than a half enhancement of $Bi_2Te_3$ ingot material (Xie et al., 2009). It is also reported that at the optimized doping concentrations assuming that scattering rate is the same as a function of doping by using a constant relaxation time and an averaged thermal conductivity, a ZT value of 1.8 can be achieved for the p-type doping in $(Sb_{0.75}Bi_{0.25})_2Te_3$ compound (Lv et al., 2010).

A ZT value of 1.4 is acquired from ternary alloyed bismuth antimony telluride (BiSbTe) at 100 °C through hot pressing nanopowders that were ball-milled from crystalline ingots under intert conditions than traditional achieved ZT value of 1 for several decades. The high performance of thin nanocomposite is attibuted to the sligh increase of electrical conductivity and large decrease of the thermal conductivity. The lower value of ZT is acquired at higher lattice disorder for $Bi_{0.5}Sb_{0.5}Te$. And experimental results and measurements indicated that a low thermal conductivity is gained due to increased phonon scattering by grain boundaries and defects. This kind of nanocomposite can be used as cost-saving and high-performance TE material for cooling and power generation (Poudel et al., 2008). Moreover, from the TEM picture of $Bi_{0.5}Sb_{0.5}Te$, it can be seen that both nanosized and microsized grains are engendered. And between the nanograins, the interface regions have a 4 nm thickness in addition to nanoprecipitates. A ZT value of 1.4 is acquired for this material due to its low thermal conductivity and slightly improved electrical conductivity (Lan et al., 2009).

Except for ternary alloys Bi-Sb-Te, some other ternary nanostructured homologous serious like $Ga_mSb_nTe_{1.5(m+n)}$ is studied for its valuable performance in TE properties. $Ga_mSb_nTe_{1.5(m+n)}$ was studied over the temperature range of 318-412 K, and a measured ZT value of 0.98 is achieved with m:n=1:10 at 482 K which is higher than that of undoped $Sb_2Te_3$ at the same temperature. This improvement is on accouts of phonon scattering caused by amorphous structure, amorphous structure and lattice distortion leading to remarkable reduction in thermal conductivity. With increase of m:n ratio (See figure 23), both the thermal conductivity and electrical conductivity will decrease and the Seebeck coeffcient will increase. The ZT values with different ratio for $Ga_mSb_nTe_{1.5(m+n)}$ are shown in the Fig. 23: ZT value will increase with m:n ratio until m:n=1:10, after that, will decrease. In comparison, a ZT value of 0.65 is obtained fro Ga doped telluride alloy like $Ga_xBi_{0.5}Sb_{1.5-x}Te_3$ at 318 K (Cui et al., 2009).

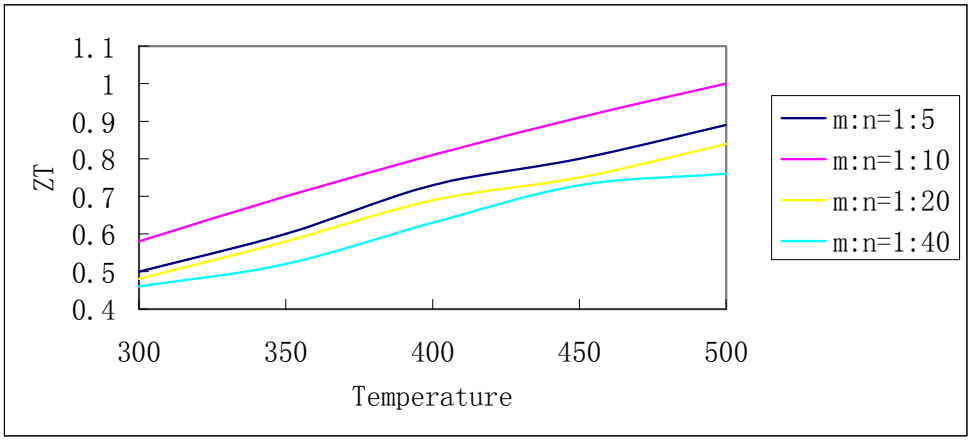


Fig. 23. The relations between temperature (K) and ZT value for $Ga_mSb_nTe_{1.5(m+n)}$ alloys. Data source from (Cui et al., 2009).

The quaternry telluride based alloys with formula $Ag_nPb_mSb_nTe_{m+2n}$ and $Ag_nPb_mSi_nTe_{m+2n}$ were reported with high ZT value. For example, $AgPb_{10}SbTe_{12}$ indicated an exceptionally high ZT value more than 2.0 at enhanced temperature arising from very low total thermal conductivity.

Recently, unit cell disorder is employed as a effective method to reduce lattice thermal conductivity through interstitial sites, rattling atoms or partial occupancies as well as the disorder inherent in the alloying materials. The following figure shows the lower thermal conductivities recently found in nanocomposites compared with previous state-of-the-art thermoelectric alloys such as $Bi_2Te_3$, PbTe and SiGe.

From the results in Fig. 24, the novel nanocomposites have lower thermal conductivity than traditional thermoelectric materials. The quaternary alloy $Hf_{0.75}Zr_{0.25}NiSb$ in the above figure with high thermal conductivity has a simple cubic structure rather than large and complicated unit cells related to low thermal conductivity. For $La_{3-x}Te_4$, because of large number of random vacancies in rare-earth chalcogenides $La_{3-x}Te_4$ with similar structure like $Th_3P_4$, rare-earth chalcogenides have a lower lattice thermal conductivity. It can be seen that $Ag_9TlTe_5$ has lower lattice thermal conductivity. Low lattice thermal conductivity can also be attained from thallium-base thermoelectric materials like $Tl_9BiTe_6$. The possible

explanation of the low value of lattice thermal conductivity is because extremely soft thallium bonding can be observed in low elastic modulus.

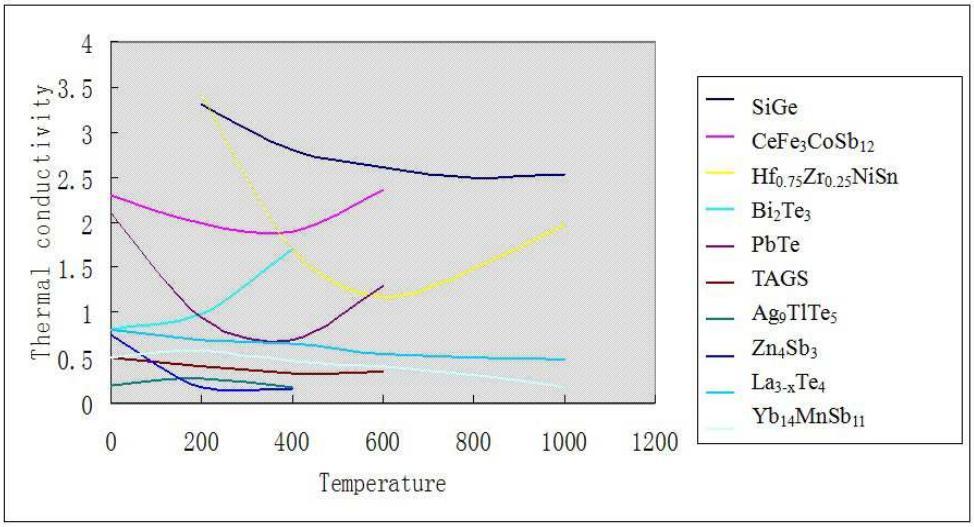


Fig. 24. Relations between temperature (K) and lattice thermal conductivity (W/m·K). Data source from (Snyder & Toberer, 2008).

A ZT value of 2.4 is obtained at 330 K at Research Triangle Institute through the manufacturing superlattice $Bi_2Te_3/Sb_2Te_3$. The significant improvement lies in the created 'nanoengineered' material which is effective in thermal insulation while maintaining the electrical conductivity. The thermal insulation comes from a intricate localized property for phonons, while the electron transmission is facilitated by optimal choice of band offsets in these semiconductor heterostructures. So the improvement in superlattice materials seems to be more promising for a reduction in lattice thermal conductivity than an increase in power factor. (Tritt et al., 2006)

**InSb**

Originally, by using a relaxation time approximation to the electron scattering, an unlimited increase of ZT was predicted as the thickness of the nanowire decreased. However, the calculation is via exact solution of the Boltzmann transport equation, which is devised by Ludwig Boltzmann, describing the statistical distribution of one particle in a fluid, including all the fundamental electron scattering mechanisims: polar optic, acoustic deformation potential, piezoelectric and ionized impurity scattering. More recently, the exact solution of the Boltzmann transport equation showed that, if all frequency dependent electron scattering mechanisms are properly taken into account, there is an effective limit to the maximum enhancement of the power factor, that can be obtained with nanowires of a given material. This limit occurs because the acoustic phonon–electron scattering increases dramatically as the thickness of the nanowire is reduced. As a result, it was predicted that a more power factor enhancement of ten times or less would be possible for GaAs quantum well superlattices, and only a two-fold enhancement might be achieved for PbTe. These

findings led to speculation that the main contribution to ZT enhancement might come from the lattice thermal conductivity reduction.

There exist large differences between different III–V materials regarding their suitability for nanowire based thermoelectric applications. Only InSb seems to be a promising candidate for which nanowires around 10 nm thick might suffice to obtain a reasonably high figure of merit. GaAs and InP nanowires appear to be of little practical use at room temperature, down to 1 nm thickness. InP nanowires yield the lowest power factor and ZT within the materials studied, and InAs lies in between the InSb and GaAs cases. Enhancements of the power factor of only 10–20 times are predicted in the narrow wire limit, while much of the ZT increase in these III–V nanowires occurs due to $\kappa_l$ reduction. Two separate sets of calculaltlions are carried out: one for the electronic transport properties, and another one for the lattice thermal transport, for nanowires made of GaAs, InP, InSb and InAs.The result showed that InSb nanowires around 10 nm thick is standing out as a great nanocomposite to exhibit higher power factor and lower lattice thermal conductivity, when compared to GaAs, InP and InAs, as a great nanocomposite to exhibit higher power factor and lower lattice thermal conductivity (Mingoa, 2004).

Recently, In doped $CoSb_3$ based skutterudite nanocomposites have drawn much attention due to their potential TE performance. A ZT value of 1.2 at 575 K is obtained from $In_{0.25}Co_4Sb_{12}$ compound. The single bulk crystal Te doped InSb has been studied for its TE properties. The maximum ZT value is 0.6 at 673 K and the maximu output power is 216 μV at 195 K (Matsumoto et al., 2005). The combined doping influence of In and Ge leads to high properties in n-type skutterudite $In_xCe_yCo_4Sb_{12}$ which was synthesized by a melt-quench-anneal-spark plasma sintering method. The doped $In_xCe_yCo_4Sb_{12}$ showed a nanostructured InSb phase with the grain size from 10 nm to 80 nm which is averagely dispersed on the boundaries of the skutterudite matrix. The evenly dispersed InSb nanophase at the boundaries is believed to notably lower the lattice thermal conductivity and enhance the thermopower. The nanostructured InSb phase also possesses a significant effect on phonon scattering resulting in remarkable reduction in lattice thermal conductivity. Additionally, the lattice thermal conductivity is further reduced due to doped Ce atoms. A reported ZT value of 1.43 was proven at 800 K in the $In_xCe_yCo_4Sb_{12}$ compound (Li et al., 2009).

**Other TE materials with low thermal conductivity**

Because of the good thermoelectric properties and available component elements, $Mg_2Si$ and $Mg_2Sn$ compounds have indicated potential utilization for TE applications. The high thermoelectric performance $Mg_2Si_{0.4-x}Sn_{0.6}Sb_x$ alloy synthesized by directly melting stoichiometric amount of atom Si, Sn and Sb under argon atmosphere, showed a ZT value of 1.1 with x=0.075 with relatively low thermal conductivity (Zhang et al., 2008). Additionally, oxygen-deficient lanthanum doped strontium titanate $Sr_{1-x}La_xTiO_3$ films showed significant reduction in thermal conductivity due to randomly dispersed and clustered vacancies which are effective to scatter phonons. Specifically, the thermal conductivity could be reduced to 0.5 W/ m K at 300 K for $S_{r0.98}La_{0.02}TiO_3$ via doping other phonon suppression methods like implanting various size nanostructures (Yu et al., 2008).Tedrahedrally bonded stannite ($Cu_2FeSnS_4$) compound $Cu_2ZnSuSe_4$ showed a narrow band gap of 1.44 eV as a result of which indicating a high TE performance at intermediate temperature. A maximum ZT value of 0.95 at 850 K for $Cu_2ZnSn_{0.9}In_{0.1}Se_4$ is achieved by means of relatively low thermal conductivity due to distorted structure and tunable electrical traits through doping (Shi et al., 2009). In the end, chalcopyritelike ($CuFeS_2$) quaternary chalcogenides $Cu_2ZnSnS_4$ and

$Cu_2ZnSnSe_4$ were studied for their TE properties with a wide band gap. It has shown that doping can generate more charge carriers thus improving electrical conductivity and distorted structure and quaternary components can lead to low lattice thermal conductivity. Specifically, a ZT value of 0.9 is obtained for $Cu_{2.1}Zn_{0.9}SnS_4$ at 860 K (Liu et al., 2009).

## 4. Applications of thermoelectric materials

This part will introduce the TE materials' applications at high temperatures and at low temperatures, nanocomposites with organic and inorganic materials and potential TE material graphane.

### 4.1 Applications at high temperatures

High temperature thermoelectric nanocomposites could be widely used in the field of air-warming system, Aeronautics and astronautics etc. It is an active realm driven by its applications. As a result, to acquire thermoelectric nanocomposite which possesses high energy conversion rate is fundamental for its applications. This process needs improved figure of merit from high electrical conductivity, high Seebeck coefficient, low thermal conductivity or any combinations of the above. This section will introduce perovskite-type oxides, double perovskites, half-Heusler alloy, boron icosahedra, zintl compound, copper aluminate and other oxides with high performance in high temperature. Besides, high temperature materials such as skutterudites and clathrates were narrated earlier in low thermal conductivity section, and chalcogenides were recounted in both low thermal conductivity section and high Seebeck coefficient section.

**Perovskite-type oxides**

Classic thermoelectric materials suffer from high toxicity, low stability and low efficiency while ceramics have been recently recognized as good thermoelectric with high stability even at elevated temperatures and low production costs. The perovskite is calcium titanium oxide mineral composed of calcium titanate, with the formula $CaTiO_3$. Perovskite-type oxides like $Ln(Co, Ni)O_3$ (Ln= La, Pr, Nd, Sm, Gd and Dy) compounds can exhibit higher ZT with low thermal conductivity in more than1200 K. The $LaCoO_3$ system is a promising thermoelectric material due to its high Seebeck coefficient of 600 mV/K at room temperature. The thermopower of $LaCoO_3$ is positive due to the partial disproportionation $2\ Co^{3+} = Co^{2+} + Co^{4+}$. Nevertheless the electrical resistivity is rather high which lowers the conversion efficiency. The amount of charge carriers and thus the electrical conductivity and thermoelectric properties in this system can be tuned by suitable Co-site and La-site substitution. Similarly, the compositions $La_{0.8}\ Ca_{0.2}MnO_3$ and $La_{0.6}\ Ca_4CoO_3$ were successfully grown by Weidenkaff et al. (Weidenkaff et al., 2008). These kinds of compounds could be used in regaining heat from the wastes. Still among perovskite-type oxides, some ceramic oxide materials such as $Na_xCo_2O_4$, site-substituted $SrMnO_3$ bear good electric conductivity and other perovskite-type oxides possess large thermopower (Robert et al., 2007). Besides, their chemical stability can prevent them from being oxidized. So, they are promising thermoelectrical materials due to simple manufacturing processes and low production costs in addition to above advantages.

**Double perovskites**

Double perovskites thermoelectric materials were reported showing high Seebeck coefficient at both high temperature and ambient temperauture. $Sr_2RuYO_6$ and $Sr_2ErRuO_6$ are such

materials. Fig. 25 indicated changes in Seebeck coefficient with temperature. From the results of Fig. 25, it can be seen that the values are negative in the whole temperature range due to majority of the charge carriers are electrons. The thermoelectric figure of merit values are large when the Seebeck coefficient of $Sr_2RuYO_6$ is -475 μV/K at 500 K and Seebeck coefficient of $Sr_2ErRuO_6$ is -400 μV/K at 500 K. From the figure 28, for $Sr_2ErRuO_6$ compound, the Seebeck coefficient is almost constant between the temperature range of 620 K and 950 K.

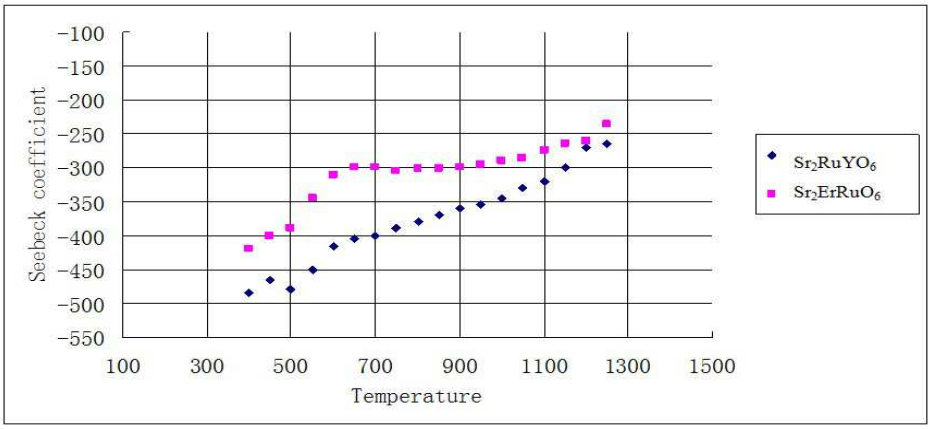


Fig. 25. The relations bewteen temperature (K) and Seebeck coefficient (μV/K) for $Sr_2RuYO_6$ & $Sr_2ErRuO_6$. Data source from (Aguirre et al., 2005).

Fig. 26 shows the relations between the total thermal conductivity and temperature for the these two compounds. The data points in Fig. 26 indicated that the trend of the thermal conductivity decreases with the increasing temperature. Obviously, $Sr_2RuErO_6$ has a lower thermal conductivity than $Sr_2RuYO_6$ attributing to that Er atom is larger than Y atom leading to a more efficient scattering center for phonons.

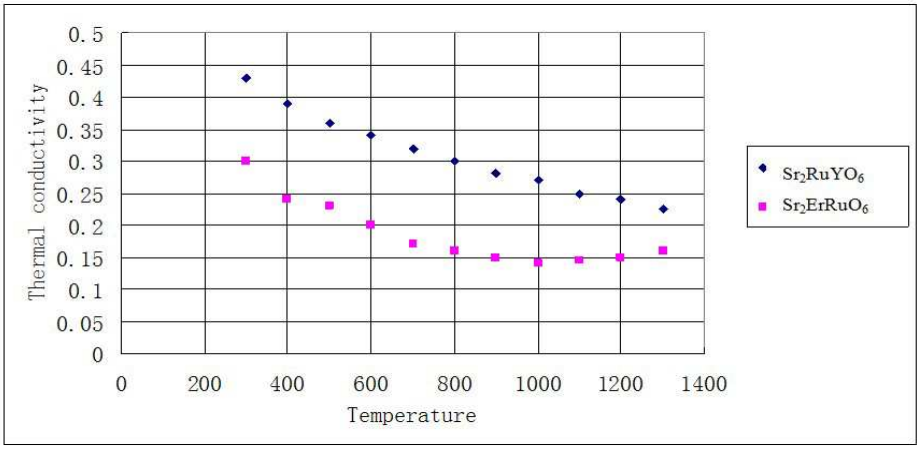


Fig. 26. The relations bewteen temperature (K) and total thermal conductivity ($W \cdot K^{-1} \cdot m^{-1}$) for $Sr_2RuYO_6$ & $Sr_2ErRuO_6$. Data source from (Aguirre et al., 2005).

Half-Heusler (HH) alloy

A Heusler alloy is a ferromagnetic metal alloy based on a Heusler phase which is intermetallic with particular composition and face-centered cubic crystal structure. This term is named after a German mining engineer and Chemist Friedrich Heusler, who studies such an alloy in 1903. Heusler alloy has the formulism $Cu_2MnSn$. While the half-Heusler alloys are considered as high-performance thermoelectric materials for high temperature. Specifically, (Ti, Zr, Hf)NiSn system consisting of three interpenetrating fcc sublattices indicated higher Seebeck (100-500 μV/K at 300 K) coefficient and relatively low resistivity. To achieve higher power factor, Sb could be incorporated in Sn site which is the main provider of carriers for charge transport for half-Heusler TiNiSn at high temperature. As a result, The (Ti, Zr, Hf)NiSn system is becoming a semimetallic material. The extrinsic charge carrier due to doping is fundamental for higher TE efficiency. Therefore, it is believed that properly alloying for these half-Heusler materials could enable these compounds to show higher TE performance at high temperature by tuning crystal structure and carrier concentrtion (Kim et al., 2004).

For example, for TiNiSn compound, incorporating Hf into Ti site and incorporating Sb into Sn site will reduce thermal conductivity. The highest ZT value of 0.78 is obtained at 770 K for $Ti_{0.95}Hf_{0.05}NiSn_{0.99}Sb_{0.01}$ compound; incorporating both Hf and Zr into Ti site and incorporating Sb into Sn site will cause an improved ZT value of 1.4 at 700 K for $(Zr_{0.5}Hf_{0.5})_{0.5}Ti_{0.5}NiSn_{1-y}Sb_y$ compound. Moreover, for n-type ZrNiSn-based alloys, incorporating Hf into Zr site and incorporating Sb into Sn site will cause an improved ZT value of 0.7 at 800 K for $Zr_{0.5}Hf_{0.5}Ni_{1-x}Pd_xSn_{0.99}Sb_{0.01}$ compound, and an enhanced ZT of 0.78 at 1070 K for $Hf_{0.75}Zr_{0.25}NiSn_{0.975}Sb_{0.025}$ compound (Culp et al., 2006). What's more, The Bi containing HH alloys has lower thermal conductivity compared to general HH alloys. A Ni doped ZrCoBi prepared by solid state reaction showing improved TE performance was reported (Ponnambalam et al., 2007). It is also reported that incorporating at the Ni site is vital for the optimization of the TE efficiency. The concentration of Ti, Zr and Hf as well as Pd or Pt substitution at Ni site can reduce the lattice thermal conductivity through mass fluctuations and strain field effects. Moreover, incorporating Pt on the Ni site of the disordered ZrNiSn-based compounds will improve both mass fluctuation and strain field fluctuation on accounts of Pt has a larger atomic mass and metallic radius than Pd. HH alloy with the formula $Zr_{0.5}Hf_{0.5}Ni_{0.5}Pd_{0.5}Sn_{0.99}Sb_{0.01}$ was such kind material with reduced thermal conductivity, thus indicating enhanced TE properties (Yang et al., 2004). A study deliberates a series of half-Heusler compounds XNiPn in which X stands for atoms such as Y, La and Bu, Pn means a pnicogen As, Sb and Bi. The results indicated that all these compounds are narrow-gap semiconductors and could be utilized as potential candidates for high properties TE materials (Larson et al., 1999).

(Zr,Hf)Co(Sb,Sn) alloys can be fabricated by mixing elemental pieces in proper quantities, and then melting several times in an arc furnace under flowing. An lowered thermal conductivity is found between 4.1 $W/m^{-1}$ $K^{-1}$ and 3.6 $W/m^{-1}$ $K^{-1}$ ranging from 300 K to 1000 K for $Zr_{0.5}Hf_{0.5}CoSb_{0.8}Sn_{0.2}$. An obvious improved ZT value is observed due to decreasing in thermal conductivity as well as increasing power factor beyond 1100 K. A ZT value of 0.51 is found for $Zr_{0.5}Hf_{0.5}CoSb_{0.8}Sn_{0.2}$ which is higher than SiGe at the same temperature 1000 K (Culp et al., 2008). Nearly single-phase NbCoSn alloys was synthesized by directional solidification employing optical floating zone melting method. This material is generally hard to fabricate because the melting point of Sn is lower than other elements in the alloy.

The nearly single-phase NbCoSn indicated a Seebeck coefficient of -250 μV/K at around 900 K and showed a relatively high carrier concentration of $4.82\times10^{26}$ $m^{-3}$. Also NbCoSn exhibited an excellent power factor of 2.5 mW/MK at around 650 K without adjusting electrical properties (Kimura et al., 2008). HH alloys $Zr_{1-x}Ti_xCoSn_ySb_{1-y}$ is also investigated for their possible use as high temperature p-type TE material. In this material, the Zr site is mainly substituted with Ti to lower thermal conductivity, which the content of Sn is varied to optimize the TE properties. Fig. 27 indicates the relation betweens temperature and thermopower. It showed that, thermopower values are high at higher temperatures due to high effective mass (Ponnambalam et al., 2008).

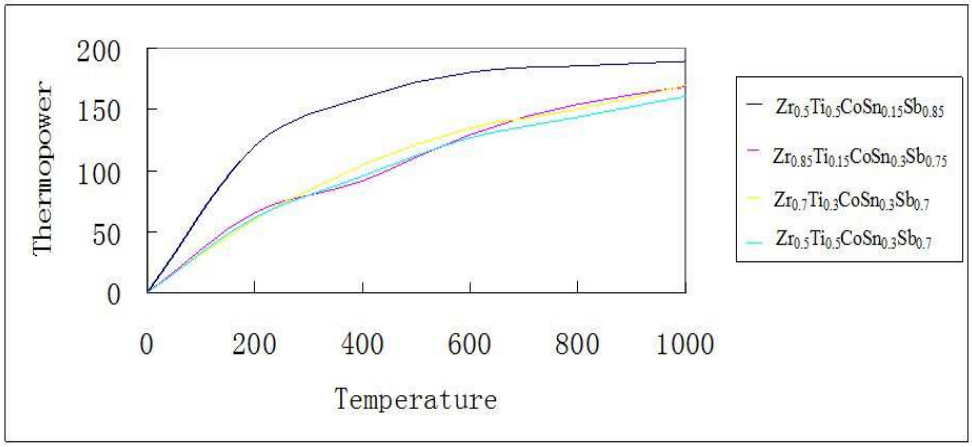


Fig. 27. Relations between thermopower (μV/K) and temperature (K) for Ti content varied $Zr_{1-x}Ti_xCoSn_{0.3}Sb_{0.7}$ series and Sn content reduced $Zr_{0.5}Ti_{0.5}CoSn_{0.15}Sb_{0.85}$ alloy. Data source from (Ponnambalam et al., 2008)

**Boron icosahedra**

Numerous novel nanocomposites were studied for the low thermal conductivity. Boron-rich cluster compounds are attractive materials because of their stability under high temperature, typically exhibiting melting points of above 2300 K, and more importantly, they also have intrinsic low thermal conductivity (Mori et al., 2007). Among the rare-earth-containing boron icosahedra compounds, only $RB_{66}$ (R=rare earth) has been investigated over a wide temperature region. $YB_{66}$ was found to exhibit low thermal conductivity with an amorphous like temperature dependence. A homologous series of n-type boron icosahedra compounds $RB_{17}CN$,$RB_{22}C_2N$ and $RB_{66}$ (R=rare earth) without doping were discovered to express low thermal conductivity in the temperature range of 300–1000 K rather than traditionally synthesized boron cluster compounds like boron carbide, $RB_{66}$ and $RB_{50}$ which have been found as p type (Mori et al., 2007).

**Zintl compound**

Moreover, it is reported that $C_{60}$-containing $Ba_{0.44}Co_4Sb_{12}$ possessing great thermal and electrical properties showed lower themal conductivity as low as 1.7 W/mK at around 650K.Also, the maximum output of the ceramic-layer-inserted p-n-joined $Si_{0.8}Ge_{0.2}$ thermoelectric elements was 48 mW/K starting from 500K to 1300K synthesized by pulse-

current sintering compared with dense bodies from gas-atomized powders. Obviously, the thermal conductivities of fine-grained Si–Ge dense bodies from ball-milled powders were greatly lowered (Otakea et al., 2004). But there is some special TE nanocomposite with lower thermal conductivity showing higher ZT value. It is reported that the compound $Ba_{0.24}Co_4Sb_{12}$ shows a ZT value as high as 1.3 at 850 K with decreased electrical conductivity and thermal conductivity due to increasing impurity contents. The reason is because of enhanced grain-boundary scattering of charge carriers and phonons, and barium fullerides formed from apart of barium in the filled skutterudite reacted with fullerene (Shi et al., 2007).

**Copper aluminate**

Another thermoelectric promising nanocomposite which is still stable at high temperatures up to 1400 K is copper aluminate ($CuAlO_2$). This TE nanocomposite could be used in thermoelectric devices and optoelectric applications dut to that $CuAlO_2$ is a transparent semiconductor and has a direct band-gap of 3.5eV. Many researchers use $CuAlO_2$ as a basic material to fabricate nanocomposite with higher value of ZT. The electrical conductivity and the Seebeck coefficient can be enhanced with the substitution of Ca for Al like $CuAl_{0.9}Ca_{0.1}O_2$.The nanocomposite $CuAl_{0.9}Fe_{0.1}O_2$ was obtained at 1140 K showing higher value of power factor up to 1.1($10^{-4}$) W/mK. Recently, the newly prepared doped $CuAlO_2$ showed the highest power factor of 1.26($10^{-4}$) with formation of $Cu_{1-x-y}Ag_xZn_yO_2$ at 1060 K, expressing a large enhancement compared with pure $CuAlO_2$. This could be proved by the XRD measurements demonstrating that the substitution of Ag and Zn for Cu improved the figure of merit. XRD also verified if using the Ag and Ni for the substitutions, the chemical reaction will be hindered between the staring materials (Yanagiya et al., 2010).

**Other Oxides**

Indium oxide indicated special TE properties when partly substituted with other cations. And indium oxide possesses great electrical conductivity and has a cubic bixbyite-like structure. Bixbyite is a manganese iron oxide meneral with a formula like $(Mn, Fe)_2O_3$. Doping $SnO_2$ into indium tin oxide bixbyite structure indicated an notably improved electrical conductivity and this kind of material is widely used for optoelectric application. Moreover, Ge incorporated $In_2O_3$ matrix with $In_2Ge_2O_7$ inclusion showed an enhanced ZT value of 0.46 at 1000 K which is the higher value obtained from polycrystalline oxides at high temperature. Additionally, $In_{1.6}Zn_{0.2}Sn_{0.2}O_3$ nanocomposite achieved a ZT value of 0.3 at 1273 K with a reduced lattice thermal conductivity resulting from mass fluctuation scattering of the phonons (Bérardan et al., 2008). What's more, $Ca_3CoRhO_6$, $Ca_3CoIrO_6$, $Sr_4Co_3O_9$ and $Ca_3Co_2O_6$ series were studied for their TE performances. Both $Ca_3CoRhO_6$ and $Ca_3CoIrO_6$ indicated a Seebeck coefficient of 150 μV/K at around 1000 K; $Ca_3CoRhO_6$ showed a lowerer power factor than $Sr_4Co_3O_9$; While $Ca_3CoRhO_6$'s power factor is more than two times than $Ca_3Co_2O_6$ at 1073 K. As a result, $Ca_3CoRhO_6$ could be considered as high promising TE material at high temperatures (Takami & Ikuta, 2008). Moreover, $Ca_3Co_4O_9$ fabricated by, chemical substitution, SPS and hot pressing indicated improved performance of TE effect. Many researches showed that substitution for Co site with Fe and substitution for Ca site with Na, Bi, Ag and Eu is an effective way to improve TE performances. Also, using the method of partially doping heavier ions in the Co site can lower the thermal conductivity. As a result, Ga ion with trivalence could be served for improving TE properties. $Ca_3Co_{4-x}Ca_xO_9$ oxides showed an enhanced ZT value than

undoped $Ca_3Co_4O_9$ specimen because Ga doped specimen possesses lower thermal conductivity than that of undoped one at around 1100 K (Nong et al., 2010).

### 4.2 Applications at low temperatures

There are many nanocomposite materials possess some high-efficient thermoelectric characteristics within low temperatures. This section will introduce such materials with Te, Sb or Bi based alloys, $FeSb_2$ and $TiS_2$, B-based compounds and cobalt oxide.

The incorportaed Te, Sb or Bi based alloys showed improved TE performance than traditional Bi-Sb-Te-Se alloys. It is reported that the $CsBi_4Te_6$ showed a high value ZT up to 0.8 at 225 K when incorporating appropriately. At cryogenic temperatures, the themoelectric properties of $CsBi_4Te_6$ can excel the traditional Bi-Sb-Te-Se alloys (Chung et al., 2000). Moreover, $Bi_{1.8}Sb_{0.2}Te_3$ was studied at low temperature for its Seebeck coefficient, ZT value and carrier concentration. $Bi_{1.8}Sb_{0.2}Te_3$ fabricated by gradient freeze method indicated a high Seebeck coefficient more than 500 μV/K and a high carrier concentration of $1.6\times10^{19}$ $cm^{-3}$, thus achieved a ZT value of 1.1 at 200 K (Huonga et al., 2004).

$Bi_{1-x}Sb_x$ nanowires ($0<x<0.30$) was studied with diameters 10 nm$<d_W<$100 nm at 77 K for its electronic transport properties. The calculation results showed that the ZT value of $Bi_{1-x}Sb_x$ nanowires is higher than that of bulk alloy. An extremly high ZT value is achieved for p-type $Bi_{1-x}Sb_x$ nanowires at 77 K with $d_W$=40 nm and x=0.13. It is also discovered that $Bi_{1-x}Sb_x$'s ZT value will be more than 1.2 for both p-type and n-type materials at 77K. The enhancement is attributed to the coalescence in energy of the subband edges of the ten hole pockets of this system and the resulting high density of states. These phenomena may not be limited to $Bi_{1-x}Sb_x$, and could serve as a strategy for the enhancement of ZT in other low-dimensional systems. It has proven that the same nanowires, under different doping conditions, can be used as either p-type or n-type legs in a TE device with ZT=1.2 at low temperature (Rabina et al., 2001). Theoretical work on transport properties in Bi was also studied. Bi nanowires have predicted that this system is a good candidate for an n-type leg for low temperature (77 K) performance. The ZT value of a Bi nanowire, oriented along the trigonal crystallographic direction and if it is properly doped, is expected to reach a ZT values of more than 1 at 77 K as the wire diameter ($d_W$) is decreased below 15 nm. Even smaller diameters are needed for the Bi nanowires to serve as good p-type legs.

Both the doped $TiS_2$ and undoped $FeSb_2$ possess the good TE properties. $FeSb_2$ was recently identified as a narrow-gap semiconductor with indications of strong electron-electron correlations. Strong electron-electron correlations are recognized to lead to a strong enhancement of the thermopower in a correlated semiconductor.

Several thermal properties of $FeSb_2$ were studied around 0 to 100K. The maximum absolute thermopower of $FeSb_2$ spans from 10 to 45 mV/K at around 10 K, greatly exceeding two reference compounds that of both $FeAs_2$ and $RuSb_2$. And $FeSb_2$ represents a promising candidate for thermoelectric cooling applications at cryogenic temperatures. Moreover, Isoelectronic substitution of antimony by arsenic $FeSb_{(2-x)}As_x$) reduces the high thermal conductivity (Sun et al., 2009). Magnesium incorporated compound $Mg_xTi_{1-x}S_2$ was studied for its thermoelectric and transport properties from 5 K to 310 K. After doping Mg for Ti in this compound, a phenomenon of a transition from metallike to semiconductorlike property because of reduction in electron concentration of $Mg^{2+}$ substitution for $Ti^{4+}$, happened meaning that $TiS_2$ essentially is a semiconductor. The result indicated that lightly substituted compound $Mg_{0.04}Ti_{0.96}S_2$'s ZT value increased significantly mainly due to its thermopower which is nearly 1.6 times more than that of $TiS_2$ at 300 K (Qin et al., 2007).

For B-based compound, $UB_4$ 's thermoelectric properties were studied along with $UB_4$'s three different boron isotope in the temperature range from 80 K to 300 K. Each of the specimens indicated a decreased TE performance with increasing temperature. The electrical resistivity decreased with increased temperature, and the natural boron, boron-10 enriched and boron-11 enriched specimen exhibited no obvious differences in electrical conductivity (Nishi et al., 2001). Another B-based TE compound is $YB_{66}$. Among the rare-earth-containing boron icosahedra compounds, $YB_{66}$ has been investigated over a wide low temperature region. And $YB_{66}$ was found to exhibit low thermal conductivity with an amorphous like temperature dependence. What's more, thermal conductivity of a $YbB_{44}Si_2$ crystal in the low temperature (12-300K) was investigated, the result of which shows that $YbB_{44}Si_2$ exhibits higher thermal conductivity value than $RB_{66}$ in lower temperature. As temperature goes up, the thermal conductivity of $YbB_{44}Si_2$ gradually goes down, but still a little higher than $YB_{66}$. A layered cobalt oxide $(Ca_{0.85}OH)_{1.16}CoO_2$ was studied for its TE performances in the temperature range from 290 K to 573 K. The experimental results from x-ray diffraction, SEM indicated that $(Ca_{0.85}OH)_{1.16}CoO_2$ is a p-type semiconductor. During this temperature range, ZT value will increase with increasing temperature (Pei et al., 2009).

### 4.3 Applications of organic and inorganic materials

Conducting polymers are attracting more and more emphasis with respect to its low thermal conductivity compared to that of an inorganic material as a traditional TE material. Hence, to better understand the characteristics and fabrications of nanostructuring composite materials is becoming neccessary. Additionally, due to the high electrical conductivity property of some polymers such as polyaniline, polypyrrole, p-phenylenevinylene, polythiophene and their derivatives, conducting polymers have already captureed much attention of its scientific application. Moreover, the conjugated polymer is flexible to be synthesized compared with traditional inorganic TE materials. While amongst the family of conducting polymers, polyaniline is considered as a critical and most studied conducting materials of the past 20 years because of good processability, stability in the air, high redox reversibility, swift change in film color, low cost, abundant chemistry characteristics and its wider applications ,say, Li batteries, capacitors (Okamoto & Kotaka, 1998), battery electrode, immobilization of enzymes, electrochromic devices (Mu et al., 1997), chemical sensors, anticorrosion coatings and light-emitting diodes (Guo & Zhou, 2007). Moreover, Carbon nanotubes have been extensively used as filling materials for polymeric composites due to their remarkable properties such as its wide accessible surface areas, great electronic traits and low resistivity. Hence, the carbon nanotube-filled polymeric composites can be applied to power devices, sensors, solar cell and supercapacitors, among which supercapacitors played an crucial role in wider applications such as auxillary power source in combination with battery in hybrid electric vehicles, back-up power sources for computer memory and short-time power source for mobile electronic devices (Zhang et al., 2009). The conducting polymer can also be used as solar cells when combined with nanocomposite materials like lead sulfide (Watt et al., 2005).

Through the years, various methods have been approved to synthesize carbon nanotube-filled polymers. In-situ chemical oxidative polymerization and ultrasonically initiated in-situ emulsion polymerization with good thermal stability and high electric conductivity have been successfully done to fabricate carbon nanotube-filled polyaniline. The carbon nanotube-filled polyanniline composite films were fabricated by electrochemical

polymerization of an aniline solution and it demonstrated higher specific capacitance, better cyclic stability. It is reported that both single-walled carbon nanotube and multi-walled carbon nanotube filled polyaniline exhibited improving electric conductivity and enhanced mechanical characteristics in supercapacitors than non-filled polymers.

In recent years, one-dimensional polyaniline have been synthesized by both chemical polymerization and electrochemical polymerization which are cheap means of gaining bulk nanofibers. The chemical fabrication consists of nanofiber seeding, electrospinning, template-based, interfacial polymerization and surfactant synthesis. But there is one big flaw involved in the chemical method: the remained surfactant and oxidants will in turn wreck sample's electrical properties. So the existing of ethanol and oligomer will reduce the effects from the dopants or current density to obtain the uniform deposited polyaniline films. While electrochemical polymerization is an environmentally friendly way to fabricate polyaniline nanofibers, and this method is a complementary way to chemical fabrication due to no surfactants and oxidants are needed (Guo & Zhou, 2007). During the production course, polyaniline chains grow on the electrode in the course of the electrochemical polymerization. Dedoped polyaniline is obtained by soaking phosphate acid doped polyaniline in ammonia solution for four hous, and their diameters range from 80 nm to 100 nm.

It is reported that aniline polymerization rate and spin activity of polyaniline are highly related to the concentration of aniline and hydrochloric acid. That is because the phenomenon that the Electron Paramagnetic resonance intensities increase obviously from 0.95 to 1.07 V during electrolysis process due to quick oxidization of aniline around 0.9 V and reduction from spinless bipolarons to polarons (Mu et al., 1997).

However, pure polymer and inorganic nanocomposite materials may not have the better TE properties than composite materials consisting of conducting polymer and inorganic TE material. The fabricated nanocomposite materials could inherit properties of both the inorganic materials and the polymers, or even with a synergistic effect. The organic-inorganic nanocomposite TE material provides the solid proof for low-cost, easy-fabrication, nontoxic and high conversion rate TE material in the future. In a two component nanostructuring composite including polymer and inorganic material, the combination of a conducting polymer and inorganic thermoelectrical material may yield high thermoelectric power and electrical conductivity. Because of the specific characteristics of polyaniline, some novel thermoelectric nanocomposite materials consisting of polyaniline (PANI) and other materials such as $Bi_2Te_3$ and $Sb_2S_3$ have been successfully synthesized using electrochemical reactions and deposited method. This kind of polymer-semiconductor composite own the traits of mechanical strengh and the solidness of semiconducting comnpounds (Subramanian et al., 2010).

For example, using inorganic bismuth nitrate as a dopant can help novel nanocomposite materials gaining higher electrical conductivity. This kind of rod-like nanocomposite thermoelectrical material has the diameter less than 100 nm. The synthesis of two component needed two solutions A and B: solution A was prepared by dissolving 200 mg of undoped PANI in 100 mg of N-dimethylformamide (MERCK) , and then mixed with 2 mg of bismuth nitrate pentahydrate as a dopant , the ratio of the PANI: dopant was 1:10. And this solution was kept under ultrasonication for 2 hours. Solution B comprised of equal volumes of bismuth nitrate solution and tellurium oxide solution. To fabricate this novel thermoelectric material, 5 ml of solution B and 20 ml of solution A were put in the electrochemical cell. ADC voltage of 20 V was applied to the solution through the

electrodes. The remaining 15 ml of solution B was added drop by drop at uniform time intervals to acquire uniform layer, ensuring uniform dispersion of both the components (Chatterjee et al., 2009).

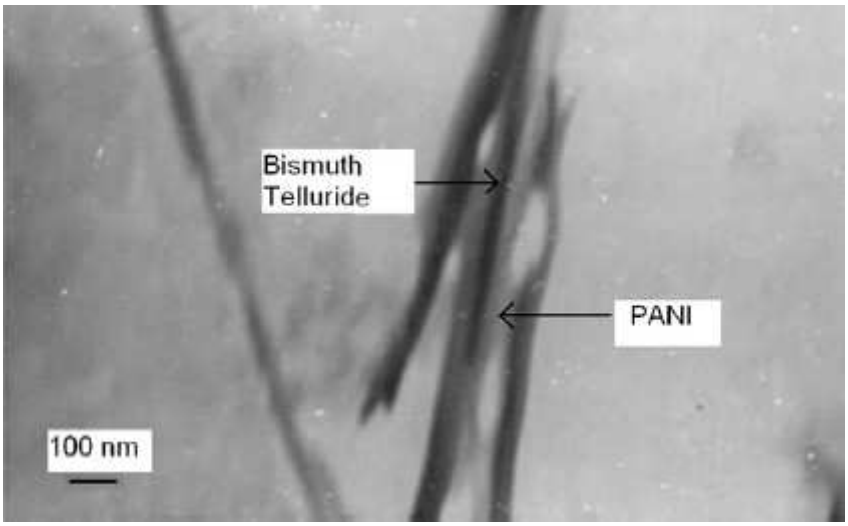


Fig. 28. TEM images of PANI/$Bi_2Te_3$ composite. Reproduced from (Chatterjee et al., 2009)

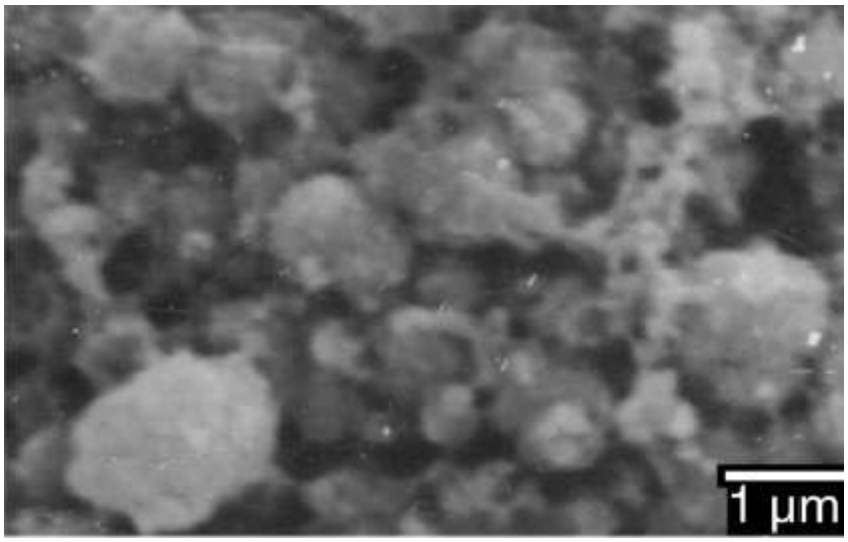


Fig. 29. SEM image of PANI/ $Bi_2Te_3$ (10000 magnification). Reproduced from (Chatterjee et al., 2009)

Transmission electron microscopy (TEM) (See Fig. 28) confirms the existence of polyaniline-$Bi_2Te_3$ and shows the rod-like nanostructure of less than 100 nm. It can be seen that the

polyaniline is amorphous and transparent, while $Bi_2Te_3$ is dark and opaque. In comparison with TEM, Scanning electron microscopy (SEM) (See Fig. 29) demonstrates the inorganic $Bi_2Te_3$ and organic polyaniline have been formed and the surface of which is uniform and continuous. Through calculations, the magnitude of thermoelectric power of the composite is between its two components within 340 K – 360 K.

Another example of two component nanocomposite material is $Sb_2S_3$ doped in PANI. This doping has more improvement of electrical conductivity of the thin film than the $Bi_2Se_3$ and $Bi_2S_3$. Usage of $Sb_2S_3$ as a dopant is because this composite is applied for television cameras and possesses the weak polar semiconducting ferroelectric characteristic. Many researchers have attempted various methods to deposit this material such as electrodeposition, chemical deposition and spray pyrolysis. While the way of doping polyaniline into the electrolyte of $Sb_2S_3$ thin film is more promising due to its three times enhancement of conductivity than that of as-deposited $Sb_2S_3$ thin film and decreasement of band gap energy on PANI doping as a result of the interfacial interaction between PANI and $Sb_2S_3$.

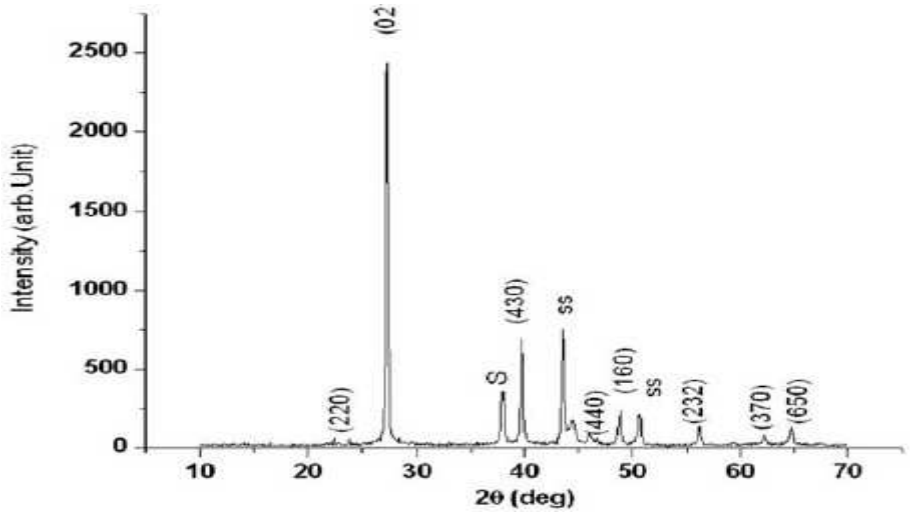


Fig. 30. XRD spectra of $Sb_2S_3$ thin films for as-deposited. Reproduced from (Subramanian et al., 2010).

Fig. 30 is the standard X-Ray Diffraction pattern of the as-deposited $Sb_2S_3$ thin film. The experiments showed that this figure is similar to the thin films doped with different concentrations of PANI dopant like 0.01M ,0.05M and 0.1M PANI. Therefore, it can be inferred that the new-fabricated thin film is polycrystalline and orthorhombic. In addition, as the lattice distortion increases, the scattering process will reduce which will in turn improve the mobility that will bring about increasement of electrical conductivity through the doping of PANI into the thin film. The figure of merit will increase on account of incorporation of PANI in the lattice of $Sb_2S_3$ resulting in lattice distortion.

As of the high Seebeck coefficient of the PbTe in nanocomposite material, it is very vital to well deposit inorganic TE material PbTe onto polyaniline to acquire great TE properties. Generally, it is difficult to homogenously disperse composite material into another polyer. As a result, PbTe-PANI composite could be fabricated by interfacial polymerization at room

temperature. The synthesized nanocomposite material powder comprised of PbTe nanoparticles, PANI/PbTe core-shell morphology and PbTe/PANI/ PbTe three layers sphere-like morphology. As the temperature increased from room teperature to 373 K, the electrical conductivity and Seebeck coefficient will show a synergistic effect compared with that of pure PbTe and PANI.

There are still lots of fabricated organic-inorganic TE composites: Bi-PANI nanocomposite by dispersing Bi nanoparticles into PANI, Ag-poly(3-octylthiophene) nanocomposite exhibiting extremely high Seebeck coefficient 1283 μV/K, $Bi_{0.5}Sb_{1.5}Te_3$-PANI nanocomposite by mixing $Bi_{0.5}Sb_{1.5}Te_3$ powder and PANI powder and then pressing them into pellets, $NaFe_4P_{12}$-PANI whisker nanocomposite by using emulsion fabrication method and in-situ compounding and carbon nanotube-polymer nanocomposite with exceedingly electrical conductivity (Wang et al., 2009).

### 4.4 Potential high ZT value TE material: graphane

Graphane is composed of carbon and hydrogen with the formula unit $(CH)_n$ in which n is large. Graphane is a single-layered 2-D polymer derived from a special graphite whose witdth is only 0.0335 nm. Adding 200,000 such graphites together, it only can build up a width of a single hair. One prominent characteristic of graphane is its electrical transport properties: indicating abnormal integral quantum Hall effect. The advantages of its low cost and rapid fabrication of its nanoscale graphane derivatives made carbon-based materials a potential promising high efficiency TE nanocomposite candidate for TE materials.

Graphane is a potential TE material for its quite large predicted ZT value. It could be as high as 5.8 depending on temeperature linearly by means of randomly introducting hydrogen vacancies to the graphane nanoribbon derivatives- armchair graphane nanoribbons (Ni et al., 2009). Furthermore, intrinsic anisotropy of thermal conductance in graphane nanoribbons were studied with width ranging from 0.5 nm to 35 nm. It found that anisotropy will disappear when its width is larger than 100 nm. The intrinsic anisotropy, created from different boundary conditions at ribbon edges, can be utilized to adjust thermal conductance for higher performance (Xu et al., 2007). What's more, large Seebeck coefficient of graphane deposited on a silicon dioxide substrate is obtained reaching 30 mV/K which is reported the highest value ever. This achievement is important for TE applications such as energy harvesting and scavenging (Dragoman & Dragoman. 2007).

## 5. Summary

To date, the most practical ZT value achieved is less than 2.0 which has been great improved than last century. ZT value will arrive at higher value like 5.0 which is not a dream in reality through researchers' constant endeavors in near future when under ideal experimentally conditions. Moreover, for small-scale electronic and optoelectronic applications, thin films may be the most suitable materials. While for large-scale applications like refrigeration and power generation, bulk TE materials with high TE properties may be fit and will be developed.

Although researchers have achieved a great deal of advances in TE materials by employing Slack's phonon-glass and electron-crystal approach or other methods, there still numerous problems ahead of us. How to choose the potential TE materials and how to tune the TE parameters to improve TE performance play an important role in pursuing the state-of-the-art materials in commecial utilizations. Up until now, a multitude of distinct TE systems and

high potential and promising TE nanocomposites are currently under investigation by a variety of global research groups. These potential nanocomposites range from semiconductors and semimetals to ceramic oxides, and from thin-film superlattice materials to large-single crystal or polycrystal materials. Consequently, there is inevitably much more work to do to obtain high-performance TE materials and devices.

Reaching higher energy efficiencies is not confined to thermoelectrical methods like creating complex structures and disorders resulting in phonon-glass properties, or leading to electron-crystal state. It is a multidisciplinary approach to quest and develop higher-efficiency TE materials and devices. As of it said, people are trying various ways to obtain higher energy conversion such as photovoltaic, mechanoelectric, electrochemical ways. And these ways are acquiring great accomplishments and are still developing. So the days when people can achieve high energy transformation rate are close by.

## 6. Acknowledgements

This work was supported by the research start-up fund from The University of Toledo. We also acknowledge the permissions from Elsevier B.V. Ltd through Copyright Clearance Center's Rightslink service to using Figures 28–30 in this paper.

## 7. References

Aguirre, M.H., Logvinovich, D., Bocher, L., Robert, R., Ebbinghaus, S.G.& Weidenkaff, A. (2008). High-temperature thermoelectric properties of $Sr_2RuYO_6$ and $Sr_2RuErO_6$ double perovskites influenced by structure and microstructure, Acta Materialis.Vol.(57): 108 – 115

Bentien, A., Christensen, M., Bryan, J.D., Sanchez, A., Paschen, S., Steglich, F., Stucky, G.D. & Iversen, B.B. (2004). Thermal conductivity of thermoelectric clathrates, Physical Review B. Vol.(69): 045107(1)- 045107(5)

Berardan, D., Guilmeau, E., Maignan, A.& Raveau, B. (2008). Enhancement of the thermoelectric performances of $In_2O_3$ by the coupled substitution of $M^{2+}/Sn^{4+}$ for $In^{3+}$, Journal of Applied Physics. Vol.(104): 064918(1)- 064918(5)

Bergvall, P. & Beckman, O. (2003). Thermoelectric properties of non-stoichiometric bismuth-antimony-telluride alloys, Solid State Electronics. Vol.(6)(No. 12):133-136

Cadavid, D. & Rodr´guez, J.E. (2008). Thermoelectric properties of polycrystalline $Zn_4Sb_3$ samples preparedby solid state reaction method, Physica B. Vol.(403): 3976–3979

Candolfi, C., Lenoir, B., Leszczynski, J., Dauscher, A., & Guilmeau, E., (2009). Beneficial influence of Ru on the thermoelectric properties of $Mo_3Sb_7$, Journal of Applied Physics. Vol.(105): 083701(1)- 083701(4)

Chatterjee, K., Suresh, A., Ganguly, S., Kargupta, K. & Banerjeea, D. (2009). Synthesis and characterization of an electro-deposited polyaniline-bismuth telluride nanocomposite -A novel thermoelectric material, Materials Characterization. Vol.(60): 1597-1601

Chung, D.Y., Hogan, T., Brazis, P., Rocci-Lane, M., Kannewurf, C., Bastea, M., Uher, C.& Kanatzidis, M.G. (2000). $CsBi_4Te_6$: A High-Performance Thermoelectric Material for Low-Temperature Applications, Science. Vol.(287)(No. 5455): 1024 – 1027

Cosnier, M., Fraisse, G. & Luo, L.G. (2008). An experimental and numerical study of a thermoelectric air-cooling and air-heating system, International Journal of Refrigeration. Vol.(31): 1051-1062

Cui, J.L., Liu, X.L., Yang, W., Chen, D.Y., Fu, H.& Ying, P.Z. (2009). Thermoelectric properties in nanostructured homologous series alloys $Ga_mSb_nTe_{1.5(m+n)}$, Journal of Applied Physics. Vol.(105): 063703(1)- 063703(6)

Culp, S.R., Poon, S.J., Hickman, N., Tritt, T.M.& Blumm, J. (2006). Effect of substitutions on the thermoelectric figure of merit of half-Heusler phases at 800 °C, Applied Physcis Letters. Vol.(88): 042106(1)- 042106(3)

Culp, S.R., Simonson, J.W., Poon, S.J., Ponnambalam, V., Edwards, J. & Tritt, T.M. (2008). (Zr,Hf)Co(Sb,Sn) half-Heusler phases as high-temperature (>700 °C) p-type thermoelectric materials, Applied Physics Letters. Vol.(93): 022105(1)- 022105(3)

Deng, S., Tang, X.F.& Zhang, Q.J. (2007). Synthesis and thermoelectric properties of p-type $Ba_8Ga_{16}Zn_xGe_{30-x}$ type-I clathrates, Journal of Applied Physics. Vol.(102): 043702(1)-043702(5)

Dragoman, D. & Dragoman, M. (2007). Giant thermoelectric effect in graphane, Applied Physics Letter. Vol.(91):203116(1)-203116(3)

Dragoman, M., Dragoman, D. & Plana, R. (2007). Modeling of rf energy sensing and harvesting using the giant thermoelectric effect in carbon nanotubes, Applied Physics Letter. Vol.(91): 173117(1)- 173117(3)

Dresselhaus, M.S., Sun, X., Zhang, Z., Cronin, S.B. & Koga, T. (1999). Low-dimensional thermoelectric materials, Physics of the Solid State. Vol.(41)(No. 5):679-682

Fornari, M. & Singh, D.J. (1999). Prediction of room-temperature high-thermoelectric performance in n-type $La(Ru_{1-x}Rh_x)_4Sb_{12}$, Applied Physics Letters. Vol.(74)(24):3666-3668

Funahashi, R.& Shikano, M. (2002). $Bi_2Sr_2Co_2O_y$ whiskers with high thermoelectric figure of merit, Applied Physics Letter. Vol.(81)(No. 8):1459-1461

Gelbstein, Y., Dashevsky, Z. & Dariel, M. P. (2008). The search for mechanically stable PbTe based thermoelectric materials, Journal of Applied Physics. Vol.(104): 033702(1)-033702(4)

Golia, Santosh., Arora, M., Sharma, R.K.& Rastogi, A.C. (2003). Electrochemically deposited bismuth telluride thin films, Current Applied Physics. Vol(3):195-197

Guo, Y.P. & Zhou, Y. (2007). Polyaniline nanofibers fabricated by electrochemical polymerization: A mechanistic study, European Polymer Journal. Vol.(43): 2292–2297

Hashimoto, K., Kurosaki, K., Imamura, Y., Muta, H.& Yamanaka, S. (2007). Thermoelectric properties of $BaSi_2$, $SrSi_2$, and LaSi, Journal of Applied Physics. Vol.(102):063763(1)-063763(5)

Huonga, N.T., Setou , Y., Nakamoto, G., Kurisu, M., Kajihara , T., Mizukami, H.& Sano, S. (2004). High thermoelectric performance at low temperature of p-$Bi_{1.8}Sb_{0.2}Te_{3.0}$ grown by the gradient freeze method from Te-rich melt, Journal of Alloys and Compounds. Vol.(368): 44-50

Ikeda, T., Collins, L.A., Ravi, V.A., Gascoin, F.S., Haile, S.M. & Snyder, G.J. (2007). Self-Assembled Nanometer Lamellae of Thermoelectric PbTe and $Sb_2Te_3$ with Epitaxy-like Interfaces, Chemisty of Materials. Vol.(19)(No. 4): 763–767

Kauzlarich, S.M., Browna, S.R.& Snyder, G.J. (2007). Zintl phases for thermoelectric devices, The Royal Society of Chemistry. DOI: 10.1039/b702266b. 2099-2107

Kim, J.H., Okamoto, N. L., Kishida, K., Tanaka,K. & Inui, H.(2007). Crystal structure and thermoelectric properties of type-III clathrate compounds in the Ba–In–Ge system, Journal of Applied Physics. Vol.(102): 094506(1)-094506(9)

Kim, S.W., Kimura, Y. & Mishima, Y. (2004). Enhancement of high temperature thermoelectric properties of intermetallic compounds based on a Skutterudite $IrSb_3$ and a half-Heusler TiNiSb, Science and Technology of Advanced Materials. Vol.(5): 485–489

Kima, S.S., Yinb, F. & Kagawa, Y. (2006). Thermoelectricity for crystallographic anisotropy controlled Bi–Te based alloys and p–n modules, Journal of Alloys and Compounds. Vol.(419): 306-311

Kimura, Y., Tamura, Y. & Kita, T. (2008). Thermoelectric properties of directionally solidified half-Heusler compound NbCoSn alloys, Applied Physics Letters. Vol.(92): 012105(1)- 012105(3)

Kishimoto, K., Akai, K., Muraoka, N., Koyanagi, T. & Matsuura, M. (2006). Synthesis and thermoelectric properties of type-I clathrate $Ge_{30}P_{16}Te_8$, Applied Physics Letters. Vol.(89): 172106 (1)-172106 (3)

Koga, T., Sun, X., Cronin, S.B., Dresselhaus, M.S., Wang, K.L. & Chen, G. (1997). Models for low-dimensional thermoelectricity, Journal of Computer-Aided Materials Design, 1998 Kluwer Academic Publishers. Printed in the Netherlands. Vol.(4):175-182

Kosuga, A., Kurosaki, K., Muta, H.& Yamanaka, S. (2006). Thermoelectric properties of Tl–X–Te (X=Ge, Sn, and Pb) compounds with low lattice thermal conductivity, Journal of Applied Physics. Vol.(99): 063705(1)- 063705(4)

Kurosaki, K., Matsumoto, H., Charoenphakdee, A., Yamanaka, S., Ishimaru, M.& Hirotsu, Y. (2008). Unexpectedly low thermal conductivity in natural nanostructured bulk $Ga_2Te_3$, Applied Physics Letters. Vol.(93): 012101(1)- 012101(3)

Lan, Y.C., Poudel, B., Ma, Y., Wang, D., Dresselhaus, M.S., Chen, G. & Ren, Z.F. (2009). Structure Study of Bulk Nanograined Thermoelectric Bismuth Antimony Telluride, Nano Letters. Vol.(9)(No. 4): 1419–1422

Larson, P., Mahanti, S.D., Sportouch, S. & Kanatzidis, M.G. (1999). Electronic structure of rare-earth nickel pnictides: Narrow-gap thermoelectric materials, Physical Review B. Vol.(59)(No. 24):15660-15668

Li, H., Tang, X.F., Su, X.L.& Zhang, Q.J. (2008). Preparation and thermoelectric properties of high-performance Sb additional $Yb_{0.2}Co_4Sb_{12+y}$ bulk materials with nanostructure, Applied Physics Letters. Vol.(92): 202114(1)- 202114(3)

Li, H., Tang, X.F., Zhang, Q.J. & Uher, C. (2008). Rapid preparation method of bulk nanostructured $Yb_{0.3}Co_4Sb_{12+y}$ compounds and their improved thermoelectric performance, Applied Physics Letters. Vol.(93): 252109(1)- 252109(3)

Li, H., Tang, X.F., Zhang, Q.J. & Uher, C. (2009). High performance $In_xCe_yCo_4Sb_{12}$ thermoelectric materials with in situ forming nanostructured InSb phase, Applied Physics Letters. Vol.(94): 102114(1)- 102114(3)

Li, Y., Xu, D.S., Zhang, Q.M., Chen, D.P., Huang, F.Z., Xu, Y.J., Guo, G.L. & and Gu, Z.N. (1999). Preparation of cadmium sulfide nanowire arrays in anodic aluminum oxide templates, Chemistry of Materials. Vol.(11): 3433-3435

Liao, C.N. & She, T.H. (2007). Preparation of bismuth telluride thin films through interfacial reaction, Thin Solid Films. Vol.(515):8059-8064

Lineykin, S. & Sam, B.Y. (2007). User-friendly and intuitive graphical approach to the design of thermoelectric cooling systems, International Journal of Refrigeration. Vol.(30):798-804

Litvinchuk, A.P., Nylén, J., Lorenz, B., Guloy, A.M.& Häussermann, U. (2008). Optical and electronic properties of metal doped thermoelectric $Zn_4Sb_3$, Journal of Applied Physics. Vol.(103): 123524(1)- 123524(6)

Liu, M.L., Huang, F.Q., Chen, L.D. & Chen, I.W. (2009). A wide-band-gap p-type thermoelectric material based on quaternary chalcogenides of $Cu_2ZnSnQ_4$ (Q=S,Se), Applied Physics Letters. Vol.(94): 202103(1)- 202103(3)

Liu, W.S., Zhang, B.P., Li, J.F., Zhang, H.L. & Zhao, L.D. (2007). Enhanced thermoelectric properties in $CoSb_{3-x}Te_x$ alloys prepared by mechanical alloying and spark plasma sintering, Journal of Applied Physics. Vol.(102): 103717(1)- 103717(7)

Lv, H.Y., Liu, H.J., Pan, L., Wen, Y.W., Tan, X.J., Shi, J. & Tang, X.F. (2010). Enhanced thermoelectric performance of $(Sb_{0.75}Bi_{0.25})_2Te_3$ compound from first-principles calculations, Applied Physics Letters. Vol.(96): 142101 (1)- 142101 (3)

Ma, Y., Hao, Q., Poudel, B., Lan, Y.C., Yu, B., Wang, D.Z., Chen, G. & Ren, Z.F. (2008). Enhanced Thermoelectric Figure-of-Merit in p-Type Nanostructured Bismuth Antimony Tellurium Alloys Made from Elemental Chunks, Nano Letters. Vol.(8)(No. 8):2580-2584

Madhavaram, R., Sander, J., Gan Y.X. & K.Masiulaniec, C. (2009). Thermoelectric property of PbTe coating on copper and nickel, Materials Chemistry and Physics. 13419(1)-13419(9)

Mangersnes, K., Løvvik, O.M. & Prytz, Ø. (2008). New filled P-based skutterudites-promising materials for thermoelectricity, New Journal of Physics. Vol.(10):1-16

Martin, J., Wang, H. & Nolas, G.S. (2008). Optimization of the thermoelectric properties of $Ba_8Ga_{16}Ge_{30}$, Applied Physics Letters. Vol.(92): 222110(1)- 222110(3)

Matsumoto, H., Kurosaki, K., Muta, H.& Yamanaka, S. (2008). Systematic investigation of the thermoelectric properties of $TlMTe_2$, Journal of Nuclear Materials. Vol.(104): 073705(1)- 073705(4)

Matsumoto, T., Yamazaki, J., Kaiwa, N. & Yamamoto, A. (2005). Thermoelectric properties and figure of merit of a Te-doped InSb bulk single crystal, Applied Physics Letter. Vol.(87): 201902(1)- 201902(3)

Mi, J.L., Zhu, T.J. & Zhao, X.B. (2007). Nanostructuring and thermoelectric properties of bulk skutterudite compound $CoSb_3$, The Journal of Chemical Physics. Vol.(101): 054314(1)- 054314(6)

Mi, J. L., Zhao, X. B., Zhu, T. J.& Tu, J. P. (2007). Improved thermoelectric figure of merit in *n*-type $CoSb_3$ based Nanocomposites, Applied Physics Letters. Vol.(91): 172116(1)-172116(3)

Mingoa, N. (2004). Thermoelectric figure of merit and maximum power factor in III–V semiconductor nanowires, Applied Physics Letters. Vol.(84)(No. 14):2652-2654

Mori,T., Martin, J. & Nolas,G. (2007). Thermal conductivity of $YbB_{44}Si_2$, Journal of Applied Physics. Vol.(102): 073510(1)- 073510(4)

Moreno, L.C., Cadavid, D. & Rodríguez, J.E. (2008). Thermoelectric power factor of LSCoO compounds, Microelectronics Journal. Vol.(39): 548-550

Mori, T., Nishimura, T., Yamaura, K. & Eiji, T.M. (2007). High temperature thermoelectric properties of a homologous series of n-type boron icosahedra compounds: A possible counterpart to p-type boron carbide, Journal of Applied Physics. Vol.(101)(No. 9):093714(1)- 093714(4)

Motohashi, T., Nonaka, Y., Sakai, K., Karppinen, M. & Yamauchi, H. (2008). Fabrication and thermoelectric characteristics of $[(Bi,Pb)_2Ba_2O_{4\pm w})_{0.5}CoO_2$ bulks with highly aligned grain structure, Journal of Applied Physics. Vol.(103): 033705(1)- 033705(6)

Mu, S.L., Kan, J.Q., Lu, J.T. & Zhuang, L. (1997). Interconversion of polarons and bipolarons of polyaniline during the electrochemical polymerization of aniline, Journal of Electroanalytical Chemistry. Vol.(446): 107–112

Ni, X.X., Liang, G., Wang, J.S. & Li, B.W. (2009). Disorder enhances thermoelectric figure of merit in armchair graphane Nanoribbons, Applied Physics Letters. Vol.(95): 192114(1)- 192114(3)

Nishi, Y., Arita, Y., Terao, K., Matsui, T. & Nagasaki, T. (2001). Boron isotope effects on the thermoelectric properties of $UB_4$ at low temperatures, Journal of Nuclear Materials. Vol.(294):209-211

Nolasa, G.S., Cohn, J.L., Slack, G.A. & Schujman, S.B. (1998). Semiconducting Ge clathrates: Promising candidates for thermoelectric Applications, Applied Physics Letters. Vol.(73)(No. 2):178-180

Nolasa, G.S., Poon, J.& Kanatzidis, M. (2006). Recent Developments in Bulk Thermoelectric Materials, MRS BULLETIN. Vol.(31):199-205

Nolasa, G.S., Kaeser, M., Littleton IV, R.T. & Tritt, T.M. (2000). High figure of merit in partially filled ytterbium skutterudite materials, Applied Physics Letters. Vol.(77)(No. 12):1855-1857

Nong, N.V., Liu, C.J. & Ohtaki, M. (2010). Improvement on the high temperature thermoelectric performance of Ga-doped misfit-layered $Ca_3Co_{4-x}Ga_xO_{9+\delta}$, Journal of Alloys and Compounds. Vol.(491): 53 – 56

Nose, K. & Yoshida, T. (2007). Semiconducting properties of zinc-doped cubic boron nitride thin films, Journal of Applied Physics. Vol.(102):063711(1)- 063711(5)

Okamoto, H. & Kotaka, T. (1998). Structure and properties of polyaniline films prepared via electrochemical polymerization.I: Effect of pH in electrochemical polymerization media on the primary structure and acid dissociation constant of product polyaniline films, Polymer. Vol.(39)(No. 18): 4349-4358

Okamoto, N.L., Oh, M.W., Nishii, T., Tanaka, K.& Inui, H. (2006). Crystal structure and thermoelectric properties of the type-I clathrate compound $Ba_8Ge_{43}$ with an ordered

arrangement of Ge vacancies, Journal of Applied Physics. Vol.(99): 033513(1)-033513(8)

Okamoto, N.L., Nakano, T., Tanaka, K. & Inui, H. (2008). Mechanical and thermal properties of single crystals of the type-I clathrate compounds $Ba_8Ga_{16}Ge_{30}$ and $Sr_8Ga_{16}Ge_{30}$, Journal of Applied Physics. Vol.(104): 013529(1)- 013529(7)

Otakea, M., Satoa, K., Sugiyamab, O. & Kaneko, S. (2004). Pulse-current sintering and thermoelectric properties of gas-atomized silicon–germanium powders, Solid State Ionics. Vol.(172): 523-526

Pedersen, B.L., Birkedal, H., Iversen, B.B., Nygren, M. & Frederiksen, P.T. (2006). Influence of sample compaction on the thermoelectric performance of $Zn_4Sb_3$, Applied Physics Letters. Vol.(89): 242108 (1)- 242108 (3)

Pedersen, B.L. & Iversen, B.B. (2008). Thermally stable thermoelectric $Zn_4Sb_3$ by zone-melting synthesis, Applied Physics Letters. Vol.(92): 161907(1)- 161907(3)

Pei, J., Chen, G.& Zhou, N. (2009). Hydrothermal synthesis, characterization, electronic structure, and thermoelectric properties of $(Ca_{0.85}OH)_{1.16}CoO_2$, The Journal of Chemical Physics. Vol.(130): 044706(1)- 044706(5)

Ponnambalam, V., Zhang, B.,Tritt,T.M. & Poon,S.J. (2007). Thermoelectric Properties of Half-Heusler Bismuthides $ZrCo_{1-x}Ni_xBi$, Chemistry and Materials Science. Vol.(36)(No. 7): 732-735

Ponnambalam, V., Alboni, P.N., Edwards, J., Tritt, T.M., Culp, S.R. & Poon, S.J. (2008). Thermoelectric properties of p-type half-Heusler alloys $Zr_{1-x}Ti_xCoSn_ySb_{1-y}$, Journal of Applied Physics. Vol.(103): 063716(1)- 063716(5)

Poudel, B., Hao, Q., Ma, Y., Lan, Y., Minnich, A., Yu, B., Yan, X., Wang, D., Muto, A., Vashaee, D., Chen, X., Liu, J., Dresselhaus, M.S., Chen, G.& Ren, Z.F. (2008). High-Thermoelectric Performance of Nanostructured Bismuth Antimony Telluride Bulk Alloys, Science Express. Vol.(320)(No. 5876):634-638

Qin, X.Y.,Zhang, J., Li, D., Dong, H.Z. & Wang, L. (2007). The effect of Mg substitution for Ti on transport and thermoelectric properties of $TiS_2$, Journal of Applied Physics. Vol.(102): 073703(1)- 073703(7)

Rabina, O., Lin, Y.M.& Dresselhaus, M.S. (2001). Anomalously high thermoelectric figure of merit in $Bi_{1-x}Sb_x$ nanowires by carrier pocket alignment, Applied Physics Letters. Vol.(79)(No. 1):81-83

Rao, A.M., Ji, X.H. and Tritt, T.M. (2006). Properties of Nanostructured One-Dimensional and Composite Thermoelectric Materials, MRS BULLETIN. Vol.(31):218-223

Rhyee, J.S., Cho, E., Lee, K.H., Lee, S.M., Kim, S.I., Kim, H.S., Kwon, Y.S.& Kim, S.J. (2009). Thermoelectric properties and anisotropic electronic band structure on the $In_4S_{e3-x}$ compounds, Applied Physics Letters. Vol.(95): 212106(1)- 212106(3)

Rhyee, J.S., Cho, E., Lee, K.H., Lee, S.M., Kim, H. & Kwon, Y.S. (2010). Thermoelectricity and localized *f*-band control by *dp*-hybridization on the $Ce_{1-x}Cu_xSe_2$ compounds, Journal of Applied Physics. Vol.(107): 053705(1)- 053705(5)

Robert, R., Aguirre, M.H., Hug, P., Reller, A.& Weidenkaff, A.(2007). High-temperature thermoelectric properties of Ln(Co, Ni)$O_3$ compounds, Acta Materialia. Vol.(55):4965-4972

Roh, J.W., Jang, S.Y., Kang, J., Lee, S., Noh, J.S., Kim, W., Park, J. & Lee, W. (2010). Size-dependent thermal conductivity of individual single-crystalline PbTe nanowires, Applied Physics Letters. Vol.(96): 103101 (1)- 0 103101 (3)

Ruan, X.F. & Xiao, W.K. (2007). Preparation and thermoelectric properties of $SiO_2/\beta$-$Zn_4Sb_3$ nanocomposite materials, Chemistry and Materials Science. Vol.(24)(No. 5):694-697

Sales, B.C., Chakoumakos, B.C.& Mandrus, D. (2000). Thermoelectric properties of thallium-filled skutterudites, Physical Review B. Vol.(61)(No. 4): 2475-2481

Sandomirsky, V., Schlesinger, Y., Butenko, A.V., Kolobov, I.G. & Ronen, A. (2003). Electric field effect controlled thermoelectricity in thin Bi films, Physica B. 1521–1522

Sekimoto, T., Kurosaki, K., Mut, H.& Yamanaka, S. (2006). LnPdSb (Ln=La,Gd): Promising intermetallics with large carrier mobility for high performance p-type thermoelectric materials, Applied Physics Letters. Vol.(89): 092108(1)- 092108(3)

Shi, L.H., Yao, D.L., Zhang, G.& Li, B.W. (2010). Large thermoelectric figure of merit in $Si_{1-x}Ge_x$ nanowires, Applied Physics Letters. Vol.(96): 173108(1)- 173108(1)

Shi, X., Chen, L., Yang, J.& Meisner, G. P. (2004). Enhanced thermoelectric figure of merit of $CoSb_3$ via large-defect scattering, Applied Physics Letters. Vol.(84)(No. 13):2301-2303

Shi, X., Chen, L.D.,.Bai, S.Q., Huang, X.Y,..Zhao, X.Y. & Yao, Q. (2007). Influence of fullerene dispersion on high temperature thermoelectric properties of $Ba_yCo_4Sb_{12}$-based composites, Journal of Applied Physics. Vol.(102): 103709(1)-103709(7)

Shi, X.Y., Huang, F.Q., Liu, M.L. & Chen, L.D. (2009). Thermoelectric properties of tetrahedrally bonded wide-gap stannite compounds $Cu_2ZnSn_{1-x}In_xSe_4$, Applied Physics Letters. Vol.(94): 122103(1)- 122103(3)

Shi, X., Kong, H., Li, C.P., Uher, C., Yang, J., Salvador, J.R., Wang, H., Chen, L. & Zhang, W. (2008). Low thermal conductivity and high thermoelectric figure of merit in n-type $Ba_xYb_yCo_4Sb_{12}$ double-filled skutterudites, Applied Physics Letters. Vol.(92): 82101(1)- 82101(3)

Snyder, G.J.& Toberer, E.S. (2008). Complex thermoelectric materials thermoelectric, nature materials. Vol.(7):105-114

Sootsman, J.R., He, J.Q., Dravid, V.P., Li, C.P., Uher, C. & Kanatzidis, M.G. (2009). High thermoelectric figure of merit and improved mechanical properties in melt quenched PbTe-Ge and PbTe-$Ge_{1-x}Si_x$ eutectic and hypereutectic composites, Journal of Applied Physics. Vol.(105): 083718(1)- 083718(1)

Subramanian, S., Chithralekha, P. & PathinettamPadiyan, D. (2010). Enhanced electrical response in $Sb_2S_3$ thin films by the inclusion of polyaniline during electrodeposition, Physica B. Vol.(405): 925-931

Sun, P.J., Oeschler, N., Johnsen, S., Iversenb, B.B.& Steglich, F. (2009). Narrow band gap and enhanced thermoelectricity in $FeSb_2$, Dalton Transactions.

Takami, T.& Ikuta, H. (2008). Magnetic and thermoelectric properties of quasi-one-dimensional oxides $A_{n+2}CoB_nO_{3n+3}$ (A=Ca,Sr, B=Co,Rh, Ir; n=1–3), Journal of Applied Physics. Vol.(103): 07B701(1)- 07B701(3)

Tardı´o, M.M., Ramı´rez, R., Gonza´ lez, R., Chen, Y.& Kokta, M. R. (2001). Enhancement of electrical conductivity in $\alpha$-$Al_2O_3$ crystals doped with magnesium, Journal of Applied Physics. Vol.(90)(No. 8):3942-3951

Tritt, T.M., Subramanian, M.A. & Editors, G. (2006). Thermoelectric Materials, Phenomena, and Applications: A Bird's Eye View, MRS BULLETIN. Vol.(31):188-198

Touzelbaev, M.N., Zhou, P., Venkatasubramanian, R.& Goodson, K.E. (2001). Thermal characterization of $Bi_2Te_3/Sb_2Te_3$ superlattices, Journal of Applied Physics. Vol.(90)(No. 2):763-767

Tsuchida, K., Tanaka, Y., Ifuku, T., Nakao, Y., Matsuda, T., Nagashima, S., Maeda, H. & Kato, A. (1996). Thermoelectric properties of oxide ceramics, Journal of Chemistry. Vol(13)(No. 5): 478-481

Wan, B.Y., Hua, C.G., Xi, Y., Xu, J. & He, X.S. (2010). Room-temperature synthesis and seebeck effect of lead chalcogenide nanocubes, Solid State Science. Vol.(12): 123-127

Wang, H., Li, J.F., Nan, C.W., Zhou, M., Liu, W.S., Zhang, B.P. & Kita, T. (2006). High-performance $Ag_{0.8}Pb_{18+x}SbTe_{20}$ thermoelectric bulk materials fabricated by mechanical alloying and spark plasma sintering, Applied Physics Letter. Vol.(88): 092104(1)- 092104(3)

Wang, X.J., Tang, M.B., Zhao, J.T., Chen, H.H. & Yang, X.X.. (2007). Thermoelectric properties and electronic structure of Zintl compound $BaZn_2Sb_2$, Applied physics letters. Vol.(90):232107(1)- 232107(3)

Wang, X.J., Tang, M.B., Chen, H.H., Yang, X.X., Zhao, J.T., Burkhardt, U.G. & Yuri. (2009). Synthesis and high thermoelectric efficiency of Zintl phase $YbCd_{2-x}Zn_xSb_2$, applied Physics Letter. Vol.(94)(No. 9): 092106(1)– 092106(3)

Wang, X.W., Lee, H., Lan, Y.C., Zhu, G.H., Joshi, G., Wang, D.Z., Yang, J., Muto, A.J., Tang, M.Y., Klatsky, J., Song, S., Dresselhaus, M.S., Chen, G. & Ren, Z.F. (2008). Enhanced thermoelectric figure of merit in nanostructured n-type silicon germanium bulk alloy, Applied Physics Letters. Vol.(93): 193121(1)- 193121(3)

Wang, Y.Y., Cai1, K.F., Yin, J.L., An, B.J., Du, Y.& Yao, X. (2009). In-Situ Fabrication and Thermoelectric Properties of PbTe-Polyaniline Composite Nanostructures, Journal of Nanoparticle Research. Manuscript Number: NANO2941:1-21

Watt, A.A.R., Blake, D., HWarner, J., Thomsen, E.A., Tavenner, E.L., Halina R.D. & Meredith, P. (2005). Lead sulfide nanocrystal: conducting polymer solar cells, Journal of Physics D: Applied Physics. Vol.(38): 2006-2012

Weidenkaff, A., Robert, R., Aguirre, M., Bocher, L., Lippert, T.& Canulescu, S. (2008). Development of thermoelectric oxides for renewable energy conversion technologies, Renewable Energy. Vol.(33): 342-347

Xie, W.J., Tang, X.F., Yan, Y.G., Zhang, Q.J. & Tritt, T.M. (2009). Unique nanostructures and enhanced thermoelectric performance of melt-spun BiSbTe alloys, Applied Physics Letters. Vol.(94): 102111(1)- 102111(3)

Xu, Y., Chen, X.B., Gu, B.L. and Duan,W.H. (2009). Intrinsic anisotropy of thermal conductance in graphene nanoribbons, Applied Physics Letters. Vol.(95): 233116(1)-233116(3)

Yamashita, O., Tomiyoshi, S. & Makita, K. (2003). Bismuth telluride compounds with high thermoelectric figures of merit, Journal of Applied Physics. Vol.(93)(No. 1):368-374

Yamashita, O. (2004). Effect of metal electrode on Seebeck coefficient of p- and n-type Si thermoelectrics, Journal of Applied Physics. Vol.(95)(No. 1):178-183

Yamashita, O.& Tomiyoshi, S. (2004). High performance n-type bismuth telluride with highly stable thermoelectric figure of merit, Journal of Applied Physics. Vol.(95)(No. 11):6277-6283

Yanagiya, S., Van Nong, N., Xu, J.X. & Pryds, N. (2010). The Effect of (Ag, Ni, Zn)-Addition on the Thermoelectric Properties of Copper Aluminate, Materials. Vol.(3): 318-328

Yang, J., Meisner, G.P. & Chen, L. (2004). Strain field fluctuation effects on lattice thermal conductivity of ZrNiSn-based thermoelectric compounds, Applied Physics Letters. Vol.(85)(No. 7):1140-1142

Young, D., Mastronardi, K., Khalifah, P., Wang, C.C.& Cava, R.J. (1999). $Ln_3Au_3Sb_4$: Thermoelectrics with low thermal conductivity, Applied Physices Letters. Vol.(74)(No. 26):3999-4001

Yu, C., Scullin, M.L., Huijben, M., Ramesh, R. & Majumdar, A. (2008). Thermal conductivity reduction in oxygen-deficient strontium titanates, Applied Physics Letters. Vol.(92): 191911(1)- 191911(3)

Yu, C., Zhu, T.J., Zhang, S.N., Zhao, X.B., He, J., Su, Z. & Tritt, T.M. (2008). Improved thermoelectric performance in the Zintl phase compounds $YbZn_{2-x}Mn_xSb_2$ via isoelectronic substitution in the anionic framework, Journal of Applied Physics. Vol.(104): 013705(1)- 013705(5)

Zawilski, B. M., Littleton IV, R. T. & Tritt, T.M. (2000). Investigation of the thermal conductivity of the mixed pentatellurides $Hf_{1-x}Zr_xTe_5$, Applied Physics Letter. Vol.(77)(No. 15):2319-2321

Zeng, G.H., Bahk, J.H., Bowers, J.E., Lu, H., Gossard, A.C., Singer, S.L., Majumdar, A., Bian, Z.X., Zebarjadi, M.& Shakouri, A. (2009). Thermoelectric power generator module of 16×16 $Bi_2Te_3$ and 0.6% ErAs: $(InGaAs)_{1-x}(InAlAs)_x$ segmented elements, Applied Physics Letters. Vol.(95): 083503(1)- 083503(5)

Zhao, X.Y., Shi, X., Chen, L.D. Zhang, W.Q., Bai, S.Q., Pe, Y.Z. & Li, X.Y. (2006). Synthesis of $Yb_yCo_4Sb_{12}/Yb_2O_3$ composites and their thermoelectric properties, Applied Physics Letters. Vol.(89): 092121 (1)- 092121 (3)

Zhao, X.Y., Shi, X., Chen, L.D., Zhang, W.Q., Zhang, W.B. & Pei, Y.Z. (2006). Synthesis and thermoelectric properties of Sr-filled skutterudite $Sr_yCo_4Sb_{12}$, Journal of Applied Physics. Vol.(99): 053711(1)- 053711(4)

Zhang, F. & Wong, S.S. (2009). Controlled synthesis of semiconducting metal sulfide nanowires, Chemistry of Materials. Vol.(21):4541-4554

Zhang, H., Zhao, J.T., Grin, Y., Wang, X.J., Tang, M.B., Man, Z.Y., Chen, H.H. & Yang, X.X. (2008). A new type of thermoelectric material, $EuZn_2Sb_2$, The Journal of Chemical Physics. Vol.(129): 164713(1)- 164713(5)

Zhang, J., Kong, L.B., Wang, B., Luo, Y.C. & Kang, L. (2009). In-situ electrochemical polymerization of multi-walled carbon nanotube/polyaniline composite films for electrochemical supercapacitors, Synthetic Metals. Vol.(159): 260-266

Zhang, L., Grytsiv, A., Kerber, M., Rogl, P., Bauer, E. & Zehetbauer, M. (2010). Thermoelectric performance of mischmetal skutterudites $Mm_yFe_{4-x}Co_xSb_{12}$ at elevated temperatures, Journal of Alloys and Compounds. Vol.(490): 19-25

Zhang, Q., He, J., Zhu, T.J., Zhang, S.N., Zhao, X.B.& Tritt, T.M. (2008). High figures of merit and natural nanostructures in $Mg_2Si_{0.4}Sn_{0.6}$ based thermoelectric materials, Applied Physics Letters. Vol.(93): 102109(1)- 102109(3)

Zhou, Y.Q., Matsubara, I., Horii, S., Takeuchi, T., Funahashi, R., Shikano, M., Shimoyama, J.& Kishio, K. (2003). Thermoelectric properties of highly grain-aligned and densified Co-based oxide ceramics, Journal of Applied Physics. Vol.(93)(No. 5):2653-2658

Zhu,T.J., Yu,C., He, J., Zhang, S.N., Zhao,X.B. & Tritt,T.M. (2008). Thermoelectric Properties of Zintl Compound $YbZn_2Sb_2$ with Mn Substitution in Anionic Framework , Journal of Electronic Materials. Vol.(38)(No. 7): 1068-1071

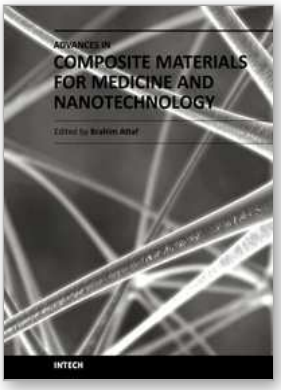


**Advances in Composite Materials for Medicine and Nanotechnology**

Edited by Dr. Brahim Attaf

ISBN 978-953-307-235-7
Hard cover, 648 pages
**Publisher** InTech
**Published online** 01, April, 2011
**Published in print edition** April, 2011

Due to their good mechanical characteristics in terms of stiffness and strength coupled with mass-saving advantage and other attractive physico-chemical properties, composite materials are successfully used in medicine and nanotechnology fields. To this end, the chapters composing the book have been divided into the following sections: medicine, dental and pharmaceutical applications; nanocomposites for energy efficiency; characterization and fabrication, all of which provide an invaluable overview of this fascinating subject area. The book presents, in addition, some studies carried out in orthopedic and stomatological applications and others aiming to design and produce new devices using the latest advances in nanotechnology. This wide variety of theoretical, numerical and experimental results can help specialists involved in these disciplines to enhance competitiveness and innovation.



INTECH
open science | open minds

**InTech Europe**
University Campus STeP Ri
Slavka Krautzeka 83/A
51000 Rijeka, Croatia
Phone: +385 (51) 770 447
Fax: +385 (51) 686 166
www.intechopen.com

**InTech China**
Unit 405, Office Block, Hotel Equatorial Shanghai
No.65, Yan An Road (West), Shanghai, 200040, China
中国上海市延安西路65号上海国际贵都大饭店办公楼405单元
Phone: +86-21-62489820
Fax: +86-21-62489821